SURFACE EFFECTS ON SPINWAVE RESONANCE IN THIN MAGNETIC FILMS

Thesis by

O. Glenn Ramer

In Partial Fullfillment of the Requirements

for the Degree of

Doctor of Philosophy

California Institute of Technology

Pasadena, California

1976

(Submitted May 13, 1976)

ACKNOWLEDGMENTS

The author would like to express his thanks to his many associates who in part made this work possible. I especially wish to thank C. H. Wilts and F. B. Humphrey; C. H. Wilts for his guidance as thesis and research advisor; F. B. Humphrey for being a close associate during the four years at Caltech and for playing a key role in my being admitted to Caltech. Helpful assistance from, discussions and correspondence with P. E. Wigen, C. E. Patton, R. C. Barker, T. Kokayashi, R. D. Henry and H. Puszkarski are acknowledged. In the course of the work, assistance from various Institute personnel has been indispensible and is acknowledged. I thank the Institute, Corning Glass Works, and the National Science Foundation for financial assistance. I thank Vere Snell and Ruth Stratton for preparing the manuscript.

Finally, I thank my wife, Sandy, for her continued encouragement and support.

ABSTRACT

Over the past few decades, ferromagnetic spinwave resonance in magnetic thin films has been used as a tool for studying the properties of magnetic materials. A full understanding of the boundary conditions at the surface of the magnetic material is extremely important. Such an understanding has been the general objective of this thesis. The approach has been to investigate various hypotheses of the surface condition and to compare the results of these models with experimental data. The conclusion is that the boundary conditions are largely due to thin surface regions with magnetic properties different from the bulk. In the calculations these regions were usually approximated by uniform surface layers; the spins were otherwise unconstrained except by the same mechanisms that exist in the bulk (i.e., no special "pinning" at the surface atomic layer is assumed). The variation of the ferromagnetic spinwave resonance spectra in YIG films with frequency, temperature, annealing, and orientation of applied field provided an excellent experimental basis for the study.

This thesis can be divided into two parts. The first part is ferromagnetic resonance theory; the second part is the comparison of calculated with experimental data in YIG films. Both are essential in understanding the conclusion that surface regions with properties different from the bulk are responsible for the resonance phenomena associated with boundary conditions.

The theoretical calculations have been made by finding the wave vectors characteristic of the magnetic fields inside the magnetic

medium, and then combining the fields associated with these wave vectors in superposition to match the specified boundary conditions. In addition to magnetic boundary conditions required for the surface layer model, two phenomenological magnetic boundary conditions are discussed in detail. The wave vectors are easily found by combining the Landau-Lifshitz equations with Maxwell's equations. Mode positions are most easily predicted from the magnetic wave vectors obtained by neglecting damping, conductivity, and the displacement current. For an insulator where the driving field is nearly uniform throughout the sample, these approximations permit a simple yet accurate calculation of the mode intensities. For metal films this calculation may be inaccurate but the mode positions are still accurately described. The techniques necessary for calculating the power absorbed by the film under a specific excitation including the effects of conductivity, displacement current and damping are also presented.

In the second part of the thesis the properties of magnetic garnet materials are summarized and the properties believed associated with the two surface regions of a YIG film are presented. Finally, the experimental data and calculated data for the surface layer model and other proposed models are compared. The conclusion of this study is that the remarkable variety of spinwave spectra that arises from various preparation techniques and subsequent treatments can be explained by surface regions with magnetic properties different from the bulk.

Table of Contents

Chapter 1
Introduction

1.1 The Thesis

Over the past few decades, ferromagnetic spinwave resonance in magnetic thin films hassbeen used as a tool for studying the properties of magnetic materials. (The reader not acquainted with ferromagnetic resonance will find a brief overview of the subject and the importance of the boundary conditions in Appendix VI.) A full understanding of the boundary conditions at the surface of the magnetic material is extremely important. Such an understanding has been the general objective of this thesis. The approach has been to investigate various hypotheses of the surface condition and to compare the results of these models with experimental data. The conclusion is that the boundary conditions are largely due to thin surface regions with magnetic properties different from the bulk. In the calculations these regions were approximated by uniform surface layers; the spins were otherwise unconstrained except by the same mechanisms that exist in the bulk (i.e., no special "pinning" at the surface atomic layer is assumed). The variation of the ferromagnetic spinwave resonance spectra in YIG films with frequency, temperature, annealing, and orientations of applied field provided an excellent experimental basis for the study. A brief review of the observed phenomena is given in the following section of this chapter.

This thesis can be divided into two parts. The first part is ferromagnetic resonance theory; the second part is the comparison of calculated with experimental data in YIG films. Both are essential in understanding the conclusion that surface regions with properties

different from the bulk are responsible for the resonance phenomena associated with boundary conditions. The theories presented in Chapters 2-4 are not new but are presented here in a complete and concise form; however, most of the equations have only appeared in the literature in the form of special cases (e.g., perpendicular resonance, parallel resonance).

The theoretical calculations have been made by finding the wave vectors characteristic of the magnetic fields inside the magnetic medium, and then combining the fields associated with these wave vectors in superposition to match the required boundary conditions. In addition to magnetic boundary conditions required for the surface layer model, two phenomenological magnetic boundary conditions are discussed in detail. The wave vectors are easily found (Chapter 2) by combining the Landau-Lifshitz (1935) equations with Maxwell's equations. Macdonald (1950) may have been the first to combine these equations to obtain a quartic equation for the propagation vectors of spinwaves when the mean magnetization is oriented perpendicular to the direction of propagation. Ament and Rado (1955) solved the problem of parallel resonance in a planar sample obtaining the same equation as that of Macdonald. Akhiezer et al (1961) extended the calculation to the case where the magnetic field and the mean magnetization were perpendicular to the sample surface. Vittoria and coworkers (1970) developed the theory for arbitrary angle of applied magnetic field in planar structures. The theory was further refined by Liu (1974).

Mode positions are most easily predicted from the magnetic wave vectors obtained by neglecting damping, conductivity, and the displacement current; these approximations are presented in Chapter 3. For an insulator where the driving field is nearly uniform throughout the sample, these approximations permit a simple yet accurate calculation of the mode intensities. For metal films this calculation may be inaccurate but the mode positions are still accurately described (see Appendix III). The final theoretical chapter (Chapter 4) presents the techniques necessary for calculating the power absorbed by the film under a specific excitation including the effects of conductivity, displacement current and damping.

The second part of the thesis is contained in Chapters 5 and 6. In Chapter 5 the properties of magnetic garnet materials are summarized and the properties believed associated with the two surface regions of YIG film are presented. In Chapter 6 the experimental data and calculated data for the surface layer model and other proposed models are compared.

1.2 Summary of Experimental Phenomena

This section describes the relevant results of spinwave resonance experiments in thin YIG films. The films were subjected to various environmental treatments which changed the surface properties of the film. The films are single crystals grown on gadolinium gallium garnet (GGG) substrates by either Liquid Phase Epitaxy (LPE) or Chemical Vapor Deposition (CVD). One experimentally interesting phenomenon is that at one of the two limiting orientations of the

applied magnetic field, parallel or perpendicular to the film plane, the resonance spectrum can show one or sometimes two spinwave modes at a higher field than the largest absorption mode; these modes are called surface modes.

The first surface mode reported in YIG films (Brown et al (1972)) was observed with the film in the parallel resonance configuration. Surface spinwave modes of this type were observed in YIG discs grown by CVD on both (100) and (110) GGG substrates. Yu et al (1975) continued the investigation of these CVD grown films. They presented the angle and temperature dependences of the spectra and discussed the creation of the surface pinning condition necessary for the existence of surface modes by controlled annealing of the films. A set of stick diagrams representing the parallel resonance spectra for a series of annealed YIG films is shown in Fig. (1-1). These spectra are from samples annealed in a dry oxygen atmosphere at the temperature indicated. The height of the lines gives an indication of the relative intensities observed. For the film annealed at 1200°C two surface modes exist.

For a .49 μm [111] oriented YIG film the spinwave spectrum for several angles of the applied magnetic field and a frequency of 6 GHz is shown in Fig. (1-2). The high field spinwave mode observed at parallel resonance ($\beta = 90°$) is a surface mode. As the applied magnetic field is rotated towards the perpendicular orientation, the high-field surface mode increases in intensity while the other modes all decrease in intensity. At about $\beta = 30°$ the surface mode becomes

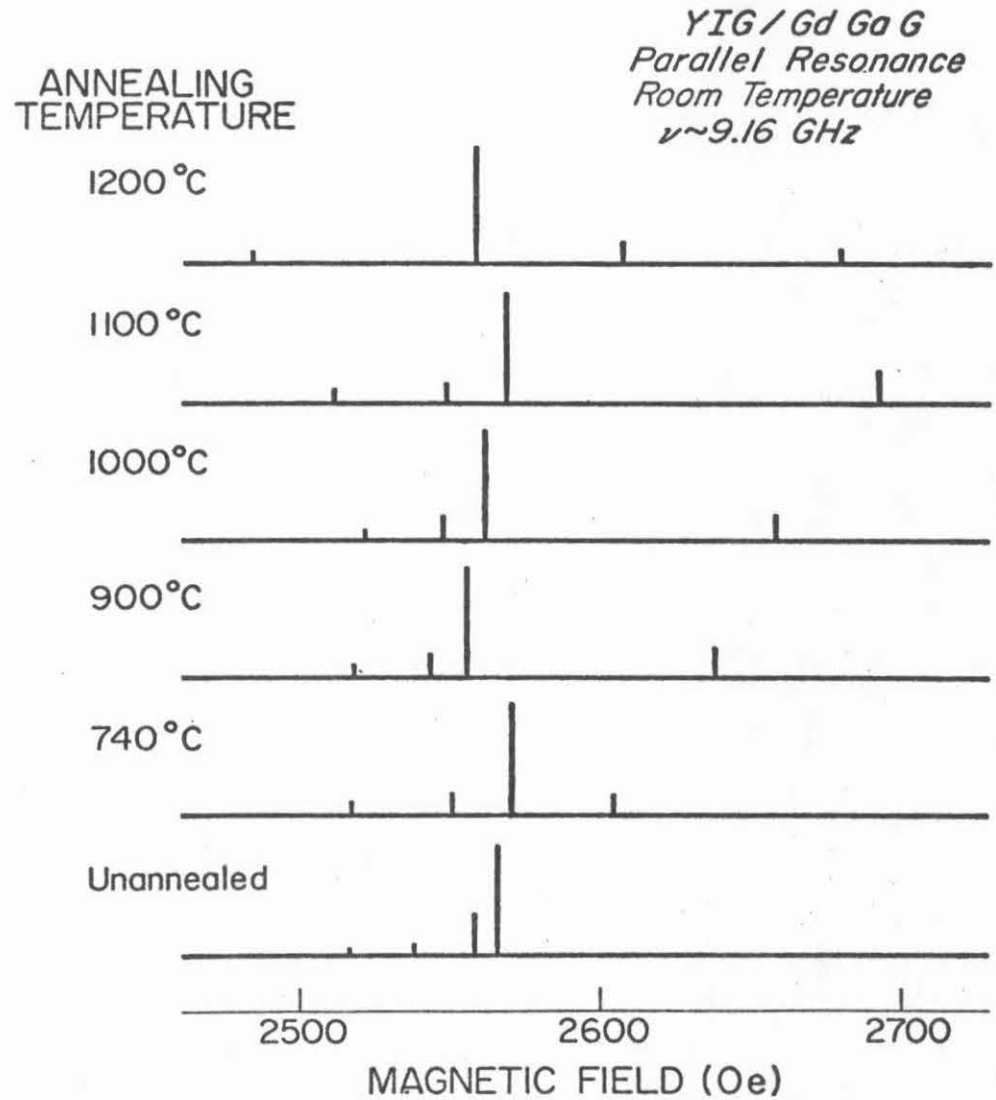

Fig. (1-1) Stick diagrams representing the parallel resonance spectra of a series of YIG films showing the effect of annealing on the resonant-field position of the spin wave modes (After Yu, et. al.,1975).

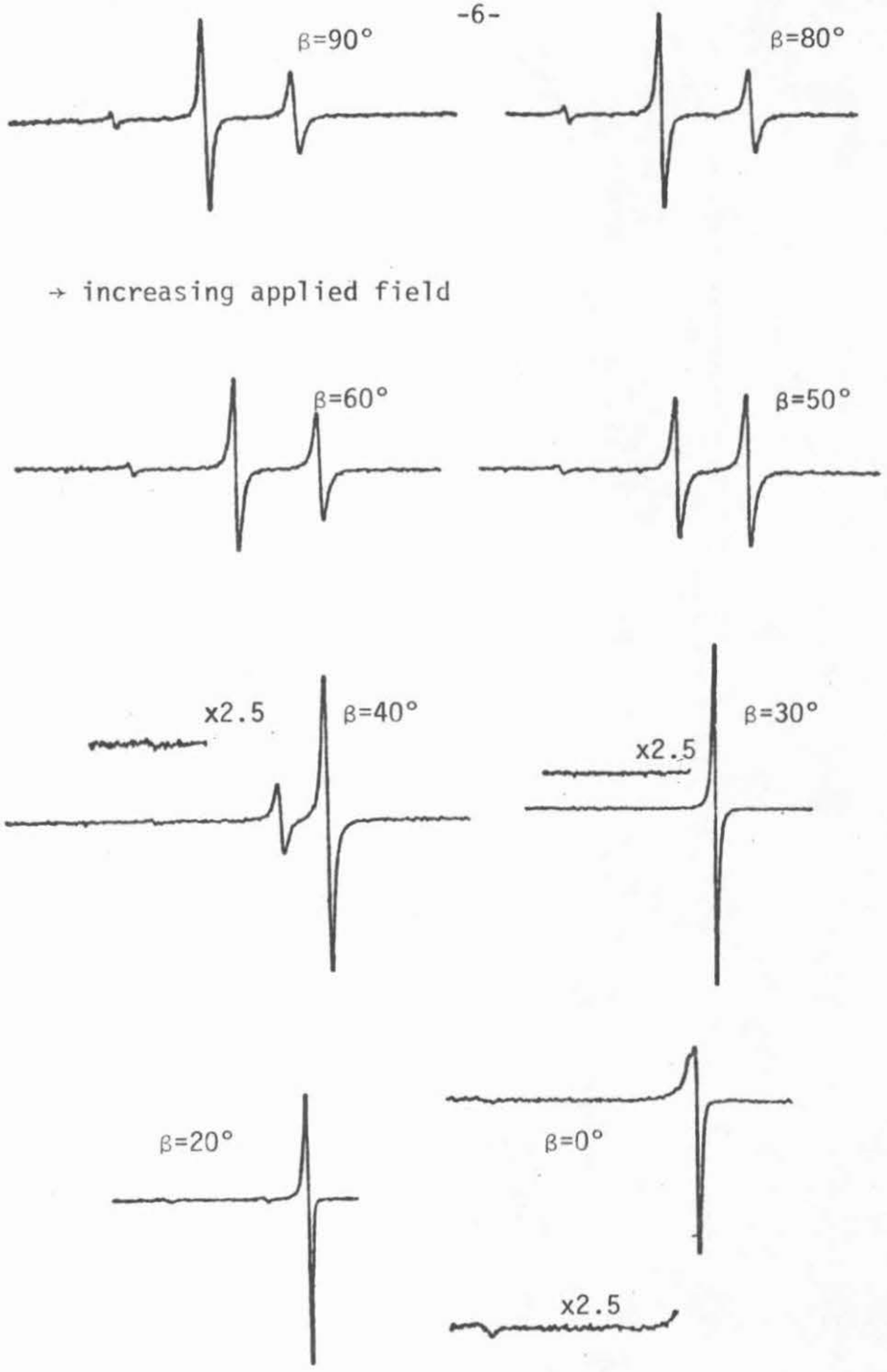

Fig. (1-2) Derivative absorption curves of the first three modes observed at eight orientations (angle of applied field, β) at 6 GHz and room temperature for a YIG film having a single surface mode at the parallel resonance orientation, β=90°.

the only mode observed; beyond this angle, the higher-order modes are again observed. In some cases (as in perpendicular resonance in Fig. (1-2)) magnetostatic contributions to the modes have been observed. However, the resonance positions and other phenomena studied in this thesis are independent of the sample shape; therefore, magnetostatic contributions are negligible.

The localization of a surface mode was investigated by etching a sample away in many steps; such experiments show indeed that the surface modes are localized at the surfaces. For a film with a single surface mode, the variation of the signal intensity with film thickness for the largest absorption mode and the surface mode is shown in Fig. (1-3). In this particular experiment the mode was localized at the film substrate interface.

Typically in a film with one surface mode localized at the interface the parallel resonance spectrum has the following temperature dependence. Upon lowering the temperature from room temperature, the surface mode increases in intensity while all other modes decrease in intensity. At a critical temperature the once surface mode has a maximum intensity and all higher order modes nearly vanish. At temperatures above the critical temperature, there is an angle (e.g., $\beta = 30°$ in Fig. (1-2)) where all higher order modes vanish.) The temperature dependence of this angle (called the critical angle) is such that it moves toward the parallel orientation and at the above critical temperature is in the plane of the film.

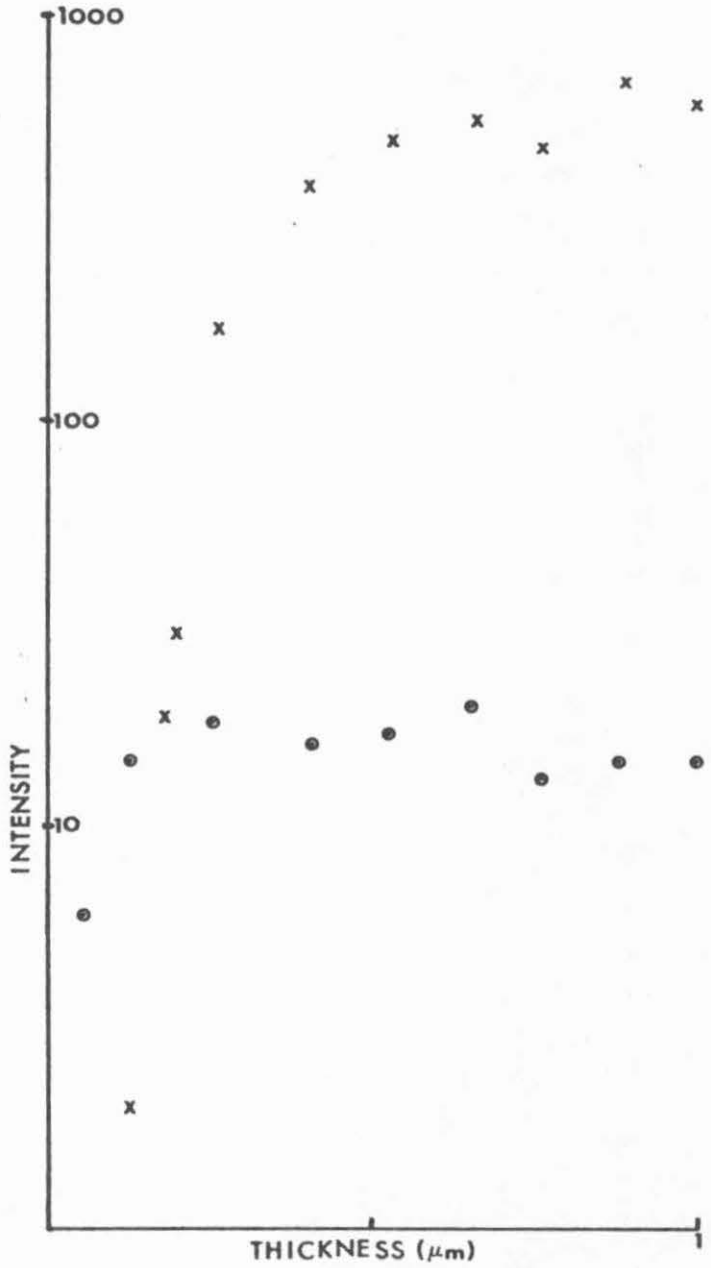

Fig. (1-3) Variation of the peak-to-peak intensity with film thickness for a body spin wave (x) and a surface spin wave (o). (After Yu et. al.,1975) Note that the intensity of the surface mode is constant as the film is etched away until the film is very thin indicating that the mode is localized at the film-substrate interface.

The existence of surface modes at the perpendicular resonance orientation in LPE grown films has been reported by Henry et al (1973). The boundary conditions necessary for this surface spinwave to exist were produced by either SiO_2 sputtering or ion implantation. Some of the properties of this surface mode are the following: (1) If the SiO_2 is removed using buffered hydrofluoric acid this surface mode persists. (2) If approximately 100Å of garnet is removed using concentrated hydrofluoric acid the surface mode disappears. (3) Upon rotating the film from the perpendicular to parallel configuration, this surface mode becomes the only spinwave observed at 30 to 40° from perpendicular. (4) No high field surface mode is observed in parallel resonance. (5) When a film is annealed at 1050°C for 30 minutes in an O_2 atmosphere the surface mode disappears. Omaggio and Wigen (1974) continued the above work by examining the surface mode behavior as a function of temperature (from 20-300K) and orientation. At room temperature the spectra were measured at 23 and 34 GHz as a function of orientation. A critical angle was observed at all temperatures and frequencies. At room temperature the perpendicular resonance spectrum was frequency independent; however, a dependence was observed at other angles of the applied field. As the temperature was decreased, the surface mode was seen to go from 106 Oe above the second spinwave mode at 300°K to 423 Oe at 85°K. Below 85°K the trend is reversed.

Stakelon (1975) irradiated a 1.7 μm YIG film with 1.5 MeV He^4 ions; ions of this energy have an estimated range of 2.5 microns through the YIG and its substrate. Therefore, defects were introduced

throughout the thickness of the sample. At room temperature the resonance linewidth increases from 1.0e to 50e after irradiation at 10^{17} ions/cm^2. Further, the resonance field for this sample was changed. At perpendicular resonance it increased and at parallel resonance it decreased; this shift is characteristic of a film with a larger magnetization than the original.

At temperatures less than 100°K photo-induced changes in the spinwave spectrum of annealed YIG thin films have been observed by Stakelon et al (1976). These changes are believed to arise due to the presence of Fe^{2+} at the surfaces of the sample.

The above experimental data show the remarkable variety of spinwave spectra that arise from various preparation techniques and subsequent treatments. Up to the present time, there has been no hypothesis or model for surface conditions that is physically meaningful and plausible which can explain such behavior. It is the conclusion of this thesis that these phenomena can be explained by surface regions with magnetic properties that are different from the bulk.

Chapter 2

The Wave Vectors

A secular equation for the spinwave propagation vectors of the spin system in a uniform magnetic material can be obtained by simultaneously solving Maxwell's equation and the Landau-Lifshitz equation of motion. It is assumed that the sample is a slab of thickness d, infinite in the x and y directions, and that the direction of the mean magnetization, $\bar{M}_o$, is described by the spherical polar angles θ and ϕ. The sum of the static Maxwellian field, $\bar{H}_o$, and the effective static anisotropy field, $\bar{H}_a$, is parallel to $\bar{M}_o$. The field $\bar{H}_o$ is a sum of the applied, $\bar{H}_{app}$, and the static demagnetizing field. The Maxwellian field, $\bar{H}$, and the magnetization, $\bar{M}$, are assumed to be of the form

$$\begin{aligned} \bar{H} &= \bar{H}_o + \bar{h} \\ \bar{M} &= \bar{M}_o + \bar{m} \end{aligned} \tag{2-1}$$

For propagation vectors normal to the film surface,

$$\begin{aligned} \bar{h} &= \bar{h}_o \, e^{i(kz + \omega t)} \\ \bar{m} &= \bar{m}_o \, e^{i(kz + \omega t)} \end{aligned} \tag{2-2}$$

The magnetization, $\bar{M}$, is assumed to change orientation in accordance with the Landau-Lifshitz equation

$$\frac{1}{\gamma}\frac{d\bar{M}}{dt} = -\bar{M} \times [\bar{H}_o + \bar{H}_a + \bar{h}_{ex} + \bar{h}_\lambda + \bar{h} + \bar{h}_a] \tag{2-3}$$

The gyromagnetic ratio γ is taken to be a positive number so that the negative sign is required. The term $\bar{h}_{ex}$ is an effective field due to exchange coupling between the adjacent non-parallel spins:

$$\bar{h}_{ex} = \frac{2A}{M^2} \nabla^2 \bar{m} = -\frac{2Ak^2}{M^2} \bar{m} \quad , \tag{2-4}$$

where A is the exchange constant and k is the wave number of the spin-wave.

The magnetic damping is treated phenomenologically by introducing $\bar{h}_\lambda$, an effective damping field. It is often written in one or the other of two nearly equivalent forms (sometimes called Landau-Lifshitz and Gilbert damping fields, respectively):

$$\bar{h}_\lambda = \frac{\lambda}{\gamma M^2} \bar{M} \times (\bar{H}_o + \bar{H}_a + \bar{h}_{rf} + \bar{h}_{ex} + \bar{h}_a) = \frac{\alpha}{M} \bar{M} \times (\bar{H}_o + \bar{H}_a + \bar{h}_{rf} + \bar{h}_{ex} + \bar{h}_a) \tag{2-5a}$$

or

$$\bar{h}_\lambda = -\frac{\lambda}{(\gamma M)^2} \frac{d\bar{m}}{dt} = \frac{-\alpha}{\gamma M} \frac{d\bar{m}}{dt} \tag{2-5b}$$

The magnitude of the damping is described by the relaxation frequency λ, or by the dimensionless damping constant $\alpha = \frac{\lambda}{\gamma M}$. Provided α is much less than unity (e.g., $\alpha < 0.1$) the difference between these two forms is not significant. It is trivial to show that Eq. (2-3) with (2-5a) is identical to Eq. (2-3) with (2-5b) if γ in the first case is replaced by $\gamma(1 + \alpha^2)$. For the ferromagnetic films treated in this thesis $\alpha < .005$. This represents a change in the gyromagnetic ratio of less than 3 parts in 10^5 ; therefore, no observable difference

occurs. Eq. (2-5b) is easier to manipulate and is used throughout the remainder of this thesis.

The effective static and time varying anisotropy fields, $\bar{H}_a$ and $\bar{h}_a$ respectively are easily calculated by variational techniques from the anisotropy energy, E_a. This energy depends on many things like the crystal make-up, the crystallographic directions of $\bar{M}$, and the stresses or strains. In the calculation of $\bar{H}_a$ and $\bar{h}_a$ spherical polar coordinates can be utilized so that the computations and notation is somewhat simplified. The static effective anisotropy field is given by

$$\bar{H}_a = \bar{a}_\theta H_{a\theta} + \bar{a}_\phi H_{a\phi} \tag{2-6}$$

where

$$H_{a\theta} = -1/M \frac{\partial E_a}{\partial \theta}$$

$$H_{a\phi} = \frac{-1}{M \sin\theta} \frac{\partial E_a}{\partial \phi}$$

The time varying anisotropy field is obtained by taking a small signal expansion of $\bar{H}_a$

$$\bar{h}_a = \frac{m_\theta}{M} \left(\frac{\partial \bar{H}_a}{\partial \theta} \right) + \frac{m_\phi}{M \sin\theta} \left(\frac{\partial \bar{H}_a}{\partial \phi} \right) \tag{2-7}$$

Since the angular derivatives of the spherical unit vectors are

$$\frac{\partial \bar{a}_r}{\partial \theta} = \bar{a}_\theta \ , \quad \frac{\partial \bar{a}_\theta}{\partial \theta} = - \bar{a}_r, \quad \frac{\partial \bar{a}_\phi}{\partial \theta} = 0, \tag{2-8}$$

$$\frac{\partial \bar{a}_r}{\partial \phi} = \bar{a}_\phi \sin\theta, \quad \frac{\partial \bar{a}_\theta}{\partial \theta} = \bar{a}_\phi \cos\theta, \quad \frac{\partial \bar{a}_\phi}{\partial \phi} = -(\bar{a}_r \sin\theta + \bar{a}_\theta \cos\theta)$$

$\bar{h}_a$ in terms of $\bar{m}$ is given by

$$\begin{bmatrix} h_{ar} \\ h_{a\theta} \\ h_{a\phi} \end{bmatrix} = \frac{1}{M} \begin{bmatrix} H_{ar\theta} & H_{ar\phi} \\ H_{a\theta\theta} & H_{a\theta\phi} \\ H_{a\phi\theta} & H_{a\phi\phi} \end{bmatrix} \begin{pmatrix} m_\theta \\ m_\phi \end{pmatrix} \equiv \frac{1}{M} \overline{\overline{H}}_a \cdot \bar{m} \qquad (2\text{-}9)$$

where

$$H_{ar\theta} = -H_{a\theta} \qquad H_{ar\phi} = -H_{a\phi}$$

$$H_{a\theta\theta} = \frac{\partial H_{a\theta}}{\partial \theta} \qquad H_{a\theta\phi} = \frac{1}{\sin\theta}\left(\frac{\partial H_{a\theta}}{\partial \phi} - H_{a\phi}\cos\theta\right) = H_{a\phi\theta}$$

$$H_{a\phi\theta} = \frac{\partial H_{a\phi}}{\partial \theta} \qquad H_{a\phi\phi} = \frac{1}{\sin\theta}\left(\frac{\partial H_{a\phi}}{\partial \phi} + H_{a\theta}\cos\theta\right)$$

When this development is used, the linearized equations of motion of the magnetization contain only $h_{a\theta}$ and $h_{a\phi}$. Therefore, for later convenience the following are defined

$$g_1 = H_{a\theta\theta}/4\pi M$$

$$g_2 = H_{a\phi\phi}/4\pi M \qquad (2\text{-}10)$$

$$g_3 = H_{a\phi\theta}/4\pi M = H_{a\theta\phi}/4\pi M$$

In the absence of microwave excitation, only static fields are present; and Eq. (2-3) reduces to the equilibrium condition

$$0 = -\bar{M}_o x[\bar{H}_o + \bar{H}_a] \qquad (2\text{-}11)$$

Eqs. (2-10) and (2-11) are used throughout the later analysis in this thesis. For the crystal structures and orientations used, they are written out explicitly in Appendix I.

The form of Eq. (2-3) ensures that $\bar{M}$ remains fixed in magnitude. This means that (for small motion) $\bar{m}$ is normal to $\bar{M}_o$ to first order; therefore only two components of $\bar{m}$ are independent. Substituting Eqs. (2-1) and (2-2) into Maxwell's equations

$$\begin{aligned} \nabla \times \bar{E} &= -1/c \frac{\partial}{\partial t} (\bar{H} + 4\pi\bar{M}) \\ \nabla \times \bar{H} &= \frac{4\pi\sigma}{c} \bar{E} + \frac{\epsilon}{c} \frac{\partial \bar{E}}{\partial t} \qquad (2\text{-}12) \\ \nabla \cdot (\bar{H} + 4\pi\bar{M}) &= 0 \\ \nabla \cdot \epsilon\bar{E} &= 0 \end{aligned}$$

gives

$$k^2 h_z \bar{a}_z - k^2 \bar{h}_o = i \frac{4\pi\sigma'\omega}{c^2} (\bar{h}_o + 4\pi\bar{m}_o) \qquad (2\text{-}13)$$

or in component form

$$\begin{aligned} 4\pi m_x + Q\, h_x &= 0 \qquad & 4\pi m_\phi + Q\, h_\phi &= 0 \\ 4\pi m_y + Q\, h_y &= 0 \qquad \text{or} \qquad & 4\pi m_\theta + \frac{Q\, h_\theta}{\cos^2\theta + Q \sin^2\theta} &= 0 \\ 4\pi m_z + h_z &= 0 \end{aligned}$$

$$Q = 1 - \frac{i}{2} \delta^2 k^2$$

$$\delta^2 = \frac{c^2}{2\pi\sigma'\omega}$$

$$\sigma' = \sigma + i\omega\epsilon/4\pi$$

The result of substituting Eq. (2-1) into Eq. (2-3) eliminating $\bar{h}$ by Eq. (2-13), and using the g_i's defined in Eq. (2-10) is

$$\begin{aligned} i\left(\frac{\omega}{\gamma} - i4\pi M\, g_3\right) m_\phi &= \pi_2\, 4\pi M\ m_\theta \\ -i\left(\frac{\omega}{\gamma} + i4\pi M\, g_3\right) m_\theta &= \pi_1\, 4\pi M\ m_\phi \end{aligned} \qquad (2\text{-}14)$$

where

$$4\pi M\, \pi_1 = + \frac{2Ak^2}{M} + \frac{i\omega\alpha}{\gamma} + H_o' + \frac{4\pi M}{Q} \quad -4\pi M\, g_2 \qquad (2\text{-}15)$$

$$4\pi M\, \pi_2 = + \frac{2Ak^2}{M} + \frac{i\omega\alpha}{\gamma} + H_o' + 4\pi M\ \left(\frac{\cos^2\theta + Q\sin^2\theta}{Q}\right) - 4\pi M\, g_1$$

$$\bar{H}_o' = \bar{H}_o + \bar{H}_a$$

This linear homogeneous set of equations for m_θ and m_ϕ has a non-trivial solution only if the determinant of the coefficients is zero. This determinantal condition is in effect an algebraic equation of the 4th degree for k^2, and the roots of the determinant provide the wave vectors for which Eq. (2-2) represents a correct solution to the equation of motion. For each of these values of k^2, Eq. (2-14) may be solved for the respective ellipticities and direction of precession of $\bar{m}$. The expansion of the determinant is

$$K^8 + A_0K^6 + A_1K^4 + A_2K^2 + A_3 = 0 \qquad (2\text{-}16)$$

$$A_0 = -(K_1^2 + K_2^2) + i\ 4\varepsilon^2$$

$$A_1 = K_1^2\, K_2^2 - 4\varepsilon^4 + i2\varepsilon^2\ [1 + \cos^2\theta - 2(K_1^2 + K_2^2)]$$

$$A_2 = i2\varepsilon^2 \left\{ 2K_1^2K_2^2 - K_1^2 - K_2^2 + \frac{[K_2^2|R|^2 + K_1^2]\sin^2\theta}{1 + |R|^2} \right.$$

$$\left. + 2i\varepsilon^2 (1 + \cos^2\theta - K_1^2 - K_2^2) \right\}$$

$$A_3 = 4\varepsilon^4 \left\{ -\cos^2\theta - K_2^2K_1^2 + K_2^2 + K_1^2 - \frac{[K_2^2|R|^2 + K_1^2]\sin^2\theta}{1 + |R|^2} \right\}$$

where

$$K_1^2 = -i\Omega'R - \eta + g_2 - i\alpha\Omega, \quad K_2^2 = i\Omega'/R^* - \eta + g_2 - i\alpha\Omega$$

$$R = \frac{(\sin^2\theta + g_2 - g_1) - \sqrt{4|\Omega'|^2 + (g_1 - g_2 - \sin^2\theta)^2}}{2i\Omega'}$$

$$\varepsilon^2 = A/2\pi M^2\delta^2 \quad , \quad K^2 = \frac{A}{2\pi M^2} k^2 \quad , \quad \eta = H_o'/4\pi M \quad , \quad \Omega = \frac{\omega}{\gamma 4\pi M}$$

$$\Omega' = \Omega + ig_3 \ .$$

Although Eq. (2-16) has appeared in many articles, it has never been published in this simple form. It is easily seen that in the limit of zero magnetization the non-zero roots are simply the propagation vectors found for non-magnetic materials ($k^2 = -2i/\delta^2$). In the limit of no conductivity or displacement effects the non-zero solutions are $K = K_1$ and $K = K_2$. The approximations presented in the next chapter are based upon the assumption that the conductivity and displacement do not significantly affect the roots K_1 and K_2. This is true for materials like YIG where ε^2 is small compared to K_1 and K_2; however, in metal films (e.g., permalloy) this assumption is not valid. The behavior of these solutions has been discussed in

detail by (Liu 1974); the roots K_1 and K_2 are discussed in chapter three of this thesis.

In two particular orientations, $\overline{M}_o$ perpendicular and parallel to the film surface, Eq. (2-16) factors allowing solutions simpler than the most general. In the perpendicular ($\theta = 0$) orientation it factors into two quadratics; at the parallel ($\theta = 90$) orientation it factors into a linear term and a cubic. In the perpendicular orientation the two quadratics are

$$K^4 + K^2 (-K_i^2 + i2\varepsilon^2) + i2\varepsilon^2(-K_i^2 + 1) = 0 \quad (i=1,2) \qquad (2\text{-}17)$$

where i=1 gives roots with positive spin precession and i=2 gives roots with negative spin precession. (Positive spin precession is determined by the vector product $-\overline{m} \times \overline{H}_o'$.) In the parallel orientation, the linear term gives the propagation vector also found for nonmagnetic materials

$$k^2 = -2i/\delta^2 \quad . \qquad (2\text{-}18)$$

It is easily shown that the excitation corresponding to this wave vector does not involve the magnetization; and the associated $\overline{h}$ is linearly polarized along $\overline{M}_o$. The other three roots come from the cubic

$$K^6 + K^4 \left\{ -(K_1^2 + K_2^2) + i2\varepsilon^2 \right\} + K^2 \left\{ K_1^2 K_2^2 + i2\varepsilon^2 (1 - K_1^2 - K_2^2) \right\}$$
$$+ i2\varepsilon^2 \left\{ K_1^2 K_2^2 - \frac{K_1^2 |R|^2 + K_2^2}{1 + |R|^2} \right\} = 0 \qquad (2\text{-}19)$$

In summary, the equations of motion will be satisfied by solutions in the form of Eq. (2-2) not merely for one wave vector but in general for a set of 8 given by Eq. (2-16). A complete solution to the boundary value problem in question, therefore, involves a superposition of waves

$$\bar{h}_n = \bar{h}_{on}\, e^{i(k_n z + \omega t)}$$

$$\bar{m}_n = \bar{m}_{on}\, e^{i(k_n z + \omega t)} \quad , \qquad (2\text{-}20)$$

with eight k_n values. In this form a solution for $\bar{m}$ will be called a spinwave excitation. A plot of the power absorbed by the material versus applied field will be called a spinwave spectrum, and peaks in this spectrum will be referred to as spinwave modes.

In all cases analyzed in this thesis the magnetization is assumed to have a constant direction throughout the sample. Except in parallel and perpendicular resonance, this is an approximation due to the static effects of any proposed boundary condition. The effects of this approximation are assumed small; however, no attempt has been made to analyze the subsequent errors. This assumption is mandatory if the results of this chapter are to be applied to a magnetic film without free surface spins.

Chapter 3

Simplest Approximation

3.1 General Discussion

The simplest approximation for calculating ferromagnetic resonance phenomena comes from neglecting displacement and conductivity ($\varepsilon \to 0$) and taking the magnetic losses into account by making perturbation calculations on the lossless solutions. The calculations give mode positions with sufficient accuracy; however, the mode intensity and linewidth are only accurate for insulators or very thin metal films ($\sim$ 500A) where the r.f. magnetic field is nearly uniform throughout the sample. In fact it can be seen from Eq. (2-13) that the approximation $\sigma = \epsilon = 0$ is equivalent to letting the external drive field penetrate the medium without attenuation or phase shift.

In the limit $\varepsilon = \alpha = 0$ Eq. (2-16) becomes

$$K^4\left(K^4 - (K_1^2 + K_2^2)\, K^2 + K_1^2 K_2^2\right) = 0 \qquad (3\text{-}1a)$$

$$K_1^2 = -i\Omega' R - \eta + g_2 \qquad (3\text{-}1b)$$

$$K_2^2 = i\Omega'/R^* - \eta + g_2 \qquad (3\text{-}1c)$$

Here the $K = 0$ roots correspond to the electromagnetic branches in the limit of infinite skin depth. The other two roots are the positive and negative precession spinwave branches, respectively. Further, K_1^2 and K_2^2 are real numbers; therefore, the wave numbers are either real or imaginary. For most spinwave modes K_1 is a real number; these spinwave modes are commonly called body modes. Spinwave modes

with imaginary K_1 are called surface modes. The K_2 root is usually imaginary. It will be shown that the excitation amplitude associated with K_2 is typically very small near the surfaces and completely negligible elsewhere. The mode shape and amplitude is therefore quite adequately described by the component associated with the wave vector K_1 . Extreme values of the anisotropies can conceivably give real values to K_2 , but such values have not been observed in the laboratory. For the K_1 and K_2 roots the ellipticity and sense of precession of the magnetization are given by

$$\left(\frac{m_\theta}{m_\phi}\right)_1 = R \qquad \left(\frac{m_\theta}{m_\phi}\right)_2 = -1/R^* \qquad (3\text{-}2)$$

Dispersion curves or plots of K_1 and K_2 versus Ω are displayed qualitatively in Fig. (3-1) for perpendicular ($\theta = 0$) and parallel ($\theta = 90°$) resonance. The real and imaginary parts of K are K' and K", respectively. In both cases, the allowed propagation constants for small Ω are imaginary, corresponding to exponentially damped or growing excitations (as a function of z). For $\theta = 0$ or perpendicular resonance, the two branches start at $K" = \sqrt{\eta}$. As Ω increases K" increases for the negative precession branch. The K" for the positive branch decreases with increasing Ω. At $\Omega = \eta$, the propagation changes from imaginary to real and $(K')^2$ increases as $(\Omega-\eta)$. This region with real K, corresponds to a propagating, plane wave type excitation. For parallel resonance ($\theta = 90°$), the behavior is similar except that the two branches are split at $\Omega = 0$, and the conversion from real K to imaginary K occurs at $\Omega = \sqrt{(\eta + 1)\eta}$. As the orientation swings from perpendicular to parallel under constant

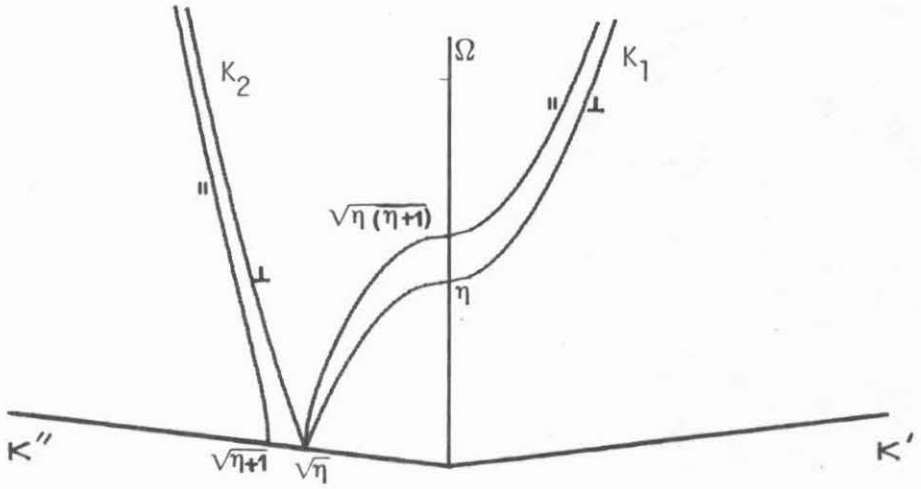

Fig. (3-1) Schematic general spinwave manifold for magnetization orientation variation from parallel to perpendicular at constant internal field, η.

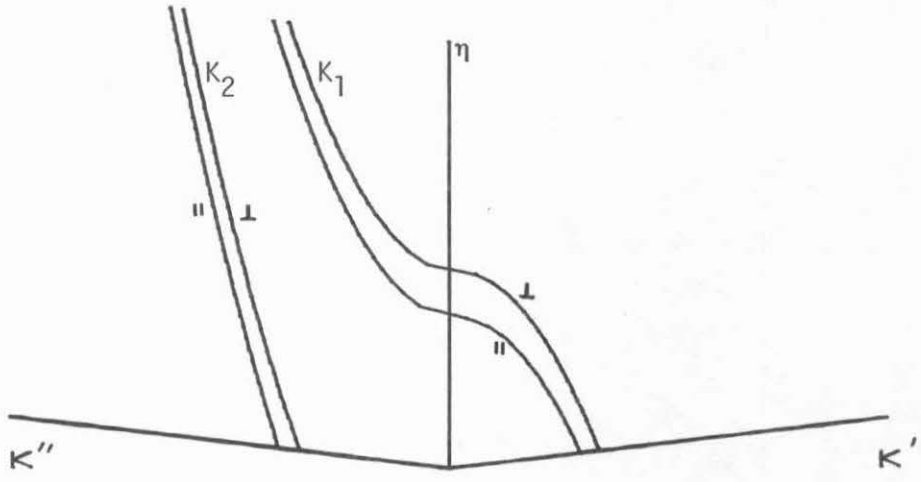

Fig. (3-2) Schematic general spinwave manifold for magnetization orientation variation from parallel to perpendicular at constant frequency, Ω.

internal bias field (η = constant) the dispersion branches sweep out the general spinwave manifold. Since the normal experimental technique is to sweep field, field swept dispersion curves at perpendicular and parallel resonance are displayed in Fig. (3-2).

In a driven lossless mechanical system resonance occurs when the external drive frequency is equal to the frequency of a normal mode. Further with damping the change in the required drive frequency is second order in the damping parameter; therefore, for small damping the change in the drive frequency is negligible. In addition, the linewidth can be linearly related to the damping constant by an approximation which becomes more accurate as the damping approaches zero. For the uniform excitation ($k_1 = 0$) it is shown below that similar considerations apply to the magnetic system. By including the time varying demagnetizing field ($\bar{h} = -4\pi \frac{\bar{k}\cdot\bar{m}}{k^2}\ \bar{k}$) and the linearly polarized drive field, $\bar{h} = h_o e^{i\omega t}\bar{a}_x$, Eq. (2-3) in component form with $k_1 = 0$ is

$$i\left(\frac{\omega}{\gamma} - i4\pi M\, g_3\right) m_\phi = m_\theta \left(\frac{i\omega\alpha}{\gamma} + H_o' + 4\pi M \sin^2\theta - 4\pi M g_1\right)$$

$$-i\left(\frac{\omega}{\gamma} + i4\pi M\, g_3\right) m_\theta = m_\phi \left(\frac{i\omega\alpha}{\gamma} + H_o' - 4\pi M g_2\right) - M h_o$$

The solution for m_ϕ is

$$m_\phi = \frac{(\eta + \sin^2\theta - g_1 + i\alpha\Omega)\, h_o/4\pi}{-\Omega'\Omega'^* + (\eta + \sin^2\theta - g_1)(\eta - g_2) - \Omega^2\alpha^2 + i\Omega\alpha(2\eta + \sin^2\theta - g_2 - g_1)} \tag{3-3}$$

If α is small, resonance occurs near the frequency where the real part of the denominator in Eq. (3-3) vanishes. Therefore, at resonance

$$-\Omega'\Omega'^{*} + (\eta + \sin^2\theta - g_1)(\eta - g_2) - \Omega^2\alpha^2 \simeq 0$$

and

$$m_\phi \approx \frac{-i(\eta + \sin^2\theta - g_1 + i\alpha\Omega)\, h_o/4\pi}{\Omega\alpha(2\eta + \sin^2\theta - g_2 - g_1)} \qquad (3\text{-}4)$$

From Eq. (3-4) one can obtain the following results:

1) $\overline{h}$ and m_ϕ are approximately 90° out of phase.

2) With a change in α the condition for resonance changes by a term which is second order in α.

From Eq. (3-3) the half power field swept linewidth, ΔH, can be determined. For perpendicular and parallel resonance

$$\Delta H \simeq \frac{2\omega\alpha}{\gamma} \qquad (3\text{-}5)$$

if ΔH is small compared to the total internal field. At all other values of θ

$$\Delta\eta \simeq 2\Omega\alpha$$

but

$$\Delta\eta \neq \frac{\Delta H}{4\pi M}$$

because of the fact that the magnetization is not aligned with the applied field.

Although figures (3-1) and (3-2) show a continuum of wave vectors, only certain ones will produce a resonant response or oscillate freely when the spins are perturbed from the equilibrium position. A particular wave vector is resonant if the associated mode shape satisfies the magnetic boundary conditions. The relations for the allowed wave vectors and expressions for the associated mode amplitudes are developed in the following sections.

3.2 Spinwave Mode Amplitude

If the magnetization variation consists of the purely sinusoidal or hyperbolic components that satisfy the magnetic boundary conditions, Eqs. (3-3) and (3-4) no longer apply though the qualitative remarks about resonant frequency and linewidth are still applicable. The amplitude and power absorbed can be obtained by balancing the total drive torque and total dissipation torque. Note that except for k = 0 these torques do not balance locally; however, the exchange interaction is so strong that insignificant changes in spinwave excitation are able to provide the local torque balance without significant change in amplitude.

The power per unit volume expended by the drive field on the magnetic system is $\bar{h}\cdot\partial\bar{m}/\partial t = \bar{h}\cdot\dot{\bar{m}}$; and the power per unit volume absorbed by the system due to the losses is $\alpha\dot{m}^2/\gamma M$. The integrals of these through the sample have to balance; therefore, the average power absorbed per unit area of film is

$$P_{abs} = \int_{-d/2}^{d/2} \frac{\alpha}{\gamma M}\left\langle \dot{m}^2 \right\rangle_t \, dz = \int_{-d/2}^{d/2} \left\langle \bar{h}\cdot\dot{\bar{m}} \right\rangle_t dz$$

where the averaging is with respect to time. Using the facts that $\bar{h}$ is linearly polarized along the x-axis and 90° out of phase with m_ϕ it is easily shown that

$$1 = \frac{ho}{\omega} \frac{\langle m_\phi \rangle}{\left\langle \frac{\alpha}{\gamma M}(1+v^2) m_\phi^2 \right\rangle} \qquad (3\text{-}6a)$$

and

$$P_{abs} = \frac{ho^2 d}{2} \frac{\langle m_\phi \rangle^2}{\left\langle \frac{\alpha}{\gamma M}(1+v^2)\, m_\phi^2 \right\rangle} \qquad (3\text{-}6b)$$

where $v=|m_\theta/m_\phi|$, d is the total film thickness, and the averages are

through the thickness of the film. Note that α , γ , M and v are included within the average since they can be functions of position. In the models considered, v is a function of position for $\overline{M}_0$ at all angles except perpendicular resonance. The parameters α, γ, and M will be considered constant except in the case of a nonuniform film. In this case M, α, and γ of the bulk and surface can all be different.

3.3 Boundary Value Problems

The three boundary conditions that have been most used to explain resonance phenomena are treated here. These are:

(1) uniaxial perpendicular surface anisotropy (Bailey et al 1973)

(2) tensorial anisotropy (Yu et al 1975)

(3) surface layers of different properties than the bulk material (Ramer and Wilts 1976)

The appropriate surface boundary conditions for the two anisotropy models are derived in Appendix I. The approach is to find the wave vectors for which the associated mode shapes satisfy the magnetic boundary conditions. Once the allowed wave vectors have been determined the resonant mode shapes and several other things can be determined. The mode amplitude and power absorbed can be determined from Eq. (3-6). The field position of the absorption peaks can be determined from Eq. (3-1) and the equilibrium conditions on the magnetization (Eq. (2-11)). Typically the calculated spinwave spectrum will have one large power absorption peak and several smaller ones. If there are no surface modes the highest field position mode will have the largest power absorption; the wave vector k_1 for this mode is the smallest of the allowed wave vectors. If there are one or two surface modes (a maximum

of two are allowed), then no specific statement can be made about the relative power absorption of the modes; for example, the surface modes have a higher field position than the body modes and the associated absorption can be larger or smaller than that for the body mode with the highest field position.

3.3.1 Perpendicular Surface Anisotropy

If the perpendicular surface anisotropy energy is assumed to have the form $E_s = -K_s \cos^2\theta$ (as first proposed by Kittel (1958)) the boundary condition on $\overline{M}$ is

$$\frac{dm_\phi}{dn} + \frac{K_s}{A} m_\phi \cos^2\theta = 0 \qquad (3\text{-}7a)$$

$$\frac{dm_\theta}{dn} + \frac{K_s}{A} m_\theta \cos 2\theta = 0 \qquad (3\text{-}7b)$$

Here n is the coordinate along the outward film normal.

For a given frequency and applied field, the spinwave excitation for a film with asymmetric surface boundary conditions is

$$m_\theta = m_{11} \cos k_1 z + m_{12} \sin k_1 z + m_{21} \cos k_2 z + m_{22} \sin k_2 z$$

$$m_\phi = \frac{m_{11}}{R} \cos k_1 z + \frac{m_{12}}{R} \sin k_1 z - R^* m_{21} \cos k_2 z - R^* m_{22} \sin k_2 z \qquad (3\text{-}8)$$

where k_1 and k_2 are given by Eqs. (3-1) and (2-16). Substitution of Eq. (3-8) into Eq. (3-7) gives a linear homogeneous set of equations for $\{m_{ij}\}$ i;j = 1,2; this set has a nontrivial solution only if the determinant of the coefficients is zero. The roots of this determinant give the allowed values of k_1 and k_2. The relations between

k_1 and k_2 and the elements of the 4 x 4 determinantal equation for determining k_1 are given in Appendix II. Schematically

$$\det [a_{ij}] = 0 \qquad (3\text{-}9a)$$

At perpendicular resonance, the symmetry is such that the positive and negative precession spinwave branches uncouple; and Eq. (3-9a) becomes

$$\prod_{i=1}^{2} \{(k_i - K_o \cot \frac{k_i d}{2})(k_i + K_o \tan \frac{k_i d}{2}) + \Delta K^2\} = 0 \qquad (3\text{-}9b)$$

where $K_o = (K_{s1} + K_{s2})/2A$ and $\Delta K = (K_{s1} - K_{s2})/2A$. The (i=1) factor gives the allowed positive precession spinwave wave vectors. If K_{s1} and K_{s2} are large and negative, the (i=2) term can give only two allowed negative precession spinwave wave vectors; however, values of the surface anisotropy of this magnitude are believed unrealistic. Therefore, for values of surface anisotropy normally required to match experimental data the spinwave excitations associated with this model have purely sinusoidal or hyperbolic excitations corresponding to the allowed values of k_1.

For each allowed k_1 and k_2 the required applied field can be calculated from Eq. (3-1) and the equilibrium condition for the static magnetization. Solutions to Eq. (3-9) for a symmetric film at perpendicular and parallel resonance are plotted in Fig. (3-3) and (3-4). For positive K_s at parallel resonance and negative K_s at perpendicular resonance there is always one and sometimes two surface modes (i.e., k_1 is negative); for the other sign of K_s there

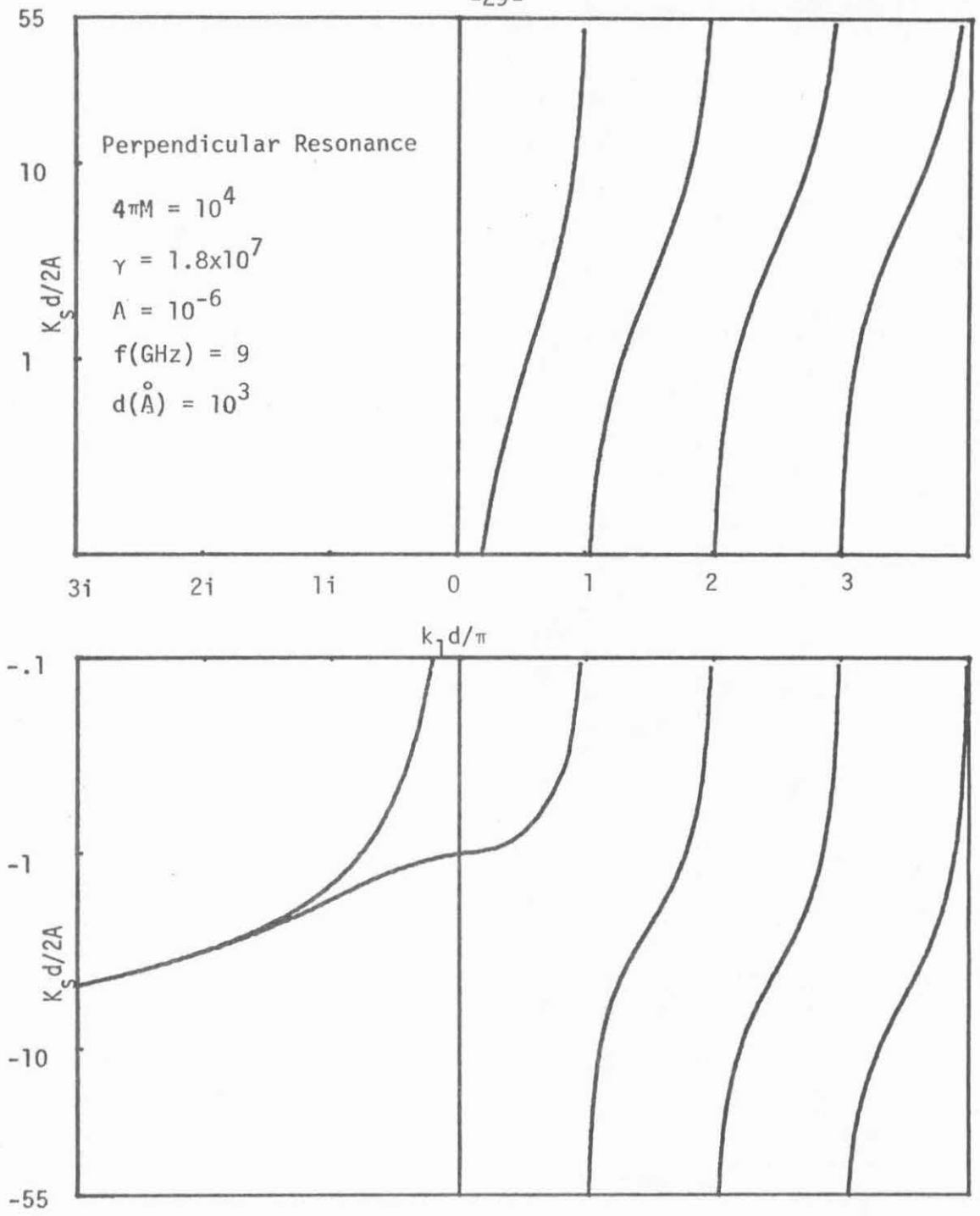

Fig. 3-3 Solutions ($k_1 d/\pi$) to Eq. (3-9) for a symmetric film at perpendicular resonance versus $K_s d/2A$.

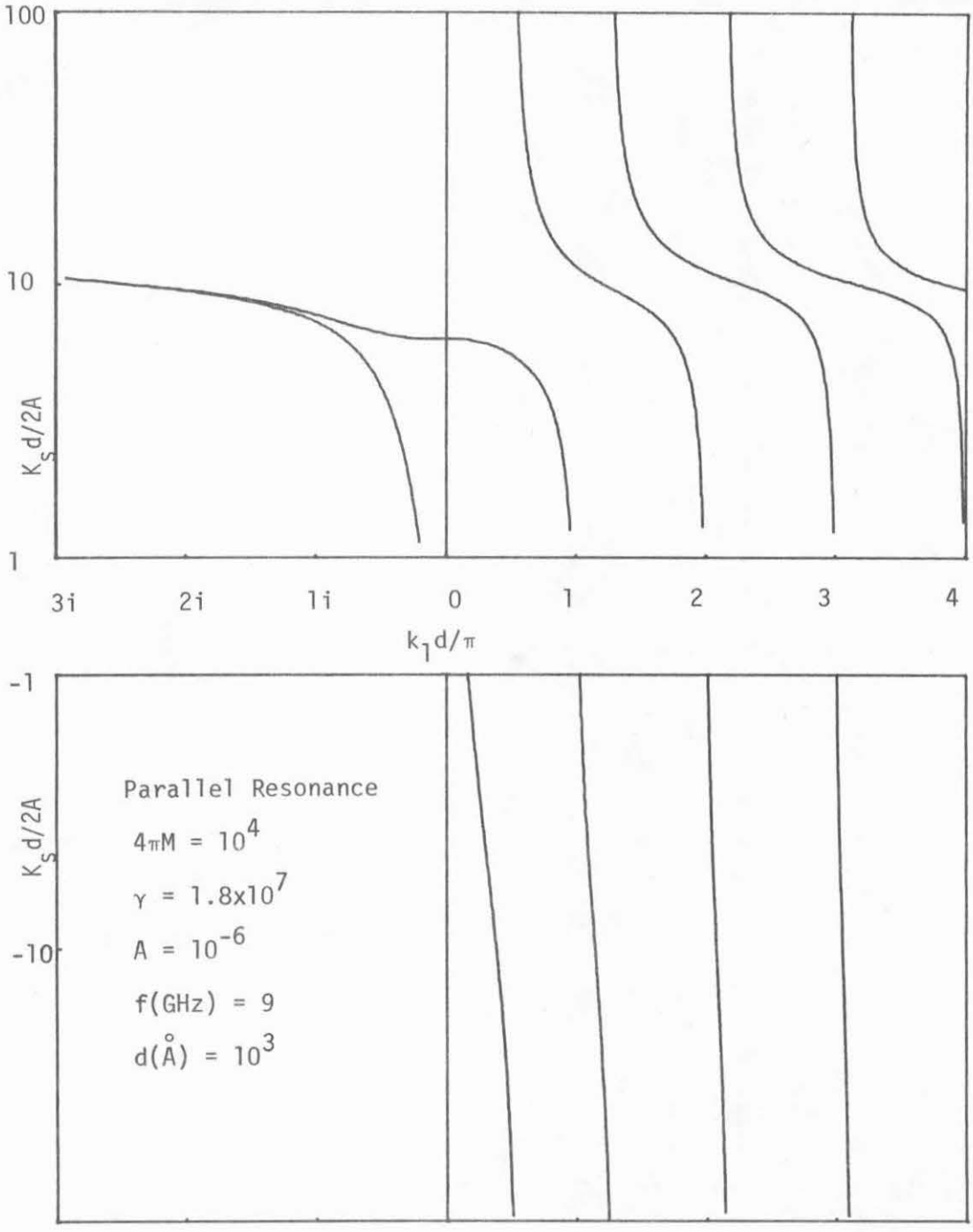

Fig. 3-4 Solutions ($k_1 d/\pi$) to Eq. (3-9) for a symmetric film at parallel resonance versus $K_s d/2A$.

are no surface modes. It can be shown that at perpendicular resonance if there are two surface modes then there is no allowed value of k_1 in the range $(0 < k_1 d/\pi < 1)$; this may not be true at parallel resonance as can be seen in Fig. (3-4).

Ratios of the coefficients in Eq. (3-8) can be determined for each allowed value of k_1 and k_2. A particular coefficient can be assumed unity or related to the applied field through Eq. (3-6a). For a symmetric film at the parallel orientation, plots of m_ϕ normalized to unity at the film center are shown in Fig. (3-5). Note that the k_2 component (i.e., $-R^* m_{21} \cos k_2 z$) is concentrated at the surfaces; this is typically the case since k_2 is usually a large imaginary number.

Since the k_2 components are concentrated at the surfaces and have a small amplitude only a small error is made if these components are neglected when calculating the power absorbed from (Eq. (3-6b). With this approximation $|v|^2 = |R|^2$ and the power absorbed per unit area of film is

$$P_{abs} = \frac{ho^2 \gamma M d}{2\alpha (1+|R|^2)} \left\{ \left(\frac{\cos\psi \sin k_1 d/2}{k_1 d/2} \right)^2 \frac{2}{\left(1 + \frac{\sin k_1 d \cos 2\psi}{k_1 d} \right)} \right\} \qquad (3\text{-}10a)$$

where

$$\psi = \tan^{-1} (m_{12}/m_{11}) \qquad (3\text{-}10b)$$

$$\frac{m_{12}}{m_{11}} = \frac{\begin{vmatrix} a_{11} & a_{31} & a_{41} \\ a_{12} & a_{32} & a_{42} \\ a_{13} & a_{33} & a_{43} \end{vmatrix}}{\begin{vmatrix} a_{21} & a_{31} & a_{41} \\ a_{22} & a_{32} & a_{42} \\ a_{23} & a_{33} & a_{43} \end{vmatrix}} \qquad (3\text{-}10c)$$

and the a_{ij}'s are given in Appendix II. For a symmetric film Eq. (3-9) factors into two parts. One factor gives wave vectors which correspond to mode shapes that are symmetric around the film center (even modes); the other factor gives wave vectors which correspond to antisymmetric mode shapes (odd modes). For the antisymmetric mode shapes $\cos \psi = 0$; therefore, these modes are not excited (i.e., $P_{abs} = 0$). For the symmetric mode shapes $\cos \psi = 1$, and the power absorbed by the symmetric modes normalized by the $k = 0$ absorption is plotted versus $k_1 d/2\pi$ in Fig. (3-6). If a highly localized surface mode exists (i.e., $k_1 d/\pi$ is a large imaginary number) the next even mode has a wave vector in the range $(\frac{1}{2} < \frac{kd}{2\pi} < 1)$(see Fig. (3-3) and (3-4)); therefore, it is possible to have a surface mode (highest field mode) with a power absorption smaller than the first body mode.

Eq. (3-9) has been expanded for the parallel resonance orientation; the result of this expansion is given in Appendix III along with other results for some permalloy films at both the perpendicular and parallel resonance orientations.

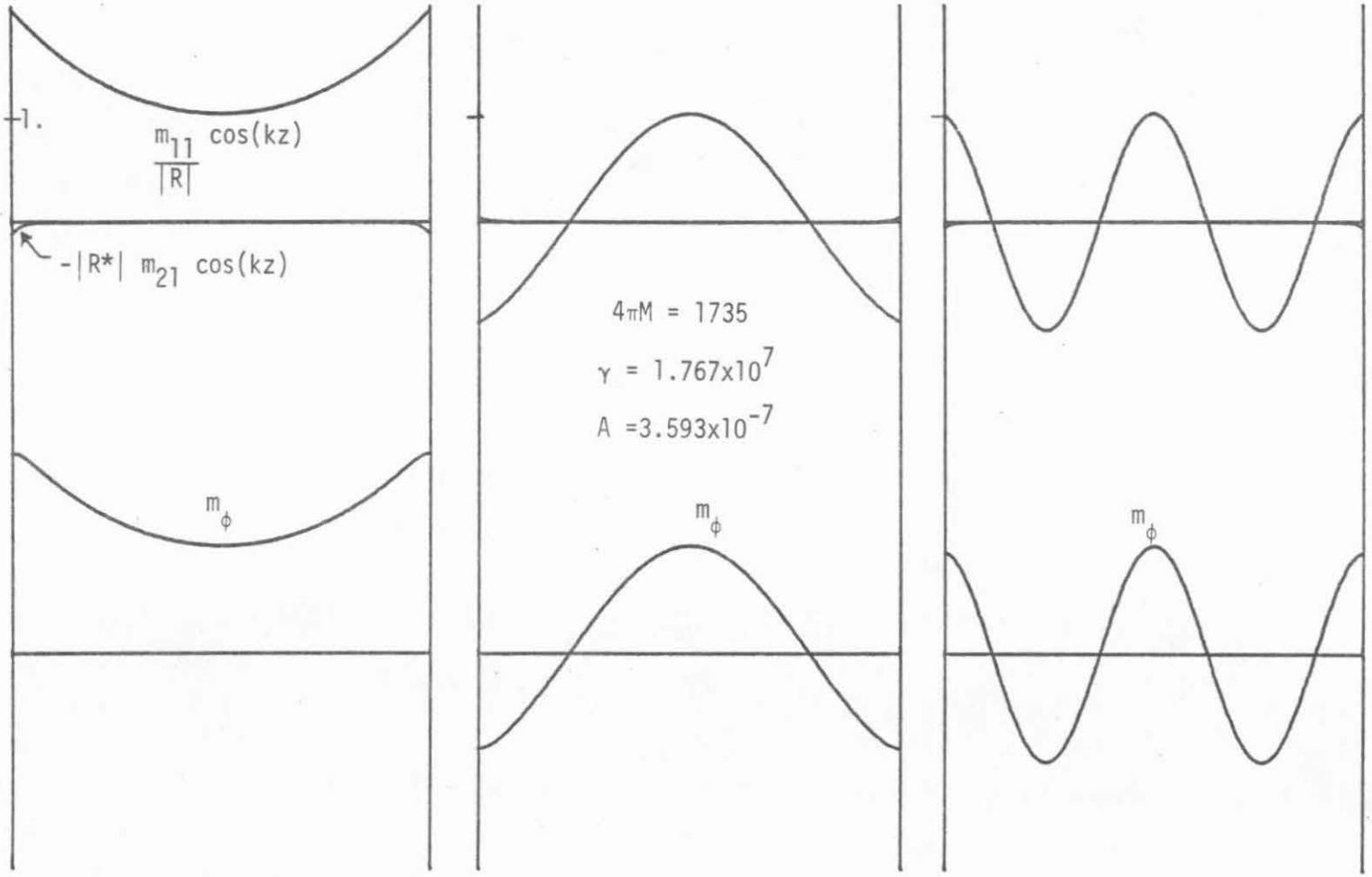

Fig. (3-5) The first three spin wave excitations at parallel resonance for a film with YIG parameters, K_s=.05 ergs/cm^2, and d=.4 microns

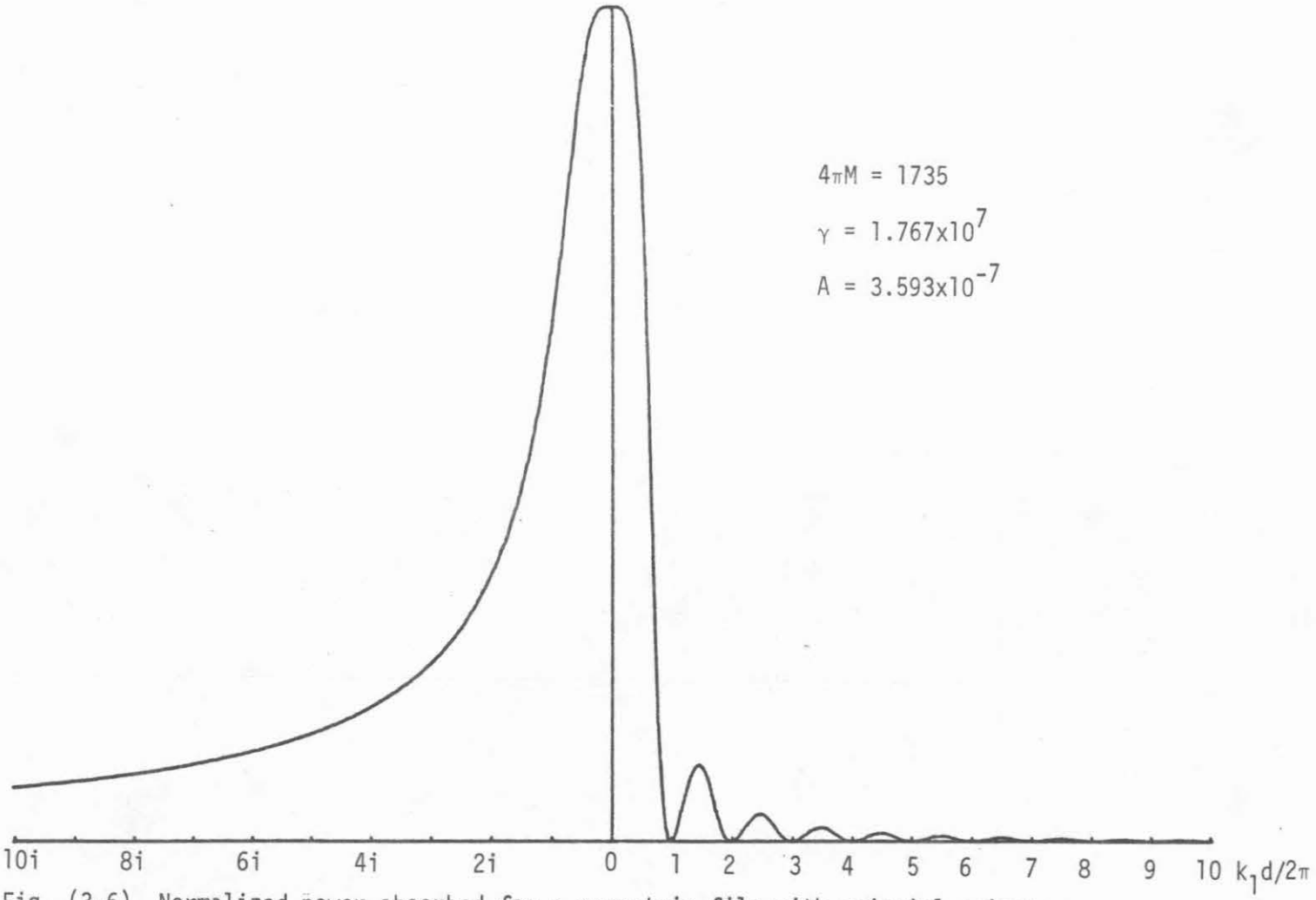

Fig. (3-6) Normalized power absorbed for a symmetric film with uniaxial anisotropy. Material constants are for YIG, d=.846 microns.

3.3.2 Tensorial Anisotropy

The tensorial anisotropy energy proposed by Yu (1975) gives the following boundary condition on $\bar{m}$ (see Appendix I) (n is the coordinate along the outward film normal)

$$A\frac{d\bar{m}}{dn} + (K_{\perp}\cos^2\theta + K_{||}\sin^2\theta)\bar{m} = 0 \qquad (3\text{-}11)$$

or

$$A\frac{d\bar{m}}{dn} + K_T(\theta)\bar{m} = 0$$

For spinwave excitations given by

$$\bar{m} = \sum_{i=1}^{2} \bar{m}_{1i}\cos k_i z + \bar{m}_{2i}\sin k_i z \qquad (3\text{-}12)$$

and asymmetric boundary conditions, the secular equation for k_i is

$$\prod_{i=1}^{2}\{(k_i - K_o\cot\frac{k_i d}{2})(k_i + K_o\tan\frac{k_i d}{2}) + (\Delta K)^2\} = 0 \qquad (3\text{-}13)$$

where d is the film thickness, $K_{T1}(\theta)$ and $K_{T2}(\theta)$ the anisotropies at the two surfaces, $K_o = (K_{T1}(\theta) + K_{T2}(\theta))/2A$, and $\Delta K = (K_{T1}(\theta) - K_{T2}(\theta))/2A$.

Equation (3-13) is identical to Eq. (3-9b) if $K_{T1}(\theta) = K_{s1}$ and $K_{T2}(\theta) = K_{s2}$; therefore, the comments after Eq. (3-9b) applying to uniaxial perpendicular anisotropy at perpendicular resonance apply at all angles here. For a symmetric film and $\bar{m}$ at an angle θ the allowed values of k_1 versus $K_s = K_T(\theta)$ are plotted in Fig. (3-3). Finally, based upon an approximation for the uniaxial anisotropy developed in chapter 4 the tensorial and uniaxial models have similar properties if

$$K_{\perp} = K_s$$

$$K_{||} = \frac{-K_s |R|^2}{1 + |R|^2} \qquad (3\text{-}14)$$

The power absorbed for a film with this boundary condition is given by Eq. (3-10a) where

$$\frac{m_2}{m_1} = \frac{m_{12}}{m_{11}} = \frac{-\Delta K \cos k_1 d/2}{k_1 \cos k_1 d/2 + K_o \sin k_1 d/2}$$

Recall that for a symmetric film and symmetric modes this expression normalized to the $k_1 = 0$ absorption is plotted in Fig. (3-6).

3.3.3 Surface Layer Model

A physically plausible model is that the surface regions of the film have a chemical composition and structure different than the bulk of the film. This can be due to diffusion of elements into the film or chemical reaction. As a first step in understanding the properties of this model, the film may be assumed to have surface layers of uniform magnetic properties which are different from the bulk properties. As required for a clearer understanding, the model can be later extended to one in which variation in properties is represented by adjacent layers with graded properties or by an explicit functional dependence. The greater part of this thesis is restricted to simple layers at each surface. The properties given these layers represent a kind of average of the properties of the actual regions. It will be shown in Chapter 6 that this model can quantitatively or in

some cases only qualitatively match most behavior observed in YIG films. Some of the failures are believed to be due to the variation of the magnetic properties near the surface; that is, the assumption of uniform layers is simply not accurate enough.

A schematic representation of the model is given in Fig. (3-7); the figure is schematic for a YIG film grown on a GGG substrate. The two surface layers are obviously different and the exact properties are unknown; but experimental and theoretical data suggest the properties which should be ascribed to each.

In each of the three uniform regions Eq. (3-1) applies when the appropriate material constants are used. It is assumed that the direction of the static magnetization in the surface region is the same as the static magnetization of the bulk; at all angles of $\bar{m}$ other than parallel and perpendicular to the film plane this is an approximation not only in the surface region but also in the bulk near the interface. Because of the exchange interaction, there is a continuous smooth transition between the angles of equilibrium; the transition region extends from the interface into both the bulk and surface layers. At 9 GHz the maximum variation for a half magnetization surface layer is about 6° for YIG and 20° for Permalloy. With the above assumptions the required boundary conditions at the interface of the magnetic regions are easily derived from torque considerations. They are

$$\frac{\bar{m}_b}{M_b} = \frac{\bar{m}_s}{M_s}$$

$$\frac{A_b}{M_b}\frac{\partial \bar{m}_b}{\partial z} = \frac{A_s}{M_s}\frac{\partial \bar{m}_s}{\partial z} \qquad (3\text{-}15)$$

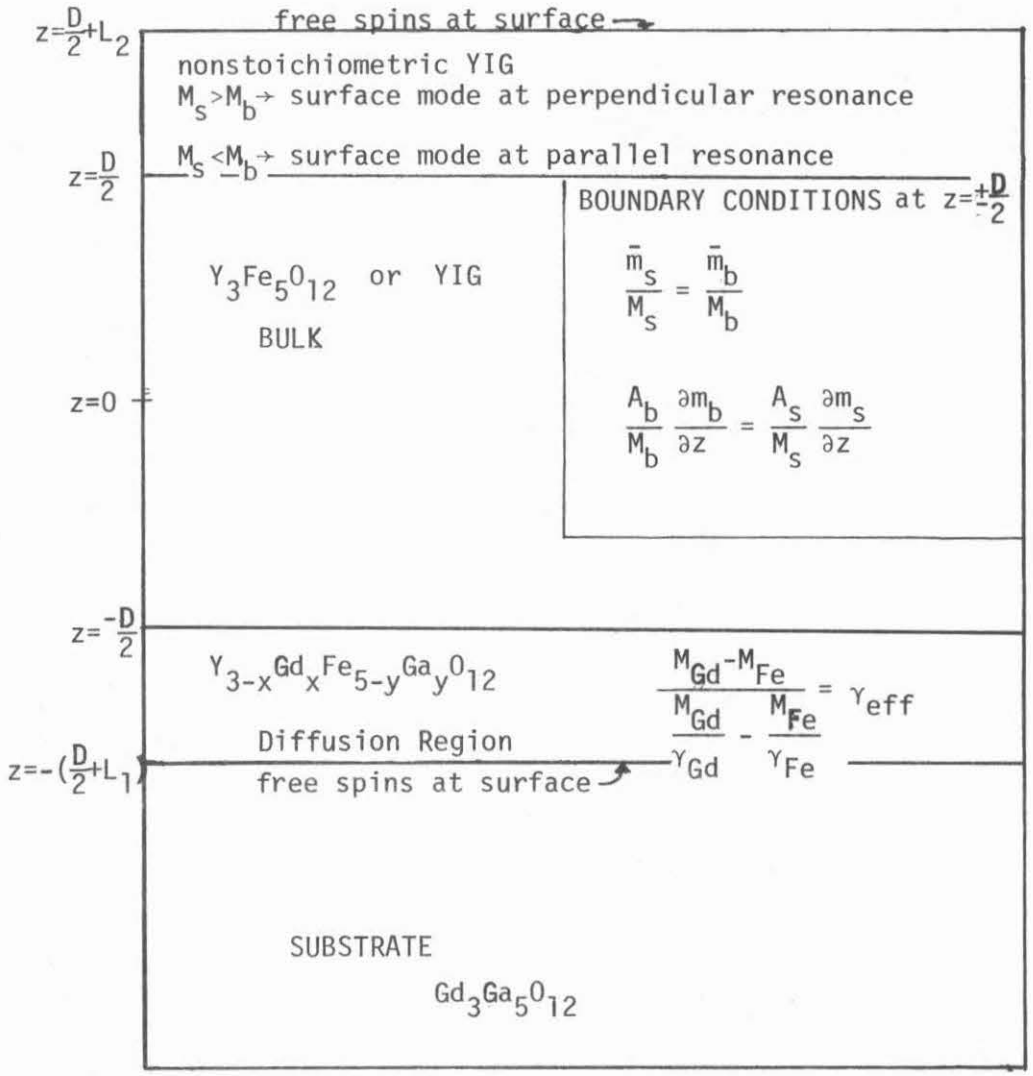

Fig. (3-7) Schematic representation of the surface layer model for YIG. It is assumed that the static magnetization in each region is in the same direction as in the bulk of the film.

where $\bar{m}_b$, $\bar{m}_s$ are the rf magnetization vectors; M_b and M_s are the saturation magnetizations; and A_b, A_s are the exchange constants in the bulk and surface regions, respectively. At all surfaces between magnetic and nonmagnetic materials the spins are taken to be free; this requires that $\frac{\partial \bar{m}}{\partial z} = 0$.

Spinwave excitations for a symmetric film with free spins at $z = \mp(\frac{D}{2} + L)$ are given by

$$
\begin{aligned}
m_{\theta b} &= m_{1b} \cos k_{1b} z + m_{2b} \cos k_{2b} z \\
m_{\phi b} &= \frac{m_{1b}}{R_b} \cos k_{1b} z - R_b^* m_{2b} \cos k_{2b} z \\
m_{\theta s} &= m_{1s} \cos k_{1s} \left(z \pm \tfrac{D}{2} \pm L\right) + m_{2s} \cos k_{2s} \left(z \pm \tfrac{D}{2} \pm L\right) \\
m_{\phi s} &= \frac{m_{1s}}{R_s} \cos k_{1s} \left(z \pm \tfrac{D}{2} \pm L\right) - R_s^* m_{2s} \cos k_{2s} \left(z \pm \tfrac{D}{2} \pm L\right)
\end{aligned}
\tag{3-16}
$$

These spinwave excitations and the boundary conditions in Eq. (3-15) give a 4 x 4 determinant for determing the k-values. The following secular equation is obtained for k_{1b}.

$$
k_{1b} A_b \tan (k_{1b} D/2) = - \left[\frac{T_{1s}[(|R_b|^2+1)(|R_s|^2+1)T_{2s}+|(1+R_b R_s^*)|^2 T_{2b}]+|R_b-R_s|^2 T_{2s} T_{2b}}{|(1+R_b R_s^*)|^2 T_{2s}+(|R_b|^2+1)(|R_s|^2+1)T_{2b}+|R_b-R_s|^2 T_{2s}} \right] \tag{3-17}
$$

where

$$
\begin{aligned}
T_{1s} &= k_{1s} A_s \tan(k_{1s} L) \\
T_{2s} &= k_{2s} A_s \tan(k_{2s} L) \\
T_{2b} &= k_{2b} A_b \tan(k_{2b} D/2)
\end{aligned}
$$

$$K_{1s}^2 = -j\Omega_s' R_s + \Delta(K_{1b}^2 + j\Omega_b' R_b - \cos^2\theta - g_{2b}) + \cos^2\theta + g_{2s}$$

$$K_{2s}^2 = K_{1s}^2 - \sqrt{4|\Omega_s'|^2 + (g_{1s} - g_{2s} - \sin^2\theta)^2}$$

$$K_{2b}^2 = K_{1b}^2 - \sqrt{4|\Omega_b'|^2 + (g_{1b} - g_{2b} - \sin^2\theta)^2}$$

$$\Delta = M_b/M_s$$

This analysis for an asymmetric film gives a secular equation in the form of an 8 x 8 determinant; this determinant is given in Appendix II. Given the frequency, the angle of the static magnetization, and the magnetic properties of the bulk and surface regions, the secular equation can be solved for the spinwave wave vectors that satisfy the boundary conditions. For each allowed wave vector the required applied field $\overline{H}_a$ can be determined from Eq. 3-1 and the equilibrium conditions for the static magnetization in the bulk region (Appendix I). (Note that (Eq. 3-17) can be applied to a film having only one surface layer by replacing D/2 by D. The other surface would naturally have free spins.)

For YIG material constants and $\theta = 0°$, $30°$, $60°$ and $90°$ the two sides of Eq. (3-17) are plotted versus $k_1 D/2\pi$ in Fig. (3-8). Note that in the range $\theta = \pi/3$ to $\pi/2$ there is a root giving a surface mode (i.e., k_1 is imaginary). The angle where $k_1 = 0$ satisfies Eq. (3-17) has been called the critical angle; a more in depth discussion of the critical angle will be given later.

Since garnets have widely varying losses depending on their composition and preparation, it is plausible that the damping parameter, α,

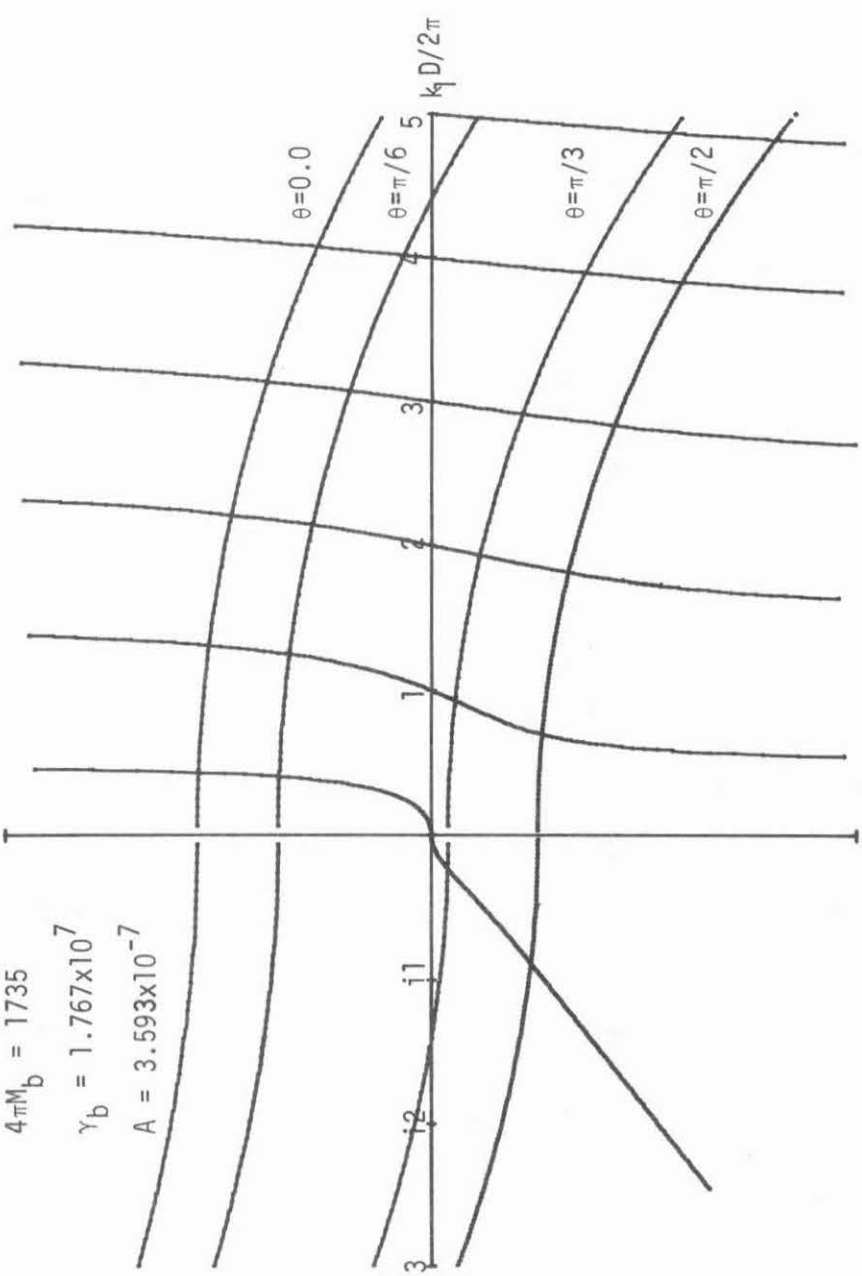

Fig. (3-8) Plot of the right and left hand sides of Eq. (3-17) versus $k_1 D/2\pi$. The material constants are for YIG with a 200Å half magnetization surface layer. The bulk thickness is .42 microns.

could be different in bulk and surface layers. The effects of this on the relative intensity of the modes can be calculated as follows. Using Eq. (3-5) and ignoring the contribution of the k_2 components the power absorbed is

$$P_{abs} = \frac{h_o^2 \left\{ \frac{\sin k_{1b} D/2}{k_{1b}/2} + 2C \frac{\sin k_{1s} L}{k_{1s}} \right\}^2}{\left\{ (1+|R_b^2|) \frac{\alpha_b}{\gamma_b M_b} \left(D + \frac{\sin(2k_{1b}D/2)}{k_{1b}} - \right) + \frac{C^2 \alpha_s}{\gamma_s M_s} (1+|R_s^2|)(2L + \frac{\sin(2k_{1s}L)}{k_{1s}}) \right\}} \qquad (3\text{-}18)$$

$$C = \frac{M_s \cos(k_{1b}D/2)}{M_b \cos(k_{1s}L)} \frac{(T_{2s}(R_b R_b^* - 1) + T_{2b}(1 + R_b R_s^*) - (R_b R_b^* + R_s^* R_b) T_{1b})}{(T_{2s}(R_b R_s^* - 1) + T_{2b}(1 + R_s R_s^*) - (R_b^* R_s + R_s^* R_s) T_{1b})}$$

This expression normalized for $k = 0$ and $\alpha_b/\alpha_s = 1$ has been plotted in Fig. (3-9) for $\alpha_b/\alpha_s = 1$, .3, and .1. The increase in absorption at $kD/2\pi = 7$ or 8 is due to the surface layer going through its uniform resonance (i.e., $k_{1s} \approx 0$). Note that the increased surface α has more effect on the surface mode intensity than on the body modes (except where $k_{1s} \approx 0$).

By making approximations in equation (3-17) one can deduce some of the physics of the surface layer model. By assuming that $R_b \approx R_s$ and that $k_{1s}L$ is sufficiently small to approximate $\tan(k_{1s}L)$, Eq. (3-17) becomes

$$A_b k_{1b} \tan k_{1b} D/2 = -A_s k_{1s}^2 L$$

This equation is in the form of the secular equation for a symmetric film with an anisotropy energy, K_m, and easy direction along M_o. In this case

$$K_m = -A_s k_{1s}^2 L \qquad (3\text{-}19)$$

Fig. (3-9) Normalized power absorbed versus $k_1 D/2\pi$ for YIG material constants and a half magnetization surface layer 470Å. Thickness of bulk film is .423 microns. ($\gamma_b = \gamma_s$)

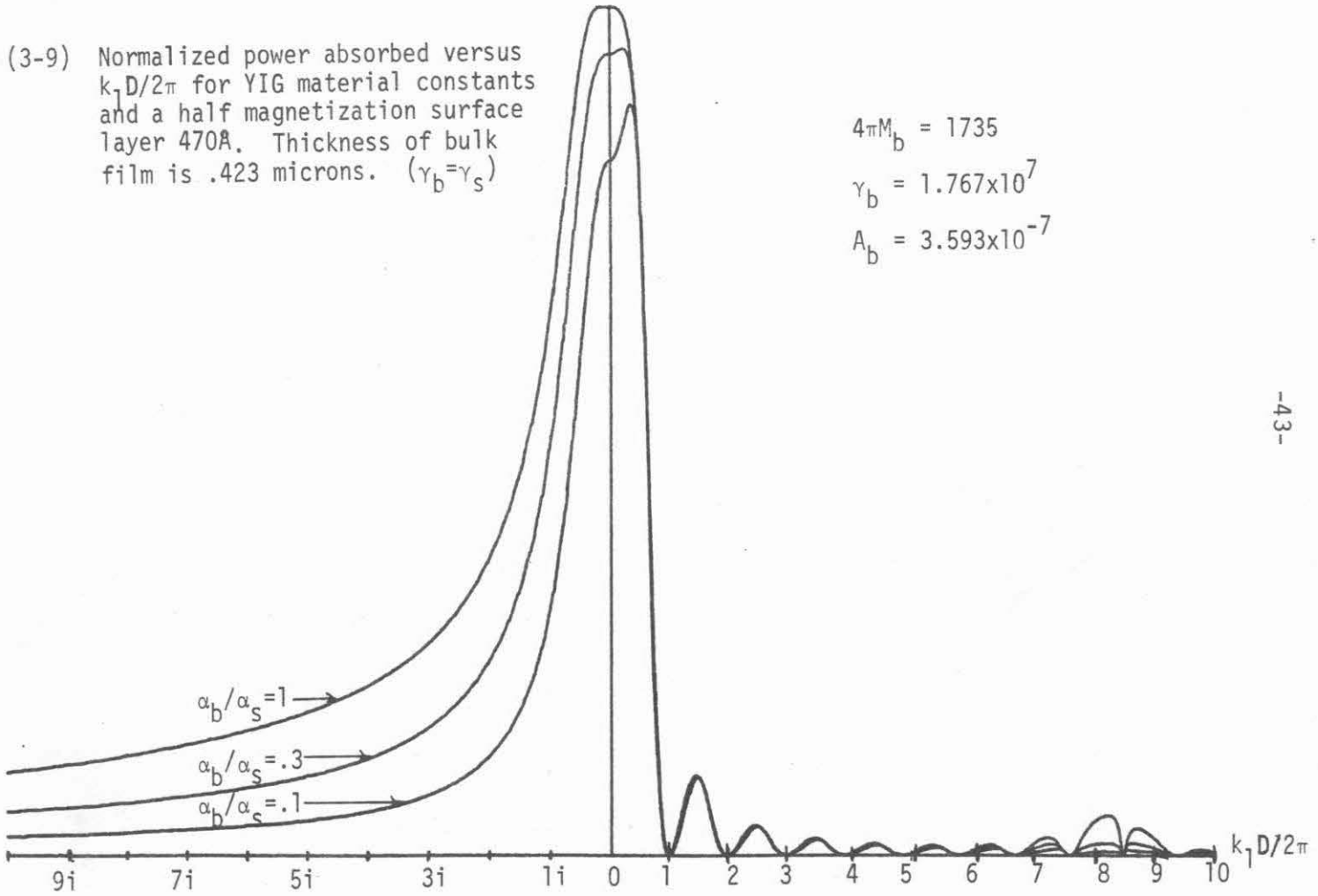

An anisotropy field can be defined

$$H_m = \frac{2K_m}{M_s L} = -\frac{2A_s}{M_s} k_{1s}^2 \qquad (3\text{-}20)$$

This is approximately the exchange field necessary to satisfy the resonance condition in the surface region. If H_m is positive the highest field mode will have a sinusoidal excitation in the bulk and an exponential excitation in the surface region. If H_m is negative the highest field mode will have an exponential excitation in the bulk (surface mode) and a sinusoidal excitation in the surface region. Fig. (3-10) shows several spinwave mode shapes at perpendicular resonance. The angle at which $H_m = 0$ is approximately the critical angle (see next section), and corresponds to the angle at which both regions resonate with a "uniform excitation".

Finally the following interesting correspondence between the surface layer ($\gamma_b = \gamma_s$) and the perpendicular uniaxial anisotropy is worthy of note. It was shown by Bajorek and Wilts (1971) that for thin surface layers on permalloy at perpendicular resonance these two models have mode positions which are in very close agreement no matter how thin the central bulk layer if the uniaxial model has the following properties. First the film is uniform with bulk properties and the same magnetization as the layered film. Secondly, the value of K_s is given by Eq. (3-19) evaluated at perpendicular resonance with $k_{1b}=0$. At parallel resonance Wilts and Ramer showed that the same close agreement existed (unpublished). For YIG material constants ($\gamma_b = \gamma_s$) Fig. (3-11) is a comparison of the two models at all angles of the applied field. It will be pointed out in Chapter 6 that the agreement is not as remarkable for thicker surface layers on YIG or when $\gamma_b \neq \gamma_s$.

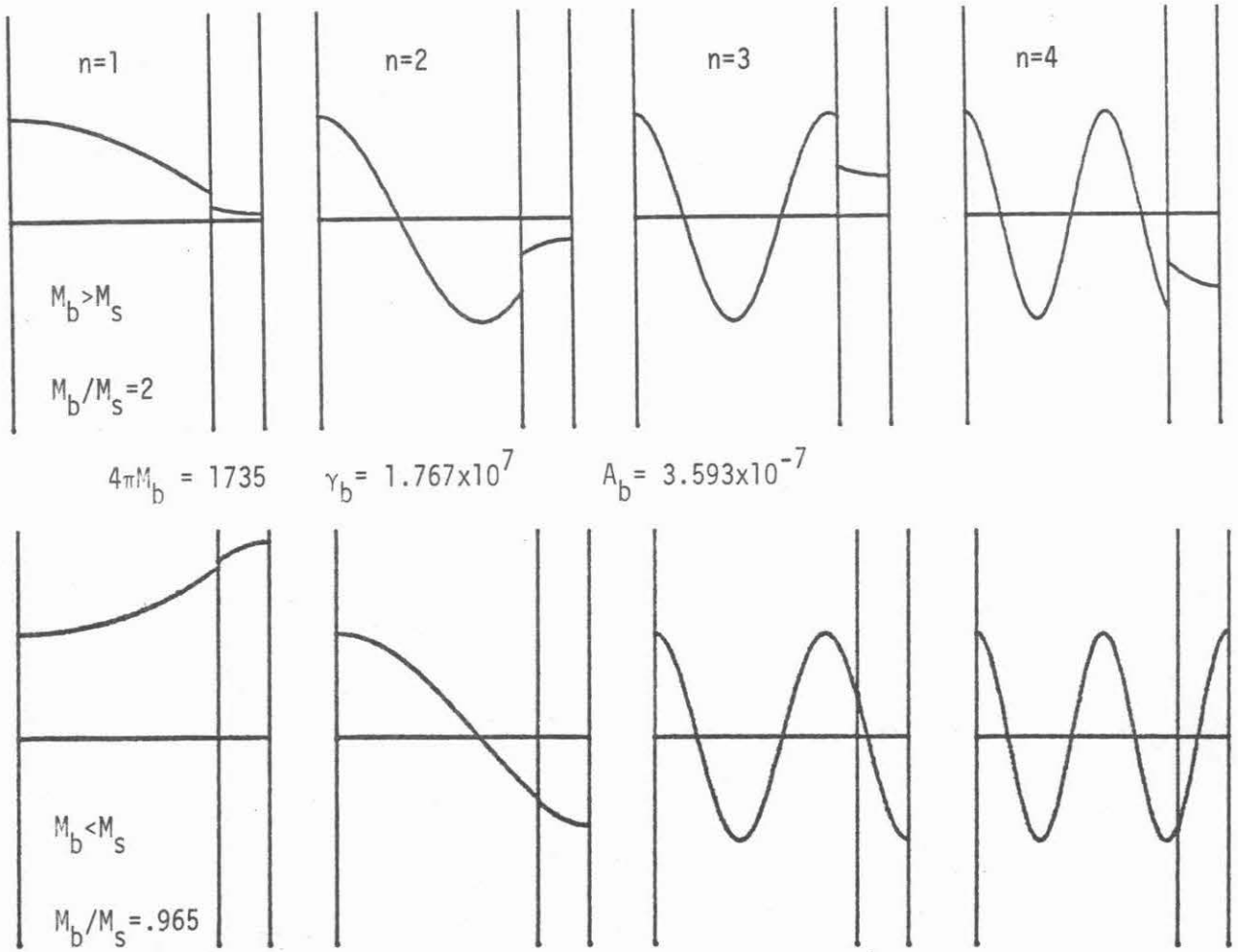

Fig. (3-10) Perpendicular resonance mode shapes for the surface layer model and one free surface. The modes are numbered with the highest field mode n=1. The parameters were for YIG, D=3700Å and L=470Å.

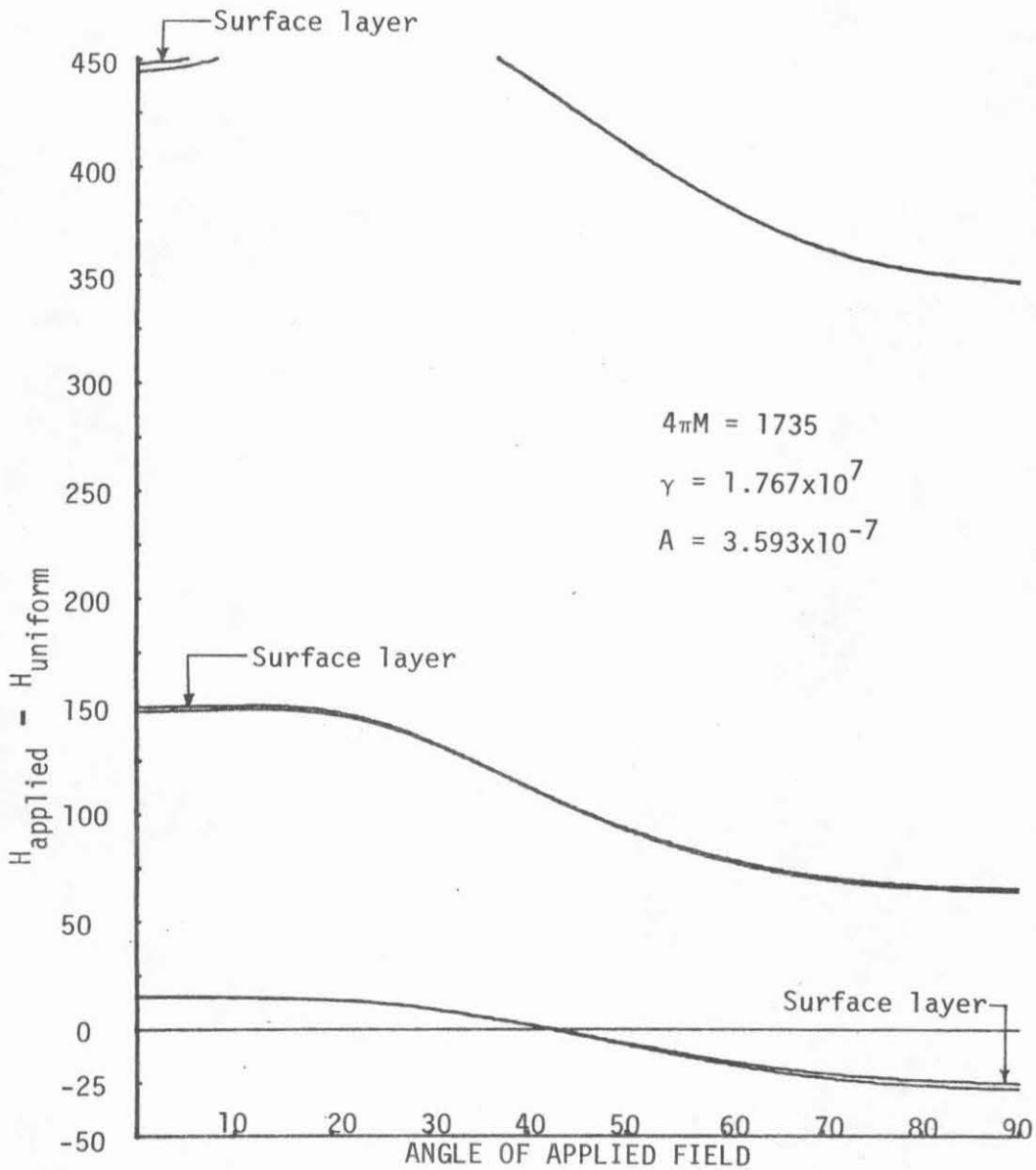

Fig. (3-11) Comparison of the surface layer model and the uniaxial model using a value of K_s deduced for very thin surface layers. The surface is a half magnetization 200A layer, D=4550A . For the surface anisotropy d=4650A and K_s=.061 ergs/cm^2.

3.4 Critical Phenomena

The typical spinwave spectrum has one large power absorption peak and several smaller ones; the mode with the largest absorption usually has the highest field position. However, in some films one and sometimes two modes have a higher field position than the mode with the largest absorption; these modes are called surface modes, and it will be shown that they have properties similar to the surface modes introduced mathematically in the previous sections. It has been observed that if the surface modes exist at one of the limiting orientations (i.e., applied field parallel or perpendicular to the film plane) they do not exist at the other. When films with surface modes are rotated with respect to the applied field from the one limiting orientation, the highest field mode increases in absorption intensity while the largest absorption peak decreases in intensity. This behavior continues until the highest field mode is observed to have the largest absorption and some of the modes that were prominent actually vanish. In some films all modes (except the highest field mode) vanish at about the same angle. In other films there are two angles where some of the modes are observed to vanish, but a particular mode does not vanish at more than one angle. Beyond the angle where a particular mode has disappeared it reappears and grows in intensity; but the highest field mode remains the largest. Even in films where the highest field mode at both limiting orientations is dominant there are angles where some of the lower field modes vanish.

In films with symmetric surface conditions or films where the air film interface has been treated to ensure that the spins at this

surface are free ($\frac{dm}{dn} = 0$), all modes except the highest field mode vanish at or very near one angle of the applied field. Since all modes do not vanish at exactly the same angle, this critical phenomenon is characterized by that angle at which the second spinwave mode vanishes, hereafter called the critical angle β_c. The temperature dependence of this critical angle is believed important in determining the particular mechanism producing the surface pinning.

In terms of the surface models the observed small amplitude high field modes are the surface modes introduced in the previous sections. For the tensorial model and a symmetric film, there is one allowed surface mode for $0>K_T(\theta)d/A>-2$ and two allowed surface modes for $K_T(\theta)d/A<-2$; the second mode, however, is antisymmetric and is not excited (i.e., cos ψ in Eq. (3-10) is zero). Further, no other antisymmetric mode is excited.

For the tensorial model and an asymmetric film, corresponding values of $K_T(\theta)$ at the two surfaces ($K_{T1}(\theta)$ and $K_{T2}(\theta)$) required for 0, 1, and 2 surface modes are plotted in Fig. (3-12). The boundaries between the regions were determined from the condition for a uniform precession mode. This condition (easily obtained from Eq. (3-13) by setting $k_1 = 0$) is given by

$$x_1 + \frac{x_2}{1 + x_2} = 0 \qquad (3\text{-}21)$$

where

$$x_i = K_{Ti}(\theta)d/A.$$

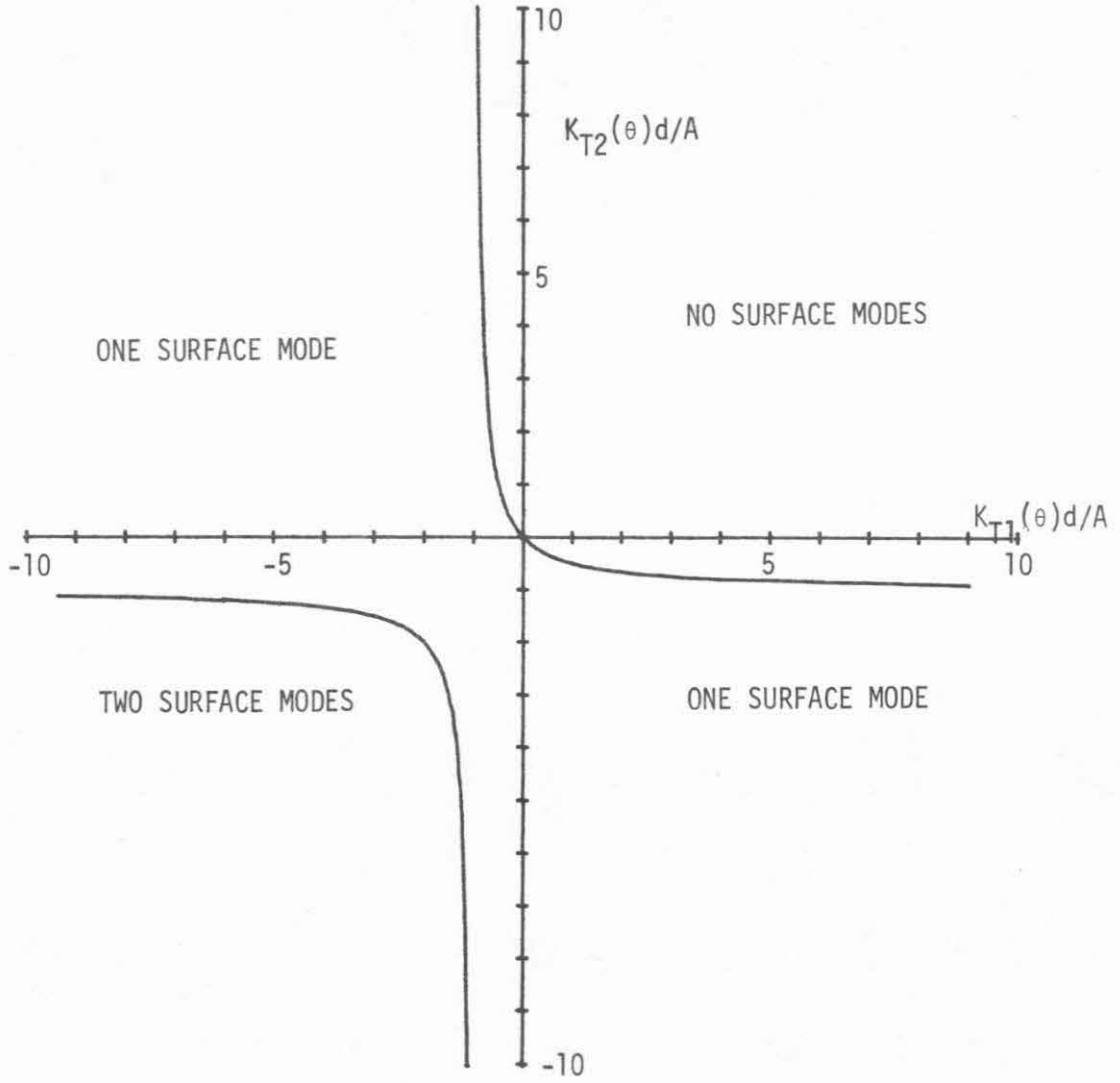

Fig. (3-12) Values of $K_T(\theta)$ at the two surfaces required for 0, 1, and 2 surface modes.

In the region for 2 surface modes and when $K_{T1} \neq K_{T2}$, the second surface mode is excited (i.e., $\cos \psi \neq 0$); this mode is called a quasi-antisymmetric surface mode. The first or high field surface mode is called a quasi-symmetric surface mode. It is easy to see from Fig. (3-6) and Eq. (3-10) how these two surface modes could have a smaller absorption than the third mode; mathematically this is due to their hyperbolic decay away from the film surface versus the sinusoidal behavior of the third spinwave (first body) mode.

If $K_{T1}(\theta/2)$ and $K_{T2}(\theta/2)$ have values which will give the spinwave spectrum two surface modes and $K_{T1}(0)$ and $K_{T2}(0)$ are both positive then as the magnetization is rotated from the parallel to perpendicular resonance orientation, the surface modes become the two highest field body modes. Further, three conditions can exist which will cause mode to vanish as observed experimentally,

$$K_{T1}(\theta) = -K_{T2}(\theta)$$

$$K_{T1}(\theta) = K_{T2}(\theta)$$

or

$$K_{T1}(\theta) = K_{T2}(\theta) = 0 \ .$$

For the condition $K_{T1}(\theta) = -K_{T2}(\theta)$ the allowed wave vectors are

$$k_1 = n\pi/d \qquad n = 1,2,3,4,\cdots \tag{3-22}$$

From Eq. (3-10) the power absorbed for n even is zero and the power absorbed for n odd is not zero unless $K_{T1}(\theta) = K_{T2}(\theta) = 0$. The modes corresponding to n odd and even are called quasi-antisymmetric and quasi-symmetric, respectively. The mode corresponding to n = 0 (the quasi-symmetric uniform precession mode) only occurs under this condition if

$K_{T1} = K_{T2} = 0$; under this condition all modes except the uniform precession mode vanish. It was pointed out that for a symmetric film the antisymmetric modes are not excited; therefore, under the condition $K_{T1}(\theta) = K_{T2}(\theta)$ quasi-antisymmetric modes become antisymmetric modes and vanish.

In the above description of the mathematical behavior of the tensorial model the variable θ is the angle of the magnetization. In the experimental situation the film is held fixed with respect to the angle, β, of the applied field; however, the direction of the magnetization varies only slightly as the magnitude of the applied field is swept over the range of interest. The surface layer and perpendicular uniaxial anisotropy models are mathematically more complex. It can be shown that they too have a mathematical behavior which can explain the above experimental behavior; in fact, this is shown roughly by the following argument. The surface layer has properties similar to the uniaxial anisotropy model (see the previous section); the uniaxial anisotropy has properties similar to the tensorial model if $K_{\perp}$ and $K_{||}$ are given by Eq. (3-14). Since the tensorial model can represent the above experimental data the others will also.

The critical angle, β_c, was defined as the angle where the second spinwave mode in a symmetric film vanishes. This angle can be estimated for the various models by solving simultaneously Eq. (3-1), the magnetization equilibrium conditions and the applicable equation for the propagation constant $k_1 = 2\pi/D$ (e.g., Eq. (3-17) for the surface layer). This is only approximate for the uniaxial

and surface layer models; the absorption amplitude is not zero because of the surface layer and the negative precession components of the mode in the bulk contribute to the excitation.

The angle of the magnetization, θ_c, when $\beta = \beta_c$, $k_1 = 2\pi/D$ discussed for the three models below. For the uniaxial perpendicular anisotropy, θ_c is plotted versus K_s in Fig. (3-13). The range of values that is reasonable for analyzing experimental data for YIG films is $(-.3 < K_s < .3)$. At the lower limit there is a highly localized surface mode at perpendicular resonance; at the upper limit there is a highly localized surface mode at parallel resonance. Within this region of K_s, θ_c only varies a few degrees. This behavior does not match the observed experimental data. For the tensorial model θ_c is given by

$$\theta_c = \tan^{-1}(-K_\perp/K_{11}) \qquad (3\text{-}23)$$

Therefore, any variation of θ_c can be matched by the appropriate choice of $K_\perp$ and K_{11}, although this would not be physically meaningful unless some understanding of the origins of $K_\perp$ and K_{11} were established. Finally for the surface layer model, the critical angle variation depends on the assumed properties of the layers; the physics required to match the observed variation is discussed in greater detail in later chapters.

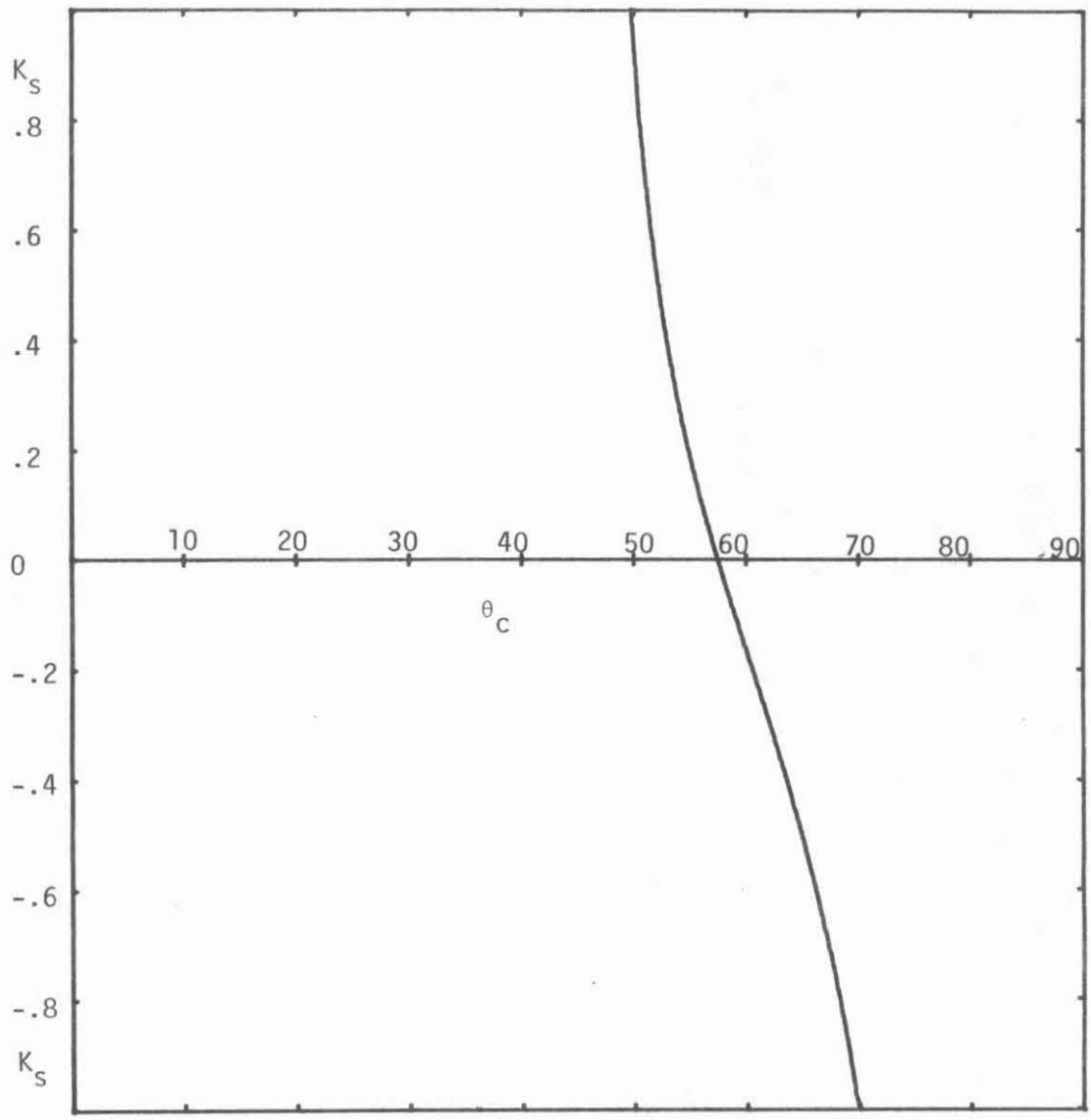

Fig. (3-13) The calculated variation of θ_c with K_s in the perpendicular uniaxial anisotropy model.

Chapter 4

Absorption Calculations

4.1 Introduction

In this chapter, the techniques used in calculating the power absorbed by ferromagnetic films are presented. The theory as developed in Chapter 2 and this chapter has been discussed by many authors; in particular the magnetics group from Yale University has been very active in this area (at the head of this group is Dr. Barker). The material in this chapter has been repeated because of simplification, additions, and for completeness. The simplifications are apparent only if one is familiar with the previous work; therefore, they are not discussed. The additions are the approximations to the boundary conditions discussed in the final section; these approximations are useful because the computer computations are simplified. The calculated power absorption data presented for an asymmetric film with surface layers were obtained using this method; this method is believed to accurately represent the resonance process.

In the typical resonance experimental situation the magnetic film is placed in a cavity or strip line at a position of no tangential electric field and a large tangential magnetic field. Since power is absorbed by the magnetic sample, a small tangential electric field is required at the surface; therefore, the fields inside the sample chamber are perturbed in order to meet this demand. The large tangential magnetic field, however, is little changed by this perturbation. Two methods for calculating the power absorbed by the

film have been used. Both of these methods have field configurations around the sample which approximate the experimental situation described above. These field configurations are briefly described below. In any case, it is implicitly assumed that the perturbation in field structure is negligibly small and that the differences in the calculated power absorption are less than experimental error or resolution.

In the first method, the magnetic field is provided by incident and anti-incident plane waves. (Due to the film structure and the possibility of a transmitted wave, it is not proper to use the term reflected wave.) The incident plane waves of amplitude $h_o/2$ are in phase, linearly polarized with magnetic field along $\bar{a}_x$, the perpendicular to the film plane projection of the magnetization. The solution requires that the anti-incident plane waves be slightly elliptically polarized with a small component of the magnetic field perpendicular to the incident plane wave; this anti-incident wave is out of phase with the incident wave and its magnitude is such that the amplitude of the total field along $\bar{a}_x$ is slightly different than h_o. In the second method the incident and anti-incident plane waves are nearly equal in magnitude and are oppositely elliptically polarized such that the magnetic fields at the film surfaces are in phase, exactly linearly polarized along $\bar{a}_x$ with amplitude h_o. In both methods the resultant electric fields can have both $\bar{a}_x$ and $\bar{a}_y$ components of arbitrary (small) amplitude and phase as demanded by the magnetic medium.

4.2 Power Absorption

The general situation shown in Fig. (4-1) is described as follows: From the space surrounding the magnetic film there are waves incident upon both surfaces of the film ($\bar{h}_i^+$, $\bar{h}_i^-$); propagating into the surrounding space away from the magnetic film are anti-incident waves ($\bar{h}_a^+$, $\bar{h}_a^-$). Inside the magnetic film the magnetic field is given by a superposition of eight terms like Eq. (2-2);

$$\bar{h}(z) = \sum_{n=1}^{8} \bar{h}_n \, e^{i(k_n z + \omega t)} \tag{4-1}$$

From the second of Maxwell's Equations (Eq. (2-12)) the electric field inside is given by

$$\bar{e}(z) = \frac{ic}{4\pi\sigma'} \, \bar{a}_z \times \sum_{n=1}^{8} \bar{h}_n k_n \, e^{i(k_n z + \omega t)} \tag{4-2}$$

where σ' is given in Eq. (2-13). The time varying magnetization is related to the magnetic field $\bar{h}(z)$ by Eq. (2-13). The ratio, $h_{yn}/h_{xn} = \nu_n$, can be obtained from the equation of motion of the magnetization (Eq. (2-14)) and Eq. (2-13);

$$\nu_n = -\frac{i\pi_1}{\Omega'} \cos\theta \quad . \tag{4-3}$$

At z = d/2 the continuity of tangential electric and magnetic fields requires that

$$\bar{h}_i^+ + \bar{h}_a^+ = h_x^{+-}\bar{a}_x + h_y^{+-}\bar{a}_y \tag{4-4a}$$

$$\bar{e}_i^+ + \bar{e}_a^+ = e_x^{+-}\bar{a}_x + e_y^{+-}\bar{a}_y \tag{4-4b}$$

where h_x^+, h_y^+, e_x^+, and e_y^+ are the components of $\bar{h}(z)$ (Eq.(4-1)) and $\bar{e}(z)$ (Eq. (4-2)) at z = d/2.

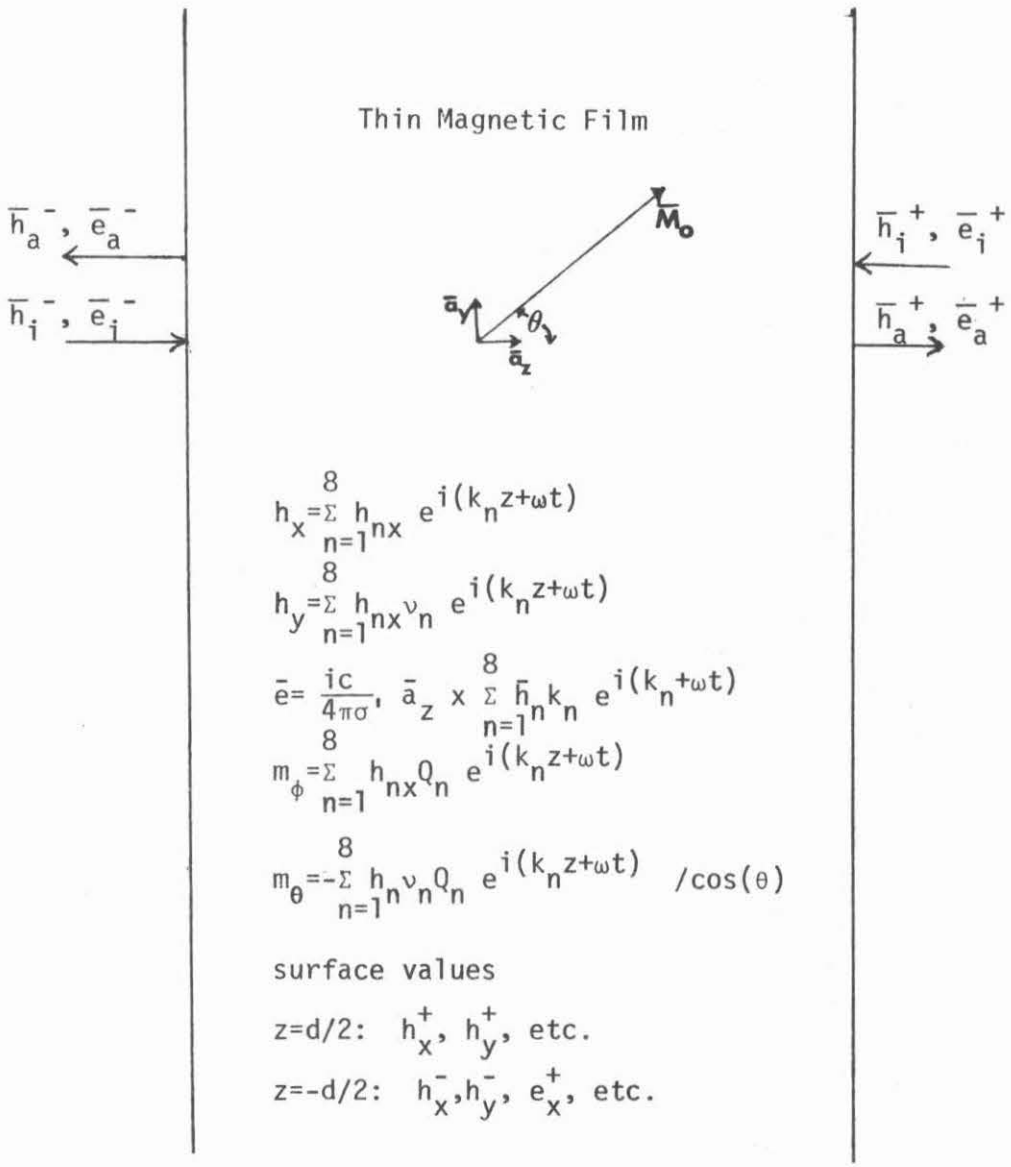

Fig. (4-1) Schematic representation of the magnetic film and mathematical fields.

By using simple relations between electric and magnetic plane waves in free space Eq. (4-4) can be written in component form as

$$h_{ix}^{+} + h_{ax}^{+} = h_{x}^{+} \tag{4-5a}$$

$$h_{iy}^{+} + h_{ay}^{+} = h_{y}^{+} \tag{4-5b}$$

$$-Z_o h_{iy}^{+} + Z_o h_{ay}^{+} = e_{x}^{+} \tag{4-5c}$$

$$Z_o h_{ix}^{+} - Z_o h_{ax}^{+} = e_{y}^{+} \tag{4-5d}$$

Finally, the following continuity equations at $z = d/2$ are easily obtained from Eq. (4-5)

$$2Z_o h_{ix}^{+} = Z_o h_{x}^{+} + e_{y}^{+} \tag{4-6a}$$

$$2Z_o h_{iy}^{+} = Z_o h_{y}^{+} - e_{x}^{+} \tag{4-6b}$$

At $z = -d/2$, a similar procedure to the above gives

$$2Z_o h_{ix}^{-} = Z_o h_{x}^{-} - e_{y}^{-} \tag{4-7a}$$

$$2Z_o h_{iy}^{-} = Z_o h_{y}^{-} + e_{x}^{-} \tag{4-7b}$$

Similar expressions to Eqs. (4-6) and (4-7) can be obtained for the anti-incident waves at each surface. These expressions are useful in obtaining an understanding of the required waves in free space.

From the Poynting theorem, the average power flow per unit surface area into a region is given by

$$\Pi = \frac{1}{TS} \int_0^T \int_{surf} \frac{c}{4\pi} (\bar{e} \times \bar{h}) \cdot \bar{n} \, dS dt \quad , \tag{4-8}$$

where the integral is over the entire bounding surface with inward unit normal $\bar{n}$, and surface area S. For sinusoidal time variations this can be written as

$$\Pi = \frac{1}{2S} \mathrm{Re}\left[\int_{\mathrm{surf}} \frac{c}{4\pi} (\bar{e} \times \bar{h}^*) \cdot \bar{n}\, dS \right] \qquad (4\text{-}9)$$

For the planar geometry considered here, the power absorbed through both surfaces per unit area of one surface (or as is commonly called per unit area of film) is

$$P = \frac{c}{8\pi} \mathrm{Re}[-\bar{e}^{+} \times \bar{h}^{+*} \cdot \bar{a}_z + \bar{e}^{-} \times \bar{h}^{-*} \cdot \bar{a}_z] \qquad (4\text{-}10)$$

where $\bar{e}^{+}$ and $\bar{h}^{+}$ are the fields at $z = \frac{d}{2}$ and $\bar{e}^{-}$ and $\bar{h}^{-}$ those at $z = -\frac{d}{2}$

$$P = \mathrm{Re}\left\{ \frac{c}{8\pi} (e_y^{+} h_x^{+*} - e_x^{+} h_y^{+*}) + \frac{c}{8\pi} (-e_y^{-} h_x^{-*} + e_x^{-} h_y^{-*}) \right\} \qquad (4\text{-}11)$$

The continuity equations Eqs. (4-6) and (4-7), the continuity of tangential fields at all interfaces between magnetic material of different properties, and the magnetic boundary conditions at all surfaces and interfaces provide enough equations to solve for the unknowns (h_x^{+}, e_x^{+}, h_{nx}, etc.) provided the incident fields ($\bar{h}_i^{+}$ $\bar{h}_i^{-}$) are specified. Therefore, the power absorbed can be calculated from Eq. (4-11). For $\bar{h}_i^{+} = \bar{h}_i^{-} = \frac{h_o}{2} e^{i\omega t} \bar{a}_x$ the above description constitutes the first method discussed in the introduction. This method is easily adapted to the study of transmission of electromagnetic radiation through films, where the second method discussed below does not contain this flexibility.

When the magnetic fields at the film surfaces are specified (i.e., method number two in the introduction), the computation or computer time required to calculate the power absorbed can be significantly reduced. If $h_x^{+} = h_x^{-} = h_o$ and $h_y^{+} = h_y^{-} = 0$, then the

power absorbed per unit area of film is

$$P = \frac{ch_o}{8\pi} \mathrm{Re}(e_y^+ - e_y^-) \tag{4-12}$$

The equations necessary for the computation of $(e_y^+ - e_y^-)$ come from the magnetic boundary conditions at all surfaces and interfaces between magnetic materials of different properties, the continuity of tangential fields at all interfaces, and the following surface equations.

$$h_x^+ = 1 = \sum_{n=1}^{8} h_{nx}\, e^{ik_n d/2} \tag{4-13a}$$

$$h_x^- = 1 = \sum_{n=1}^{8} h_{nx}\, e^{-ik_n d/2} \tag{4-13b}$$

$$h_y^+ = 0 = \sum_{n=1}^{8} h_{nx}\, \nu_n\, e^{+ik_n d/2} \tag{4-13c}$$

$$h_y^- = 0 = \sum_{n=1}^{8} h_{nx}\, \nu_n\, e^{-ik_n d/2} \tag{4-13d}$$

$$e_y^+ - e_y^- = -\frac{c}{2\pi\sigma} \sum_{n=1}^{8} k_n h_{nx} \sin\frac{k_n d}{2} \tag{4-13e}$$

This set of equations is one more in number than for method one, but $e_y^+ - e_y^-$ can be directly determined.

Due to the factoring of Eq. (2-16) at parallel and perpendicular resonance orientations, the power absorption calculations at these orientations are simplified. At parallel resonance the tangential fields associated with the six wave vectors from Eq. (2-19) and the two wave vectors from Eq. (2-18) are linearly polarized perpendicular

and parallel to $\bar{M}_o$, respectively. In terms of the equations this gives

$$h_{nx} = 0 \qquad n = 7,8 \tag{4-14a}$$

$$v_n = 0 \qquad n = 1,2,3,4,5,6 \tag{4-14b}$$

With these conditions, Eqs. (4-13) are reduced to

$$h_x^+ = 1 = \sum_{n-1}^{6} h_{nx}\, e^{ik_n d/2} \tag{4-15a}$$

$$h_x^- = 1 = \sum_{n=1}^{6} h_{nx}\, e^{ik_n d/2} \tag{4-15b}$$

$$e_y^+ - e_x^- = \frac{-c}{2\pi\sigma'} \sum_{n=1}^{6} k_n h_{nx} \sin k_n d/2 \tag{4-15c}$$

Since the summation extends only to $n = 6$, the parallel resonance calculation is simplified. For the perpendicular resonance orientation Eq. (2-16) factors into two quadratics in K^2 (Eq.(2-17)). Associated with each quadratic are four field components with circular polarization; the sense of precession or rotation of this polarization is positive (negative) for the fields with wave vectors from the $i = 1$ ($i=2$) equation. Using method two, the linearly polarized inputs ($h_x^+ = 1$, $h_y^+ = 0$, $h_x^- = 1$, $h_y^- = 0$) are resolved into two oppositely polarized circular waves of half magnitude; these polarizations are completely uncoupled, i.e., the response of the system associated with one sense of precession is not affected by the other. In general, this is true at perpendicular resonance for any magnetic boundary condition that requires isotropic pinning of the magnetization.

The power absorbed can be calculated for each of the two circular drive fields individually (see Appendix IV). The power absorbed due to the negative precession drive is small, slowly varying and can be neglected when compared to the resonant characteristics of the positive precession response.

The equations necessary to solve for the power absorbed in the following four cases are given in Appendix IV.

1. A film with asymmetric perpendicular uniaxial anisotropies and the magnetization at a general angle, θ.

2. A film with asymmetric tensorial anisotropies and the magnetization at a general angle, θ.

3. A film with asymmetric tensorial or perpendicular uniaxial anisotropies; the magnetization is in the perpendicular resonance orientation. The symmetries discussed above and method two are utilized.

4. A film with asymmetric surface layers with the magnetization in the perpendicular resonance orientation. The symmetries discussed above and method two are utilized.

In the first two examples the equations for both method one and two are presented.

4.3 Approximate Absorption Calculations

The calculations discussed in the previous section are not too unreasonable for the anisotropy models where the maximum number of equations is 9; however, when the asymmetric surface layer problem was considered it was found to have 24 unknowns. The surface layer model also required the roots of three equations like Eq. (2-16) to be found. Even the symmetric film calculation at perpendicular resonance had 9 equations. An approximation was believed to be in order. The calculated power absorption data presented in Chapter 6 for an asymmetric film with surface layers were obtained using this approximation. The positive and negative precession spin wave vectors were approximately factored from Eq. (2-16). Secondly, the boundary condition at the interface between the layers was approximated such that the negative precession wave vectors were not required. These approximations were found to give very good results for symmetric films at parallel resonance where they are the least accurate. The approximation to the secular equation will be presented here and the approximation to the boundary condition is presented in Appendix V. Results from the calculations are presented for the perpendicular uniaxial anisotropy and the surface layer model at the end of this section.

Equation (2-14) written in matrix form is

$$\begin{bmatrix} \pi_2 & -i\Omega'^{*} \\ i\Omega' & \pi_1 \end{bmatrix} \begin{bmatrix} m_\theta \\ m_\phi \end{bmatrix} = 0 \qquad (4\text{-}16)$$

or

$$\overleftrightarrow{G}\,\overline{m} = 0$$

With $\varepsilon = 0$ the matrix G can be exactly diagonalized by a similarity transformation $U^{+}\overleftrightarrow{G}\,U$ (Kobayashi, 1973).

$$U = \begin{bmatrix} \dfrac{1}{(1+|R|^2)^{1/2}} & \dfrac{R}{(1+|R|^2)^{1/2}} \\ \dfrac{-R^*}{(1+|R|^2)^{1/2}} & \dfrac{1}{(1+|R|^2)^{1/2}} \end{bmatrix} \qquad (4\text{-}17)$$

Upon applying this transformation to $\overleftrightarrow{G}$, the following is obtained

$$\overleftrightarrow{A}U^{+}\,\overline{m} = \begin{bmatrix} A_{11} & A_{12} \\ A_{21} & A_{22} \end{bmatrix} U^{+} \begin{bmatrix} m_\theta \\ m_\phi \end{bmatrix} = 0 \qquad (4\text{-}18a)$$

$$A_{11} = K^4 + K^2\,(-K_2^2 + i2\varepsilon^2) + i2\varepsilon^2\left(-K_2^2 + \frac{|R|^2 + \cos^2\theta}{1+|R|^2}\right) \qquad (4\text{-}18b)$$

$$A_{12} = -A_{21}^{*} = \frac{-i2\varepsilon^2 R\,\sin^2\theta}{(1+|R|^2)} \qquad (4\text{-}18c)$$

$$A_{22} = K^4 + K^2\,(-K_1^2 + i2\varepsilon^2) + i2\varepsilon^2\,(-K_1^2 + \frac{1 + \cos^2\theta\,|R|^2}{1 + |R|^2}) \quad (4\text{-}18d)$$

As before, the dispersion relation is given by det (A) = 0; however, if A_{12} and A_{21} are negligible, it is approximately given by $A_{11}=A_{22}=0$. The secular equation approximation (Yelon et al 1974) is to neglect A_{12} and A_{21} (Note A_{12} and A_{21} are zero for perpendicular resonance).

The ellipticity and sense of precession of the components of the magnetization for A_{11} and A_{22} are found by examining each eigenvector independently. The eigenvectors obviously are

$$\mu_1 \begin{pmatrix} 1 \\ 0 \end{pmatrix} \quad \text{for} \quad A_{11} = 0 \qquad (4\text{-}19a)$$

and

$$\mu_2 \begin{pmatrix} 0 \\ 1 \end{pmatrix} \quad \text{for} \quad A_{22} = 0 \qquad (4\text{-}19b)$$

where

$$U^+ \begin{pmatrix} m_\theta \\ m_\phi \end{pmatrix} = \mu_1 \begin{pmatrix} 1 \\ 0 \end{pmatrix} \qquad (4\text{-}19c)$$

$$U^+ \begin{pmatrix} m_\theta \\ m_\phi \end{pmatrix} = \mu_2 \begin{pmatrix} 0 \\ 1 \end{pmatrix} \quad . \qquad (4\text{-}19d)$$

Multiplying the above by U gives

$$\begin{pmatrix} m_\theta \\ m_\phi \end{pmatrix} = \mu_1 \begin{pmatrix} 1/(1 + |R|^2)^{1/2} \\ -R^*/(1 + |R|^2)^{1/2} \end{pmatrix} \Rightarrow \frac{m_\theta}{m_\phi} = -1/R^* \qquad (4\text{-}20)$$

and

$$\begin{pmatrix} m_\theta \\ m_\phi \end{pmatrix} = \mu_2 \begin{pmatrix} R/(1 + |R|^2)^{1/2} \\ 1/(1 + |R|^2)^{1/2} \end{pmatrix} \Rightarrow \frac{m_\theta}{m_\phi} = R \qquad (4\text{-}21)$$

Therefore, $A_{11} = 0$ gives two spinwaves with negative precession; like the negative precession spinwaves of perpendicular resonance, these will contribute little to the resonance phenomena. The spinwaves given by $A_{22} = 0$, however, have positive spin precession and are the major contributors to the resonance behavior. The spinwave ellipticities here are the same as those associated with the K_1 and K_2 wave vectors in Eq. (3-2).

If the boundary conditions are such that the positive and negative precession spinwaves are not coupled, then one would proceed as follows: 1) the linearly polarized input ($\bar{h}^+$ of method two) would be resolved into two oppositely polarized elliptical waves with $h_{xp} = h_x^+/(1 + |R|^2)$, $h_{xn} = |R|^2 h_x^+/(1 + |R|^2)$ and ellipticies $(R \cos\theta)$, $(-\cos\theta/R^*)$, respectively. (These can be matched by the film plane projection of the positive and negative precession spinwave fields respectively); 2) The power absorbed for each of these polarizations would be calculated as in the perpendicular resonance case discussed earlier.

Of the three boundary conditions treated in this thesis only the tensorial model falls into the class of uncoupled positive and negative precession spinwaves. Therefore, further approximations had to be made to simplify the calculations involving the other two. The uniaxial anisotropy model is approximately a tensorial model with (see Appendix V)

$$K_\perp = K_s \qquad (4\text{-}22a)$$

$$K_{\parallel} = - \frac{K_s |R|^2}{1 + |R|^2} \qquad (4\text{-}22b)$$

By using the procedure outlined above it was found that the "exact" spectra and those due only to the positive precession spinwaves had almost exactly the same characteristics (i.e., mode position, mode linewidth and relative mode amplitude); but, the power absorbed by the positive precession mode, P^+, was not in good agreement with the "exact" calculation. It was found, however, that if h_{xp} was changed to

$$h_{xp} = \frac{h_o}{(1 + |R|^2 \cos^2 \theta)} \qquad (4\text{-}23)$$

then even the power absorbed was in very good agreement at all angles of the magnetization. A comparison is given in Table (4-1). Here the amplitude, linewidth, and peak positions of P^+ is compared with method two calculations for a symmetric permalloy film; the power absorbed by the negative precession spinwaves was small and slowly varying.

An approximate boundary condition for the positive precession spin waves at the interface of two magnetic layers was deduced from Eq. (3-17) (See Appendix V)

$$\frac{1}{((1 + |R_s|^2)(1 + |R_b|^2))^{1/2}} \frac{\mu_{2b}}{M_b} = \frac{1}{(1 + R_b R_s^*)} \frac{\mu_{2s}}{M_s} \qquad (4\text{-}24a)$$

$$\frac{A_b}{M_b (1 + R_b R_s^*)} \frac{d\mu_{2b}}{dz} = \frac{A_s}{M_s((1 + |R_s|^2)(1 + |R_b|^2))^{1/2}} \frac{d\mu_{2s}}{dz} \qquad (24b)$$

A comparison of the "exact" and approximate, P^+, calculations at parallel resonance (the orientation at which the approximation should be the least accurate) is given in Table (4-2) for a YIG film. (Note: Eq. (4-23) was used for h_{xp}.) The excellent agreement found in this case and the uniaxial case presented earlier, lets one use this approximation with confidence that the calculated data represents the resonance process.

Table (4-1)

θ	"Exact" Amplitude (erg/cm^2)	P^+ Amplitude (erg/cm^2)	"Exact" Position (Oe)	P^+ Position (Oe)	"Exact" ΔH* (Oe)	P^+ ΔH* (Oe)
0	6.884×10^6	6.884×10^6	3179.9	3179.9	43.1	43.1
	4.503×10^5	4.503×10^5	2878.5	2878.5	21.1	21.1
	6.005×10^4	6.005×10^4	2122.1	2122.1	18.4	18.4
	1.450×10^4	1.45×10^4	876.8	876.8	17.6	17.6
30	1.038×10^7	1.038×10^7	2082	2081.9	40.5	40.5
	3.811×10^5	3.853×10^5	1799.4	1799.3	21.3	21.3
	4.144×10^4	4.378×10^4	1047.2	1047.0	18.4	18.4
80	1.502×10^7	1.502×10^7	882.4	882.4	38.1	38.1
90	1.513×10^7	1.513×10^7	860.9	860.6	37.9	38.0

Film Properties

M = 887.4 G

Rho = 14.3 Micro-Ohm-cm

d = 2023 Å

Alpha = .00457

A = 1.143×10^{-6}

$K_{s1} = K_{s2} = .22$ Erg/cm^2

f = 9.44 GHz

γ = 1.8484×10^7 inv Oe-sec

$g_1 = g_2 = g_3 = 0$

* ΔH is the inflection point linewidth

Table (4-2)

Film Properties

M_b = 138.1 G

$\alpha_b = \alpha_s$ = .00105

$A_b = A_s = 3.593 \times 10^{-7}$ Erg/cm

f = 9.16 GHz

$\gamma_b = \gamma_s = 1.767 \times 10^{7}$ inv Oe-sec

M_b/M_s = 1.95

L = 470 Å

D = 4230 Å

Mode NR	FMR Position (Oe)		Linewidth (Oe)		Absorption (erg/cm^2)	
	FMR (P^+)	Position "Exact"	Linewidth (P^+)	"Exact"	(P^+)	"Exact"
1	2596.6	2595.6	3.9	3.9	1.053×10^{7}	1.054×10^{7}
2	2494.0	2494.0	3.9	3.9	2.018×10^{7}	2.015×10^{7}
3	2426.6	2426.6	3.9	3.9	1.426×10^{6}	1.426×10^{6}

Chapter 5

Surface Layer Properties

5.1 Introduction

It has been asserted earlier that the surface layer model can be made to match the experimental resonance spectra observed in YIG; however, the required surface layers must represent a realistic average of the properties believed to exist in the surface regions. Some evidence for the existence of surface regions of different properties than the bulk properties is given below. Etching experiments on YIG films have shown that the source of surface modes is located within 100-800Å of the surface. An example of the mode field position behavior during an etching experiment on a film with two surface modes is provided in Fig. (5-1). The lower surface mode made the transition to a body mode in the first 200 or 300Å of etching. Presumably this mode was concentrated at the film-air interface. The field position of the other surface mode was invariant until the film was less than 1500Å thick. The remarkable behavior below this thickness indicates that there was an interface surface region of considerable thickness with properties different from the bulk. This second mode only appeared if the film had been annealed in this case at 1200°C for 6 hours; this in itself is suggestive that a diffusion may occur between substrate and film.

Surface modes were observed at perpendicular resonance by Henry et al (1973) after overcoating with SiO_2 or argon implantation. It is physically plausible that these processes would give a region

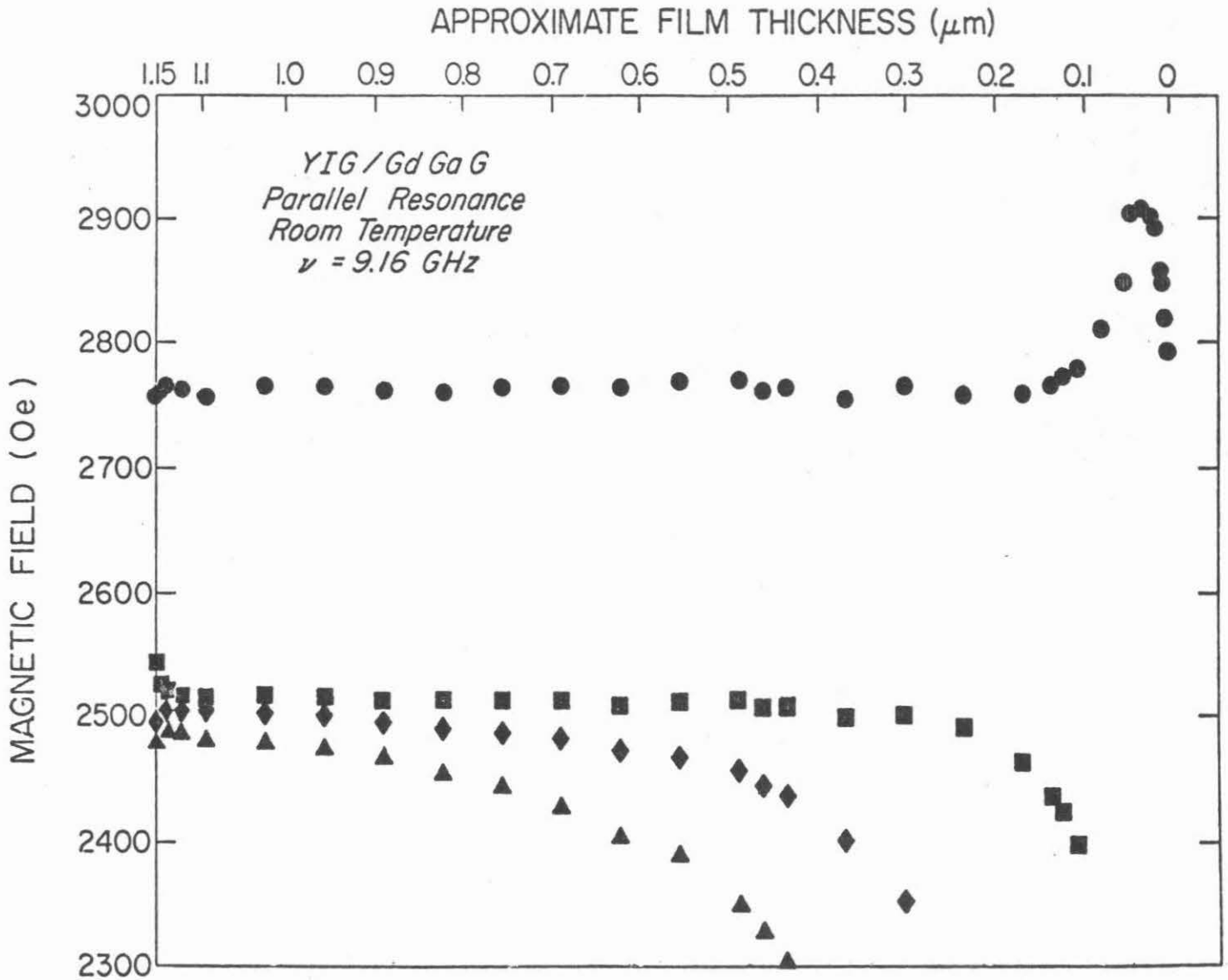

Fig. (5-1) Effect of etching on the resonant-field position of the high-field spin wave modes for a YIG film having two surface modes. After Yu et. al. (1975)

at the air-film interface with magnetic properties different than the bulk.

In the following section some of the properties of bulk garnet materials are described. The final section presents some of the properties to be ascribed to the two surface layers of a YIG film; other properties will be presented in the next chapter as needed to explain the experimental data.

5.2 Properties of Garnet Materials

The simplest chemical formula for garnet materials is $R_3P_2Q_3O_{12}$. The basic crystal structure is cubic with eight formula units per unit cell, i.e., 160 atoms 96 of which are oxygen. Each oxygen ion lies at a vertex that is common to four polyhedra of oxygen, one octahedron, one tetrahedron, and two dodecahedra, as indicated in Fig. (5-2). The orientations of the polyhedra vary throughout the unit cell, although the type of symmetry for each is retained. The cations occupy the interstitial sites. The cations denoted by P and Q occupy the octahedral or [a] sites and the tetrahedial or [d] sites, respectively. The other metal ions, R, are surrounded by eight oxygen ions located at the corners of a skewed cube, or, as it is often called, a dodecahedron, [c] sites.

In the magnetic garnets, R is typically a trivalent combination of rare-earth and yttrium ions; P and Q are trivalent combinations of Fe^{+3}, Ga^{+3} and Al^{+3}. An example is $(Gd_{0.7}Y_{1.55}Yb_{0.75})\ Ga_{0.9}Fe_{4.1}O_{12}$. In a magnetized state the net moment of the P^{3+} ions in the (a) sites and the net moment of the R^{3+} ions are in one direction and

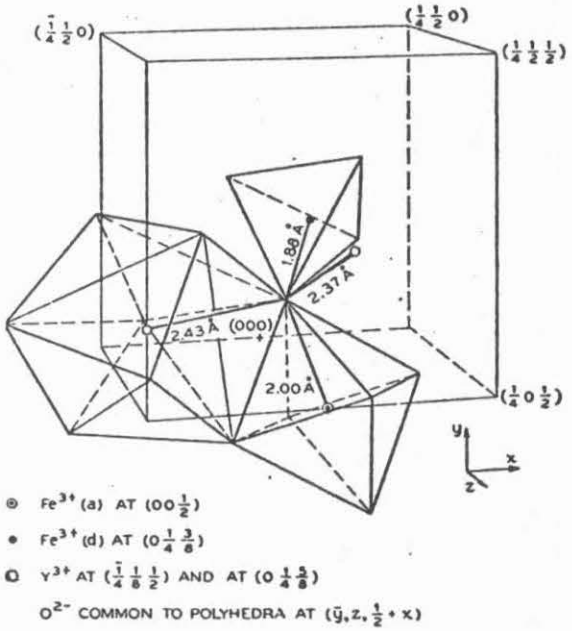

Fig (5-2) Structure of yttrium iron garnet (After Gilleo, et. al., 1958)

that of the Q^{3+} ions in the (d) sites are in the opposite direction. The alignment is due to superexchange interactions of the Q^{3+} ions in (d) sites with those in (a) and (c) sites via O^{2-} intermediaries. The moment of an Fe^{3+} ion is 5 Bohr magnetons.

In rare earth substituted YIG the variation of the net moment of the Fe^{3+} system with temperature is similar to that of ferromagnetic metals. The moment contribution due to magnetic R^{3+} ions, however, is quite different as shown in Fig. (5-3) for $Gd_3Fe_5O_{12}$. The net moment at absolute zero (that for R ions and (a) site Fe^{3+} less that for (d) site Fe^{3+}) can be fairly large. As the temperature increases for garnets like $Gd_3Fe_5O_{12}$ the net moment decreases to zero at a temperature called the compensation temperature. Above the compensation temperature the moment for Fe^{3+} in the (a) sites dominates and does so up to the Neel temperature where the moment again drops to zero.

Fig.(5-4)shows the net magnetization of several garnets as a function of temperature. Introduction of Ga^{3+} and Al^{3+} for Fe^{3+} is known to reduce the moment and the Neel temperature of the material.

"The rules for ionic site preference in the garnets may be summarized as follows:

1. The octahedral and tetrahedral sites appear to prefer exclusively ions with spherical or pseudospherical electronic configuration. The dodecahedral sites are not selective in this regard.

2. Site preferences depend on relative ionic sizes: (a) If an ion has a spherical electronic configuration in both octahedral and tetrahedral crystal fields, the larger the ion, the greater

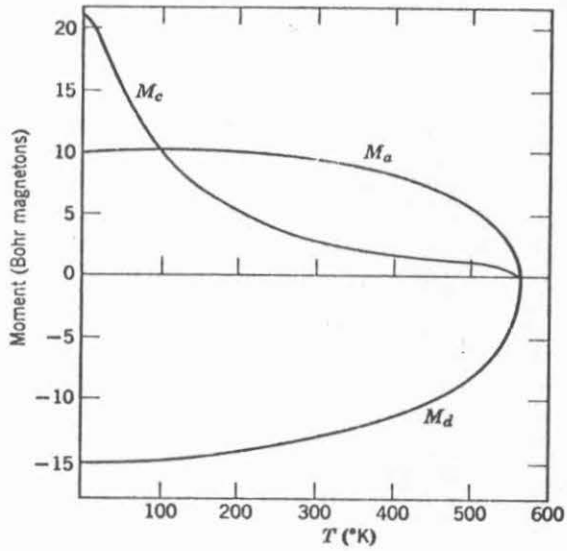

Fig. (5-3) The magnetization of the GdIG sublattices per formula unit as a function of temperature (After R. Pauthenet)

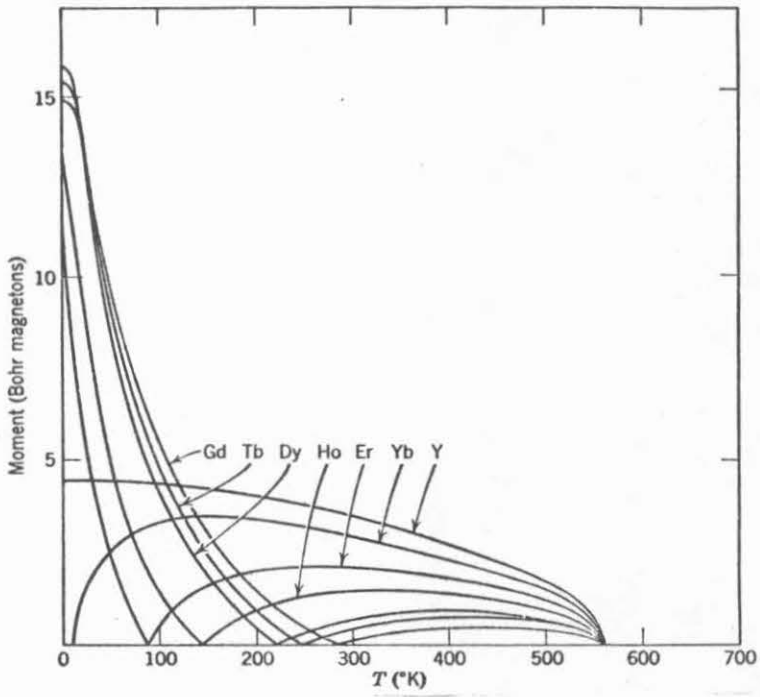

Fig. (5-4) Experimental values of the spontaneous magnetization of various simple garnets as a function of temperature. The formula unit is $P_3Fe_5O_{12}$ where the P is indicated for each curve (After R. Pauthenet)

will be the preference for the octahedral site. The dodecahedral sites are usually occupied by the largest metal ions present. (b) The substitution of one ion for another in a particular garnet is limited by the relative sizes of all of the ions involved." (Geller 1970)

The garnets are magnetostrictive and the dominant crystalline anisotropy of the rare-earth garnets is cubic with easy axis along the body diagonals; however, a number of techniques are known to add large anisotropies to these films. An example of these large anisotropies is the growth induced anisotropy in bubble related garnets. This anisotropy results from site ordering of the two or more rare-earth ions incorporated in the particular garnet; the magnitude of this anisotropy is in part determined by the size differences of the R ions involved. (Rosencwaig et al (1971), Gyorgy et al (1973).

Another anisotropy observed at low temperatures (i.e., less than 100°K) is associated with Fe^{2+} ions in octahedral sites. In the situations where this anisotropy has been most studied, the Fe^{2+} was generated by introducing Si^{4+} into the lattice. The Si^{4+} is believed to be in the tetrahedral sites because of the small size and preference for a coordination number of four. The Fe^{2+} is believed to be in the octahedral sites because of the larger size and a preference for a coordination number of six. The Fe^{2+} ion is about the same size as the Sc^{3+} ion which prefers octahedral sites exclusively in the garnets. There are four types of octahedral sites, distinguished by a different local symmetry and characterized by the local trigonal axis which lies in one of the four $\langle 111 \rangle$ directions. Electrons

(Fe^{2+} ions) in sites whose trigonal axis is nearest to the magnetization direction have a slightly lower energy than those in other sites. At low temperatures the excess electrons become trapped in those sites and produce anisotropy. The magneto-optical effects of this anisotropy have been thoroughly studied. Irradiation with white light leads to a redistribution of electrons that essentially destroys the anisotropy (Gyorgy et al (1970)).

5.3 Surface Layers in Garnet Films

It was schematically pointed out in Fig. (3-7) that the properties to be ascribed to the two surface layers are different. The properties of a particular layer depend upon the history associated with the film; therefore, it is impossible for universal properties to be determined; however, some properties that could be easily associated with a particular layer are given below. In general, any magnetic material constant may be different; this includes the magnetization, M, the gyromagnetic ratio, γ, the exchange constant, A, the damping parameter, α, and the anisotropies, K_a. Of these A and α are expected to make little difference for very thin layers but may play a role if the layers become thicker. Variations of M, K_a, and γ however, have considerable effect on the field position of the spinwave modes. Significant variation in γ is unlikely except near compensation in ferrimagnets, therefore this effect should only appear as a sensitive function of temperature. Variations in M or K_a have effects that are not easily separated.

5.3.1 Film-Air Interface

The physical mechanism producing the surface anisotropy or spin pinning at this surface is not clear; however, through etching experiments, it has been isolated to a thin surface region. In any orientation a mode localized at a surface will exist if the surface layer tends to resonate at a larger field. Two possible origins of this are: (a) a layer with different anisotropy energies than the bulk or (b) a layer of different magnetization. In the latter case, the surface mode appears in perpendicular resonance ($\theta = 0°$) if the surface magnetization is increased, and in parallel resonance ($\theta = 90°$) if the surface magnetization is decreased.

One possible source of a larger surface magnetization is the existence of oxygen vacancies in the surface region causing Fe^{2+} ions in the octahedral sites. A reduction of the total moment in the octahedral sites would increase the total magnetization. Further, the Fe^{2+} may have the effect of producing significant anisotropies at lower temperatures, and these anisotropies could be sensitive to irradiation by light.

5.3.2 Film-substrate Interface

This surface region is believed to be of variable chemical composition $Y_{3-y}Gd_yFe_{5-x}Ga_xO_{12}$ where the thickness of the layer, and y and x are dependent on prior annealing treatment. The behavior of the Gd moment in the partially substituted YIG should be little different than that of stoichiometric GdIG shown in Fig. (6-2) except for a reduced value of M_{Gd}. If the Gd magnetization is suf-

ficiently high, the strong temperature dependence of the gadolinium magnetization will produce a compensation temperature where the net magnetization vanishes. Further, it is expected that at temperatures below compensation the resultant magnetization in the surface layer will be anti-parallel to the applied field since the principal exchange coupling is through the iron sublattices and because the surface layer is believed thin compared to the width of a typical domain wall. The gyromagnetic ratio for a ferrimagnet varies with the sublattice magnetization in accordance with an effective g factor (Wangsness (1953, 1954, 1956))

$$g_{eff} = \frac{M_{Fe} - M_{Gd}}{\frac{M_{Fe}}{g_{Fe}} - \frac{M_{Gd}}{g_{Gd}}}$$

The temperature dependence of the critical angle associated with this interface can be explained if $g_{Fe} > g_{Gd}$ and if the surface layer has a compensation temperature near 110°K. From effective g measurements in GdIG, it was deduced by Calhoun et al (1958) that g_{Gd} is slightly lower than g_{Fe}. By varying the frequency and measuring the perpendicular FMR field, g_{Fe} was determined to be 2.008±.002. Based on these considerations, the values of g_{Fe} and g_{Gd} were chosen to be 2.008 and 2.000, respectively. In order to have a compensation temperature near 110°K, it was estimated from experimental and molecular field analysis data of Figures (5-3) and (5-4) that the room temperature magnetizations in the surface layer should be in

the range .4 $M_{Fe} < M_{Gd} < .3\ M_{Fe}$. In the analysis, the room temperature ratio of M_{Gd} to M_{Fe} was varied within the above limits with M_{Fe} chosen 15-25% lower than the bulk value due to the possibility of gallium substitution.

Any atomic substitution in the surface layer may also give rise to an in-plane strain since the layer is epitaxial with thick film and substrate. Through magnetostrictive interactions this can give rise to a substantial perpendicular uniaxial anisotropy such as is well known in bubble material garnets. This anisotropy is to a large extent indistinguishable from a change in magnetic moment. Therefore in what follows a change in $4\pi M$ in the surface layers could be in part a change in this anisotropy.

Chapter 6

Comparison of Experimental and Calculated Data

6.1 Introduction

The previous chapters have introduced experimental phenomena (Chapter 1), theory (Chapters 2-4), garnet material properties (Chapter 5). This chapter will address the thesis that observed surface phenomena in thin YIG films can be explained by surface layers with magnetic properties different from the bulk. Calculations utilizing the other models of surface pinning are also provided where instructive.

Experimental data from four films are compared with calculated spinwave spectra. Comparison of calculations with experimental data from other than these four films are qualitative. The material constants for these four films are given in Table (6-1); for convenience the samples have been designated CIT 1, CIT 2, OSU 1, OSU 2. The two samples measured in this laboratory were cut from a single garnet film grown by CVD process on a [111] oriented wafer. One sample (CIT 2) was annealed in dry O_2 for 6 hours at 900°C. The unannealed sample (CIT 1) has a surface mode at perpendicular resonance while the sample CIT 2 has one at parallel resonance. The surface mode of the CIT 1 sample is believed localized at the air-film surface since it had been overcoated after growth; the surface mode of the CIT 2 sample was shown to be localized at the air-film interface by etching away the outer surface. The data for the other two films are taken from a

TABLE (6-1)

Sample	CIT 1	CIT 2	OSU 1	OSU 2
Orientation	[111]	[111]	[100]	[100]
Total Thickness (μ)	.467	.47	.467	.471
Annealing Temp. (°C)	-	900	1000	1200
Annealing Time (Hr)	-	6	6	6
Frequency (GHz)	5.966	5.966	9.16	9.16
A (erg/cm)	3.593×10^{-7}	3.593×10^{-7}	3.593×10^{-7}	3.593×10^{-7}
BULK CONSTANTS				
D (Å)	4450	3800	4200	3620
$4\pi M_b$ (Oe)	1701.2	1701.2	1735	1735
γ_b (sec^{-1} Oe^{-1})	1.767×10^{7}	1.767×10^{7}	1.767×10^{7}	1.767×10^{7}
AIR-FILM SURFACE LAYER				
L_s (Å)	200	700	0	290
M_b/M_s	.821	1.38	-	1.45
γ_b/γ_s	1	1	-	1
α_b/α_s	.3	.54	-	@
SUBSTRATE-FILM SURFACE LAYER				
L_s (Å)	20	200	470	800
M_b/M_s	1.1	1.1	1.95	1.4

TABLE (6-1) CONT.

γ_b/γ_s	1	1	.9977	.999
$4\pi M_{Fe}$ at 300°K (Oe)	-	1545	1400	1500
$4\pi M_{Gd}$ at 300°K (Oe)	-	0	510	261
α_b/α_s	1	.9	@	@
TENSORIAL ANISOTROPY MODEL				
D ($\mathring{A}$)	4680	4300	4280	3860
$K_{\perp,1}$ (ergs/cm^2)	-.049	.1	.114	.118
$K_{\parallel,1}$ (ergs/cm^2)	.023	-.040	-.048	-.0505
$K_{\perp,2}$ (ergs/cm^2)	.0019	.019	0	.067
$K_{\parallel,2}$ (ergs/cm^2)	-.001	- .01	0	-.0265
UNIAXIAL ANISOTORPY MODEL				
D ($\mathring{A}$)	4680	4300	4270	3850
D calculated* ($\mathring{A}$)	4712	4489	4441	4391
K_{s1} (ergs/cm^2)	-.0488	.1	.1085	.112
K_{s1} calculated*	-.061	.161	.14	.195
K_{s2} (ergs/cm^2)	.0019	.019	0	.065
K_{s2} calculated*	.0019	.019	0	.075

* calculated from the surface layer model for comparison with other value obtained from a best fit to the experimental data (see the text)
@ not determined

paper by Yu, Tuck, and Wigen (1975). Both films were cut from a single garnet film grown by CVD on a [100] oriented wafer. One of the films (OSU 1) was annealed at 1000°C for 6 hours and has a single surface mode at parallel resonance. The other film (OSU 2) was annealed at 1200°C for 6 hours and has two parallel resonance surface modes. In the latter case, two surface modes indicate that both surfaces of the film have been altered. This was confirmed by an etching experiment (see Fig. (5-1)).

Typical experimental data consist of a set of spinwave spectra obtained at different angles of applied field. Field locations of the three highest field modes are shown for a case in Fig. (6-1). The most important feature in this figure is the separation of the modes from the (calculated) uniform mode location. Because of the large variation in the uniform mode location, there is a great loss of detail unless this separation is plotted instead of the actual mode location. All subsequent figures will show only the separations from the calculated uniform mode location. Comparison of experimental data with the calculated uniform mode location has one inherent difficulty; Fig. (6-1) shows that a small error in alignment will affect the uniform mode position negligibly at perpendicular and parallel resonance, but a significant error may result at other angles (e.g., a .1° error in alignment changes the uniform field by about 5 Oe at $\beta = 30°$). This may be the source of some of the difference between the calculated and experimental data presented later.

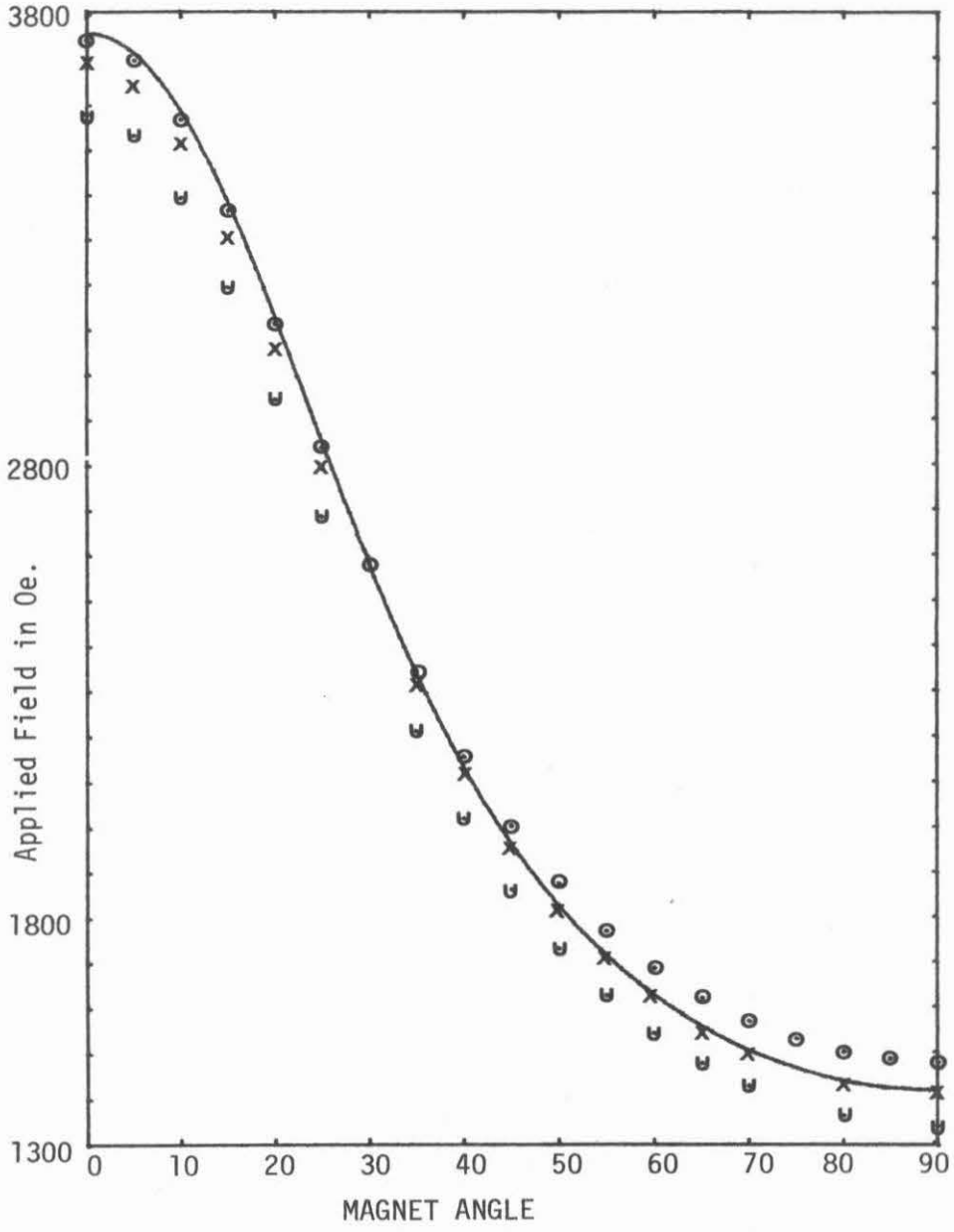

Fig. (6-1) Angle dependence of the resonant-field position of the highest three field modes of sample CIT2. The solid curve is the calculated field position for the uniform precession mode.

In attempting to duplicate the experimental spectra, the surface layer thickness, magnetization and in the case of substrate-film layer the ratio of M_{Gd} to M_{Fe} were varied to give a best fit to the mode locations at all angles. The material constants that were determined for the four films are given in Table (6-1). Film thickness for YIG is usually measured by an optical interference method. In the thickness range of .5 μm, this appears to give an accuracy only of the order of 10%. Since the spinwave spectra are very sensitive to thickness, it was necessary to vary the film thickness from the optically measured value.

The orientation of the magnetization depends on the orientation of the applied field with respect to the crystallographic axes. For simplicity of calculation, the experimental data were taken with the applied field in the orientation described below. For the [100] oriented films the applied field was in a (100) plane at an angle β from the film normal. For the [111] oriented films the applied field was at an angle β from the film normal in a plane defined by the normal and a line in the film plane 30° from the $[\bar{1}\bar{1}2]$ axis.

6.2 Comparison of the Angular Spinwave Mode Field Position Data

Surface layers can force the bulk material to support surface or body modes as the highest field mode depending on whether the surface layers tend to resonate at a higher or lower field than the bulk. A layer with a reduced magnetization will resonate at a higher field at the parallel orientation and a lower field at the perpendicular. Therefore, a film with a reduced magnetization layer will have a surface mode at parallel and not at perpendicular. A layer with increased magnetization produces the opposite effect.

Figures (6-2) and (6-3) show the angular dependence of the resonance fields for the observed and calculated spinwave spectra in the samples CIT 1 and CIT 2, respectively. For both films, the best fit to the experimental data was obtained by using two surface layers, and a total film thickness of about .47 μm. The calculated and experimental data for the two [100] oriented films (OSU 1 and OSU 2) are shown in Figures (6-4) and (6-5). The best fit for sample OSU 1 was obtained by using a single surface layer. Two surfaces were obviously required for sample OSU 2. The best fit to the data for both films was obtained using a total thickness of about .47 μm. The thickness reported by Yu et al (1975) was .56 μm; this reported thickness is clearly inconsistent with the experimental perpendicular resonance mode spacings and must be in error. The above mode position calculations utilized Eq. (3-17) for the sample with one free surface and the 8 x 8 determinant in Appendix II for the films with 2 layers. The respective g's and magnetization equilibrium relations for the [100] and [111] oriented films are given in Appendix I.

One important observation can be made from the layer thickness data given in Table (6-1).The total thickness required to match the mode position data in an annealed film is slightly larger than that required for an unannealed film or film annealed at a lower temperature. The effect, however, is small.

It is instructive to compare the above with the results from the tensorial and uniaxial surface anisotropy models. The best fit to

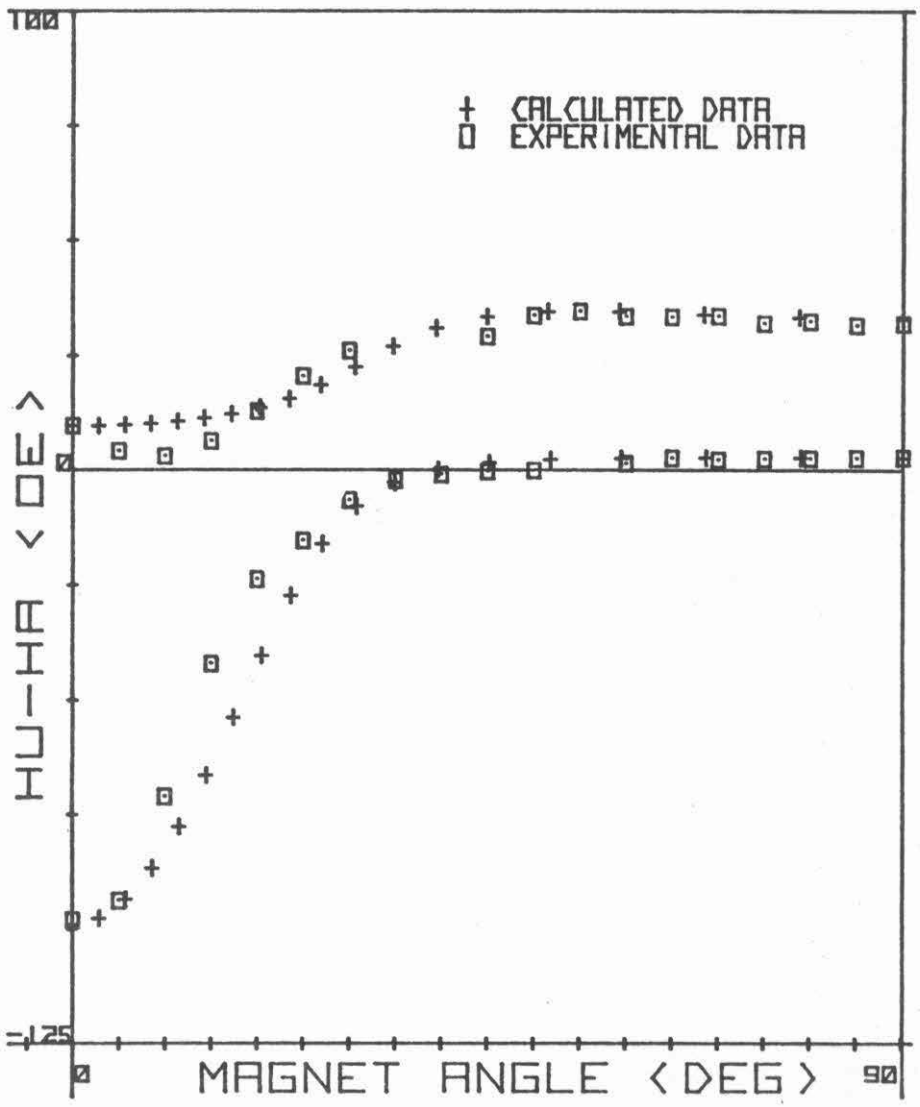

Fig. (6-2) The angle dependence of the magnetic field separation of the observed and calculated positions of the spin-wave modes, HA, from the calculated position of the uniform mode, HU, for sample CIT 1.

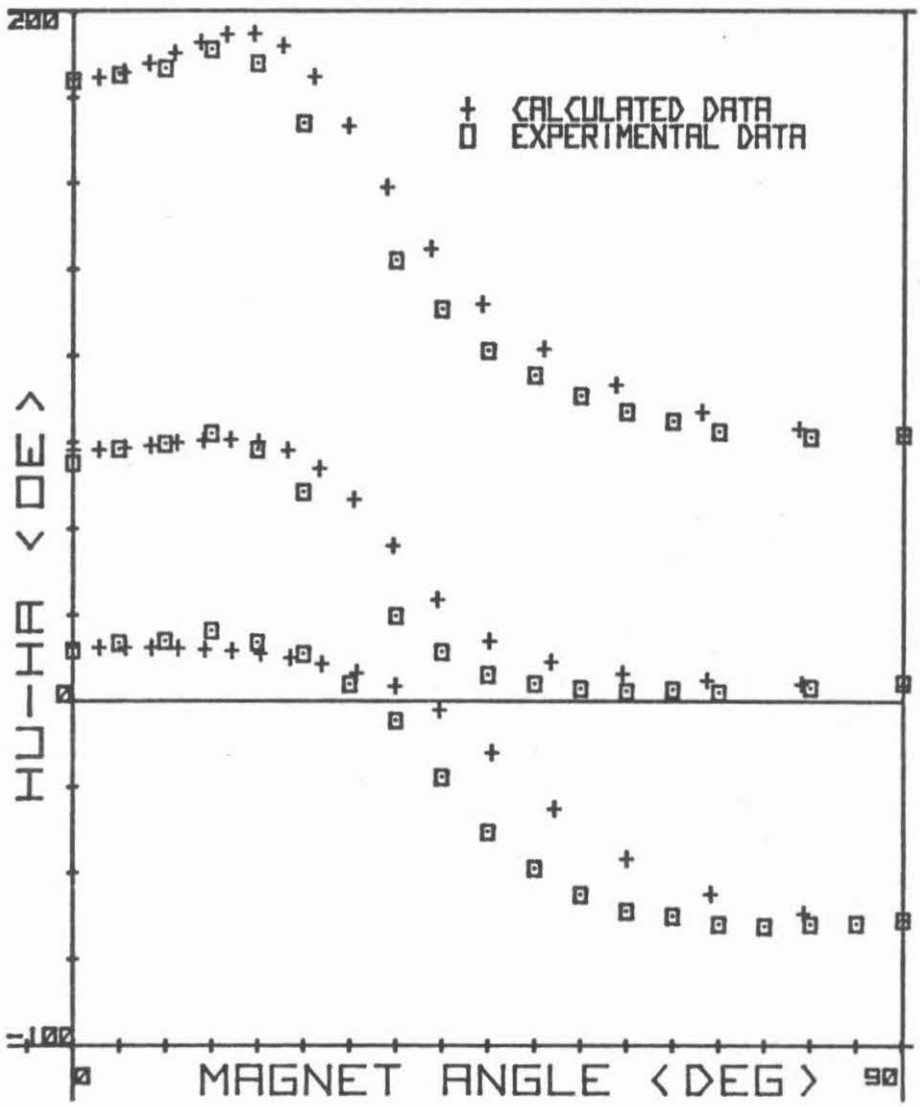

Fig. (6-3) The angle dependence of the magnetic field separation of the observed and calculated positions of the spinwave modes, HA, from the calculated positions of the uniform mode, HU, for sample CIT 2.

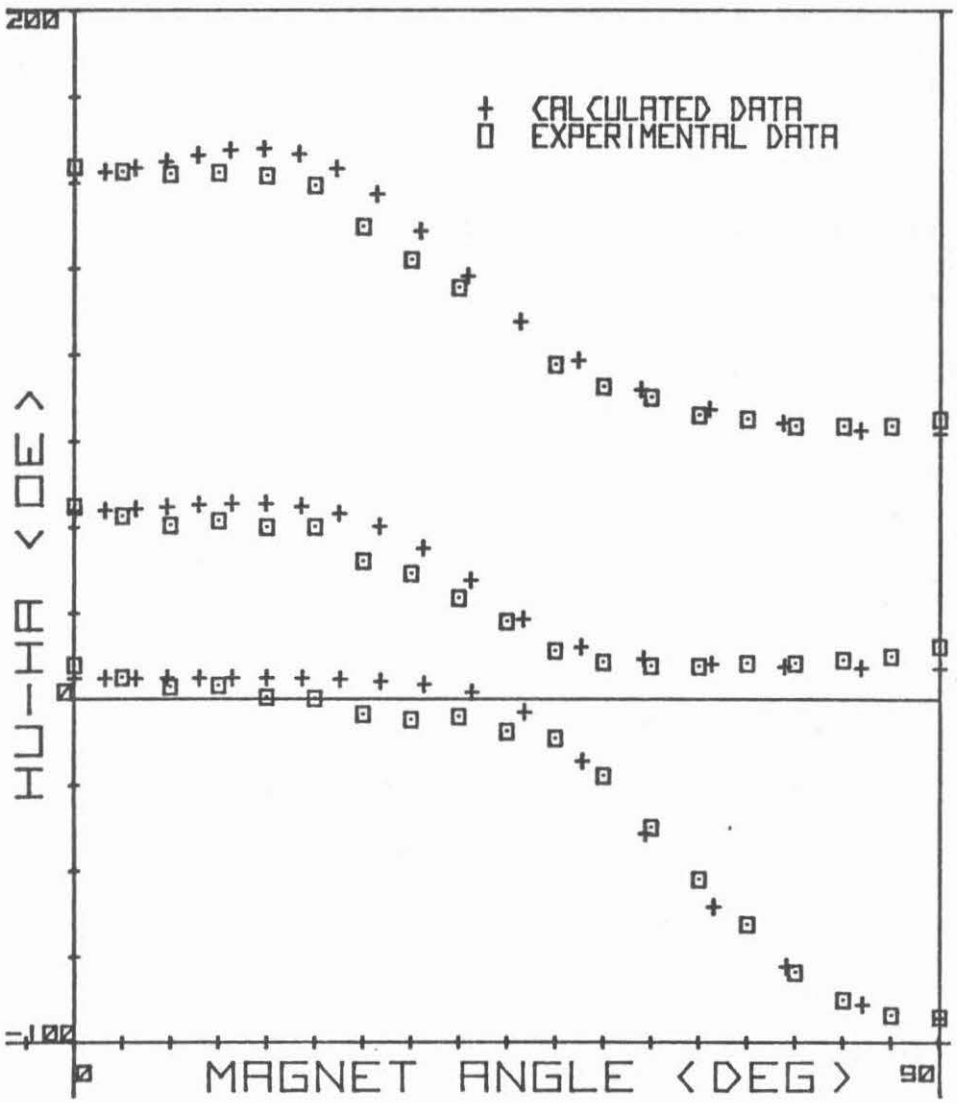

Fig. (6-4) The angle dependence of the magnetic field separation of the observed and calculated positions of the spinwave modes, HA, from the calculated position of the uniform mode,HU, for sample OSU 1.

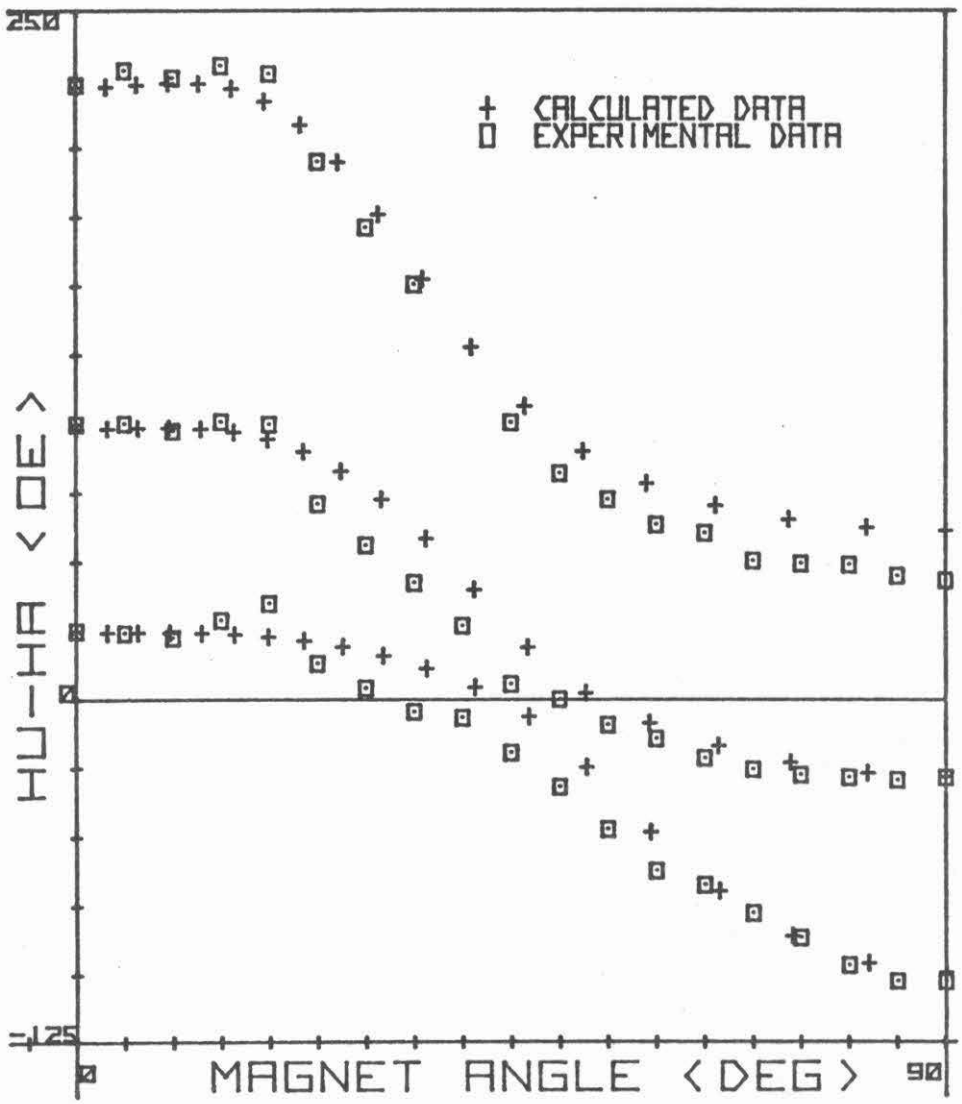

Fig. (6-5) The angle dependence of the magnetic field separation of the observed and calculated positions of the spin-wave modes, HA, from the calculated position of the uniform mode, HU, for sample OSU 2.

the experimental data from sample OSU 1 is shown for all models in Fig. (6-6). A first conclusion would be that nothing has been proven since all the models can be made to predict the same behavior; however, closer observation of Table (6-1) shows the following contradictory result in the cases of the tensorial and uniaxial models. The thickness required for two films with different annealing histories but initially from the same wafer are significantly different. Further, the thickness required to match the mode data in an annealed film is smaller (not larger) than that required for an unannealed film or film annealed at a lower temperature. Since this is such good evidence that the pinning cannot be due to a surface interaction of the type postulated, it is considered in greater detail below. Basically it is to be shown that the mode position data for samples OSU 1 and OSU 2 cannot be matched with reasonable accuracy if OSU 2 is required to be of equal or greater thickness than OSU 1. The mode spacings at perpendicular resonance simply will not allow it. Similar arguments can be made for the two CIT films. The perpendicular uniaxial model will be used for this discussion; however, since $K_{\perp}$ and $K_{\parallel}$ are related via the critical angle similar statements can be made for the tensorial model. For sample OSU 2 the two surface energies were chosen to match the field position of the two parallel resonance surface modes; this match actually has only a slight dependence upon the thickness of the film. The film thickness was then chosen to match the separation of the perpendicular resonance modes. Is it possible to match the OSU 1 data with this

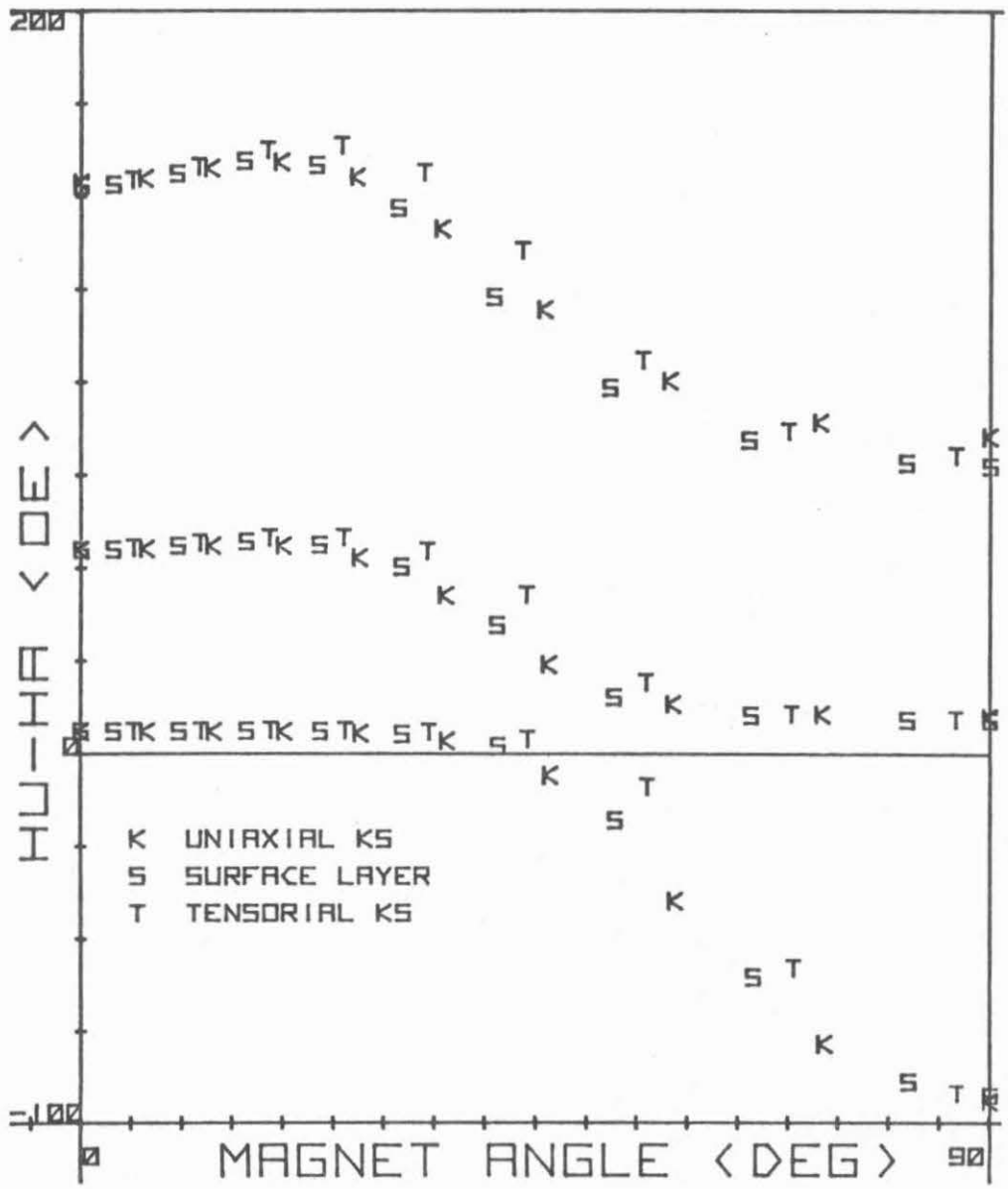

Fig. (6-6) A comparison of the calculated angle dependence of the magnetic field separation of spinwave modes from the uniform mode for the surface layer, uniaxial anisotropy, and the tensorial anisotropy models for sample OSU 1.

thickness? For sample OSU 1 the value of K_{s1} at one surface was determined by matching the position of the surface mode at parallel resonance (again this is nearly independent of film thickness). Using this value and K_{s2}= 0 at the other surface, and the above thickness, the separation of the perpendicular resonance modes from the uniform mode is 7.4, 66.6 and 186.8 Oe. Note that these are not near the experimental values of 9, 56 and 154.5 Oe. If K_{s2} is greater than zero the separation at the higher order modes is greater than above. If K_{s2} less than zero the higher order mode separations can be reduced but a perpendicular resonance surface mode is produced; this was not experimentally observed. The only way to obtain complete agreement is to increase the thickness. Conversely, if the film with two surface modes had the thickness which gives a good fit for OSU 1, then the mode spacings for OSU 2 at perpendicular resonance are 19.6, 80.3, 186.0, which is not in agreement with the experimental values of 25.1, 100.1, 223.1. Considering the accuracy of the experimental measurements, these differences are very large.

The above suggests that the tensorial and uniaxial models can at best represent some sort of averaging of the surface layer properties; this was initially proposed by Bajorek and Wilts (1971). In section (3.3.3) it was pointed out that the surface layer and uniaxial anisotropy have similar properties if K_s is determined from Eq. (3-19) and the film thickness, d, is determined by requiring the total magnetization in the two models to be the same. Table (6-1) gives a comparison of this K_s and thickness with the K_s and thickness required to

match the experimental data. Note that the agreement is good for the films with thin layers while for the films with thicker layers the agreement is not necessarily good at all.

6.3 Comparison of Spinwave Mode Intensity and Linewidth Data

Experimentally it is observed that the linewidth of the surface modes is typically wider than the other resonance modes. For sample CIT 1 the surface mode linewidth is larger by as much as a factor of two. Using the theory presented in Chapter 4 the observed spinwave mode intensity and linewidth variation can be explained if the damping parameter, α_s, of the surface layers is assumed larger than the damping parameter in the bulk of the material. Two experimental facts from earlier work support this assumption. First, the resonance linewidth of rare-earth substituted garnets ("bubble materials") can be many times (20-100) larger than that observed in good YIG films. Secondly, the resonance linewidth of films irradiated with He^4 ions (Stakelon et al (1975)) is wider than the linewidth of non-irradiated films. Therefore, disordering of the lattice (ion implantation) and impurity substitution ("bubble materials") both apparently increase the losses. Since the surface layers are believed caused by either a diffusion (impurity substitution) process or by lattice disordering (ion implantation) the assumption that $\alpha_b/\alpha_s < 1$ is plausible.

For sample CIT 1 the ratio $\alpha_b/\alpha_s = .3$ was required to match the linewidth variation observed at perpendicular resonance. With this ratio the theory also gives reasonable quantitative agreement (Table 6-2) for the intensity and linewidth variation in the two observed modes at all angles where the mode position is accurately matched (see Fig. 6-2). If the experimental and calculated data are compared

based upon mode separation from the uniform precession mode, then there is reasonable quantitative agreement for all angles. For comparison, calculated data using the uniaxial model are also provided in Table (6-2). Note, this model does not qualitatively match the experimental data and cannot unless an additional mechanism is postulated at the surfaces; the same comments are true of the tensorial model.

For the annealed [111] oriented film (sample CIT 2) even better results were obtained as shown in Table (6-3). At angles where the calculated and experimental field positions match (Fig. (6-3)), the linewidth and intensity data (calculated and experimental) are again in good agreement if $\alpha_b/\alpha_s = .54$ in the 700 Å layer and $\alpha_b/\alpha_s = .9$ in the 200 Å layer. Data from the uniaxial model are also provided for comparison. The uniaxial model shows no difference in linewidth between the surface and body modes and the mode intensities are in poor agreement with the experimental results. Note that at perpendicular resonance orientation the second mode is smaller than the third for both models; this is expected since the second mode is quasi-antisymmetric and should be smaller than the quasi-symmetric third mode. For this sample (CIT 2), absorption derivative curves were shown earlier in Fig. (1-2) for eight angular orientations.

6.4 Comparison of Temperature Dependence Data

The temperature dependence of the critical angle and the parallel resonance spectrum have been reported by Yu et al (1975). Measurements were made with films that showed both one and two parallel resonance surface modes at room temperature; these cases will be discussed

TABLE (6-2)

For film properties see Table (6-1) sample CIT 1.
All amplitudes given below are normalized to 100% for the largest amplitude mode.

Angle	Surface Layer				Uniaxial Anisotropy				Experimental			
	ΔH		% Amp		ΔH		% Amp		ΔH		% Amp	
	1	2	1	2	1	2	1	2	1	2	1	2
0	11.5	5.7	25.6	100.	5.7	5.7	50.2	100.	11.6	5.7	15.4	100.
10	11.9	6.2	31.8	100.	6.1	6.1	62.1	100.	11.1	5.8	22.0	100.
15	@	@	@	@	@	@	@	@	8.1	5.8	90.9	100.
20	12.0	7.4	74.6	100.	7.1	7.0	100.	71.9	6.9	6.9	100.	11.
30	9.2	7.7	100.	7.4	7.5	6.9	100.	6.7	7.0	a	100.	a
40	8.0	@	100.	.03	7.2	a	100.	a	7.5	a	100.	a
50	7.1	7.5	100.	.31	6.7	@	100.	.3	7.2	7.2	100.	.7
60	6.5	6.5	100.	2.5	6.3	@	100.	1.1	7.0	6.9	100.	1.3
70	6.1	6.3	100.	3.0	5.9	5.3	100.	2.7	6.3	6.3	100.	1.7
80	5.9	6.2	100.	3.3	5.7	5.2	100.	3.0	5.4	5.4	100.	2.1
90	5.8	6.2	100.	3.8	5.6	5.2	100.	3.0	5.4	5.4	100.	2.1

@ not determined

a not observed

TABLE (6-3)

Angle	Surface Layer Model						Uniaxial Model						Experimental					
	ΔH			% Amp			ΔH			% Amp			ΔH			% Amp		
	1	2	3	1	2	3	1	2	3	1	2	3	1	2	3	1	2	3
0	5.7	5.7	5.9	100.	2.9	6.3	5.7	5.6	5.6	100.	2.0	4.5	5.7	@	@	100.	1.0	3.0
10	6.1	6.2	6.5	100.	2.3	5.9	6.1	6.0	6.1	100.	2.3	4.0	5.9	@	@	100.	1.0	2.0
20	7.1	7.3	8.0	100.	4.9	4.5	7.0	6.9	7.2	100.	2.9	2.5	7.3	7.6	@	100.	3.0	2.0
30	7.6	8.1	9.0	100.	4.1	1.2	7.4	6.9	7.5	100.	1.6	.44	6.9	a	a	100.	a	a
40	8.1	a	8.4	100.	0.	.04	7.1	@	7.1	100.	1.0	.22	6.9	6.9	@	100.	24.0	1.4
50.	9.0	7.1	7.4	100.	59.4	3.5	6.6	6.6	6.7	100.	34.3	2.3	8.0	6.9	6.6	100.	91.7	5.5
60	9.1	6.5	6.8	77.1	100.	7.1	6.1	6.2	6.2	100.	78.4	6.0	8.3	6.6	6.6	62.3	100.	7.6
70	8.9	6.1	6.4	58.6	100.	8.2	5.9	5.9	5.9	94.2	100.	8.8	8.9	5.8	6.6	45.0	100.	7.6
80	8.8	5.9	6.1	52.2	100.	8.8	5.7	5.7	5.7	82.3	100.	9.5	8.8	5.8	6.0	42.0	100.	9.1
90	8.7	5.8	6.0	50.5	100.	9.0	5.6	5.6	5.6	79.5	100.	10.	8.8	5.8	5.8	42.0	100.	8.7

@ not determined

a not observed

For film properties see Table (6-1) sample CIT 2
All amplitudes are normalized to 100% for the largest amplitude mode

individually below. The sample (OSU 3) with one parallel resonance surface mode was [100] oriented, .37 μm thick, and annealed at 1000° for 6 hours; this is not one of the films listed in Table (6-1). Upon lowering the temperature below 300°K, the parallel resonance surface mode increased in intensity while the body modes decreased; at a critical temperature the once surface mode presumably became a uniform precession mode and the other body modes were not excited. The position of the critical angle was observed to shift toward the parallel orientation (Fig. (6-9)) such that at the above critical temperature the critical angle was in the plane of the film. Below the critical temperature, Yu observed no critical angle or surface mode (i.e., only body modes were observed).

It has been pointed out in Chapter 3 that the uniaxial model is incapable of explaining these experimental results. The tensorial model can be made to match almost any variation but physical explanation of the variation in $K_{\parallel}$ and $K_{\perp}$ is not convincing. The degree to which the surface layer model predicts the above behavior is explored below. For the following reasons the temperature dependence calculation was made using the material constants associated with OSU 1:

1) Only the temperature dependence data were given for sample OSU 3, so that accurate material constants are not known.
2) The computer analysis showed that the temperature variation of the critical angle depends almost entirely on the magnetic characteristics of the film-substrate surface layer so that the difference in total thickness is unimportant.

3) The two samples had identical annealing histories: therefore, it is reasonable that the surface properties should be approximately the same.

4) The detailed temperature dependence of the interface layer magnetization can only be estimated in an approximate way.

Using the properties for the substrate-film layer given in Chapter 5 the temperature dependence was calculated roughly by holding M_{Fe} constant and increasing M_{Gd} linearly with decreasing temperature. In view of the largely qualitative nature of the comparison sought, a more accurate treatment of the temperature variation of M_{Gd} and M_{Fe} was not warranted.

Figures (6-7) and (6-8) show the calculated temperature dependence of the two highest field modes at parallel and perpendicular resonance; Fig. (6-9) shows the calculated temperature dependence of the critical angle. Note that the calculated and experimental data are in qualitative agreement down to the critical temperature where the critical angle is observed in the film plane, and the uniform precession mode is excited at parallel resonance. However, at a lower temperature or higher M_{Gd} the model predicts a phenomenon that was not observed by Yu, that is, a low temperature perpendicular resonance surface mode and associated critical angle (below 100° in Figs. (6-9) and (6-8)). It was speculated that this disagreement in experimental and predicted behavior was due to over-simplification of the model. In any real system, diffusion will not produce a uniform layer but rather an inhomogeneous region with a compensation layer that moves through

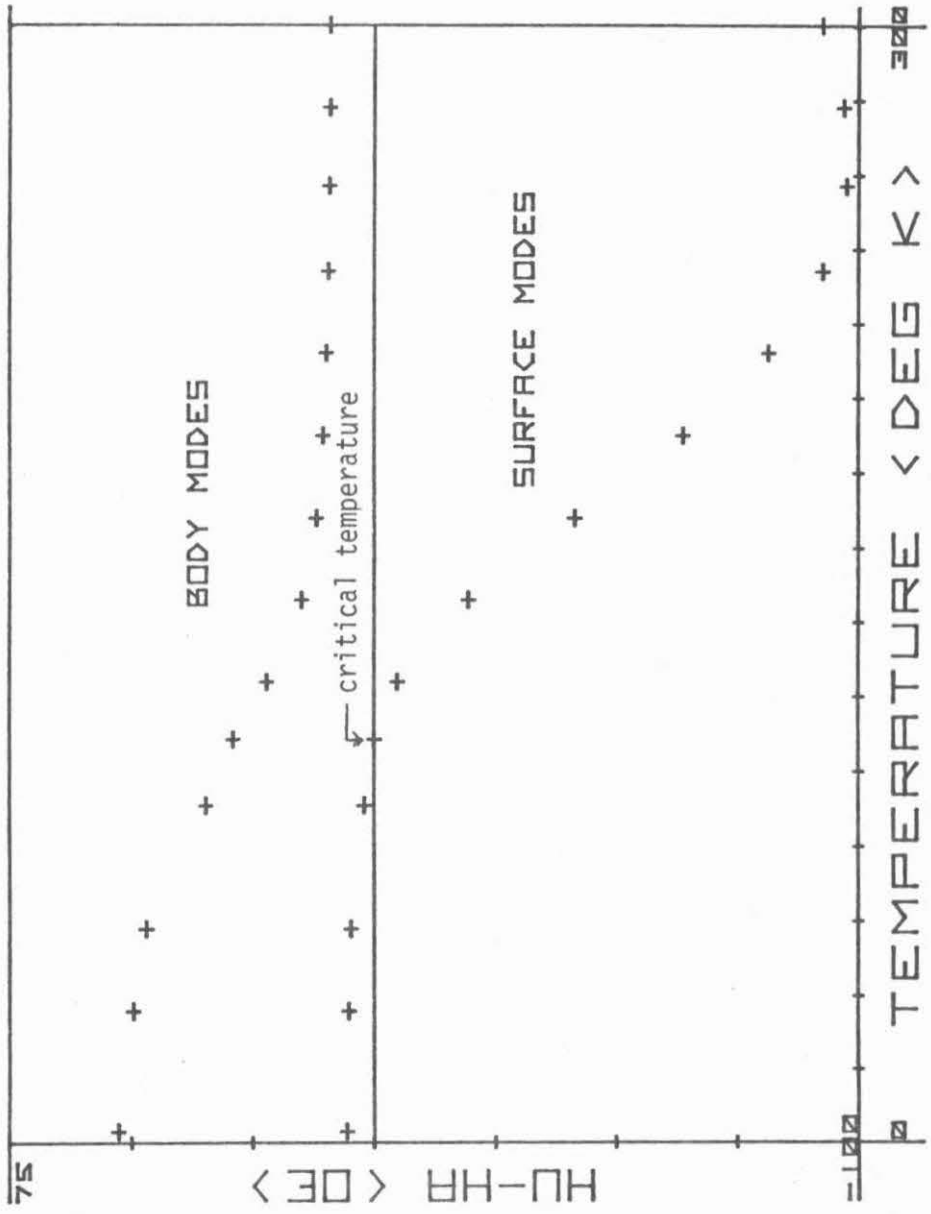

Fig. (6-7) The calculated temperature dependence of the magnetic field separation of the positions of two parallel resonance spinwave modes, HA, from the position of the uniform mode, HU, for sample OSU 1.

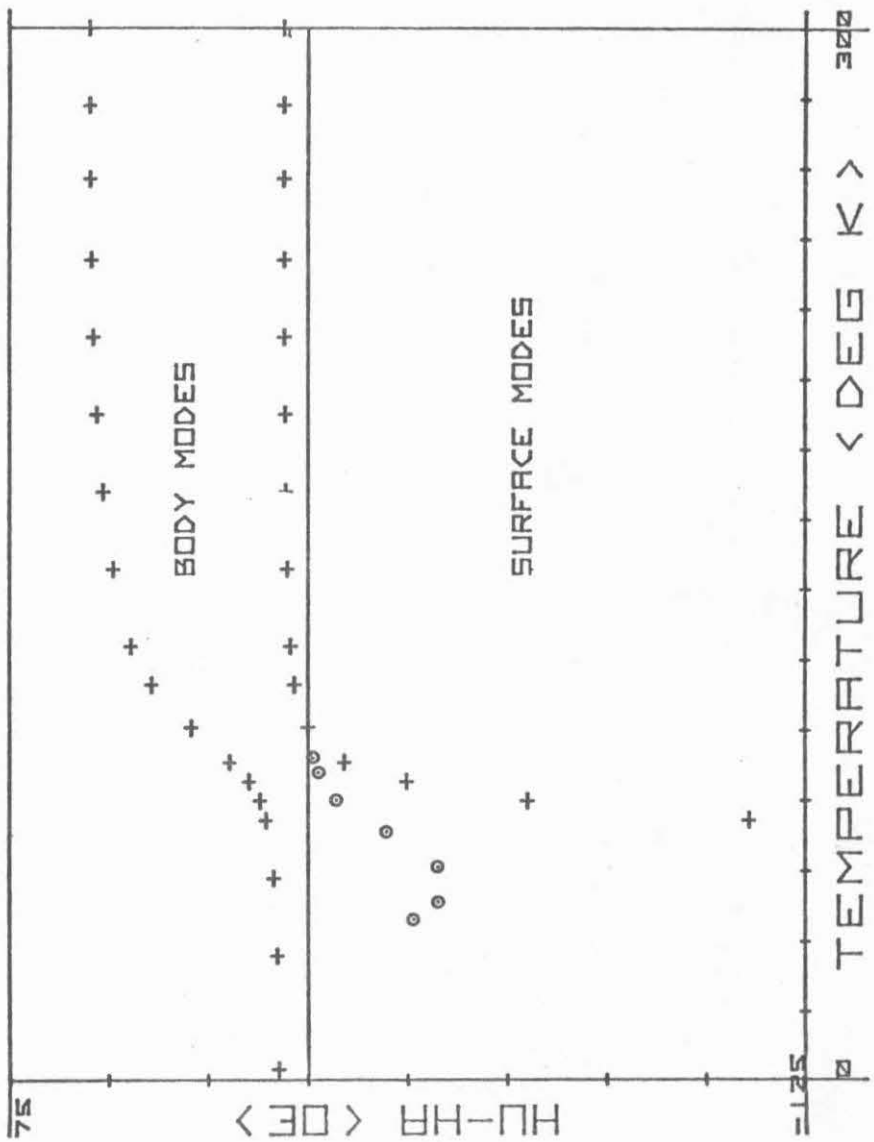

Fig. (6-8) The calculated temperature dependence (+) of the magnetic field separation of the positions of two perpendicular resonance spinwave modes, HA, from the position of the uniform mode, HU, for sample OSU 1. Rough positions of the surface mode observed with sample CIT 3 are also given (⊙).

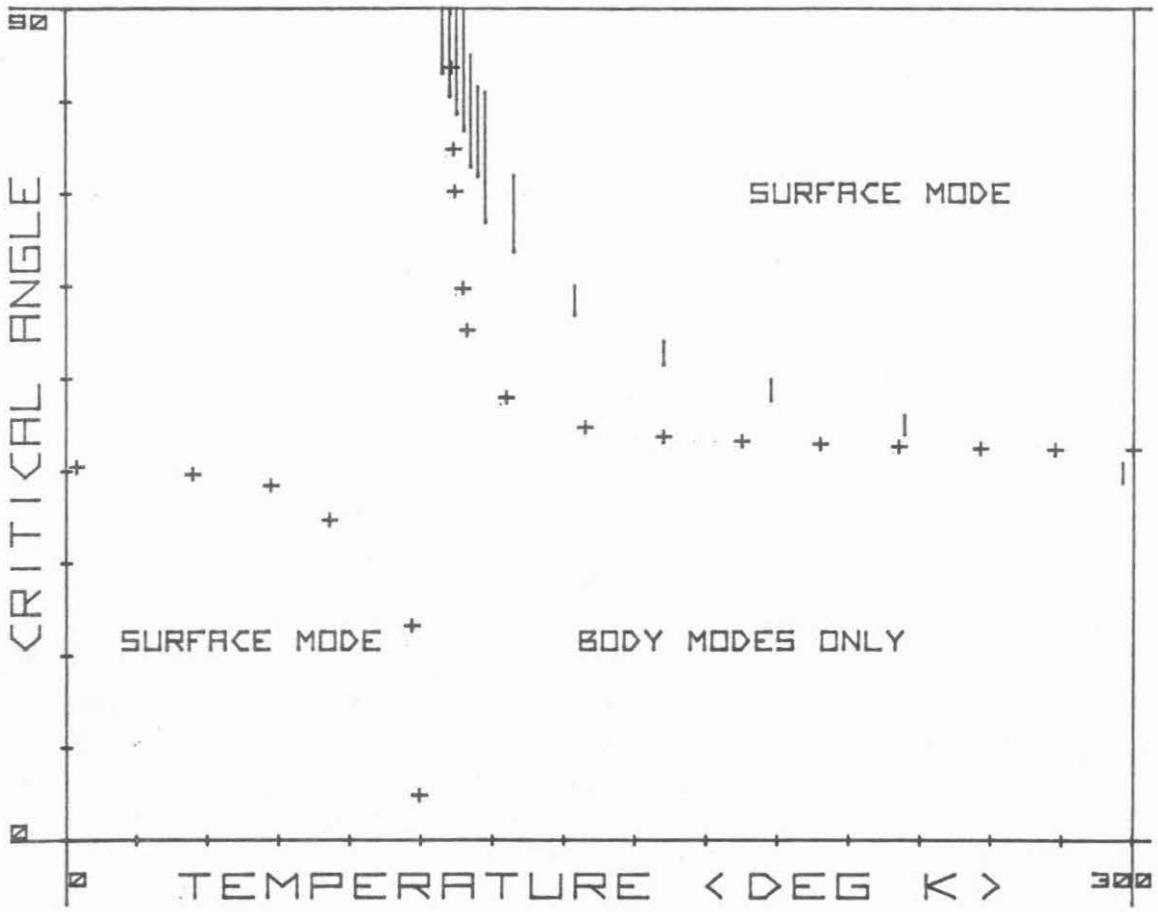

Fig. (6-9) The calculated temperature dependence of the critical angle for sample OSU 1, with the experimental data for sample OSU 3 (see text for properties of OSU 3)

it as the temperature changes. In order to try to understand the effects of nonuniformity, the interface region was represented by three adjacent surface layers of different thicknesses and different properties. Here the results were not entirely straightforward. Some geometries produced results similar to the above and others predicted completely different behaviors; however, in all cases, there was a low temperature perpendicular resonance surface mode. A final mathematical attempt involved integration of the equations of motion through the thickness of an inhomogeneous film at perpendicular resonance; this also predicted a low temperature perpendicular resonance surface mode.

In view of these results one therefore would expect a low temperature perpendicular resonance surface mode if the above assumptions are valid. Experimentally Yu and Wigen did not see such a mode; sample CIT 2 was carefully examined and showed no such mode. However, the expected mode was observed by Ramer and Wigen on a narrow linewidth, [111], LPE film annealed in a dry O_2 atmosphere for 6 hours (sample CIT 3). For this sample, the perpendicular resonance absorption derivative curves at six temperatures between 90° and 50°K are shown in Fig. (6-10); note the clear indication of the surface mode below 80°K. It was confirmed by etching away the outer surface that this mode was associated with the film substrate interface. In spite of this apparent agreement, an inconsistency between the surface layer model and the data was noted. This is shown in Fig. (6-8) where the observed surface mode resonant field for sample CIT 3 is roughly plotted versus temperature for comparison with the predicted behavior

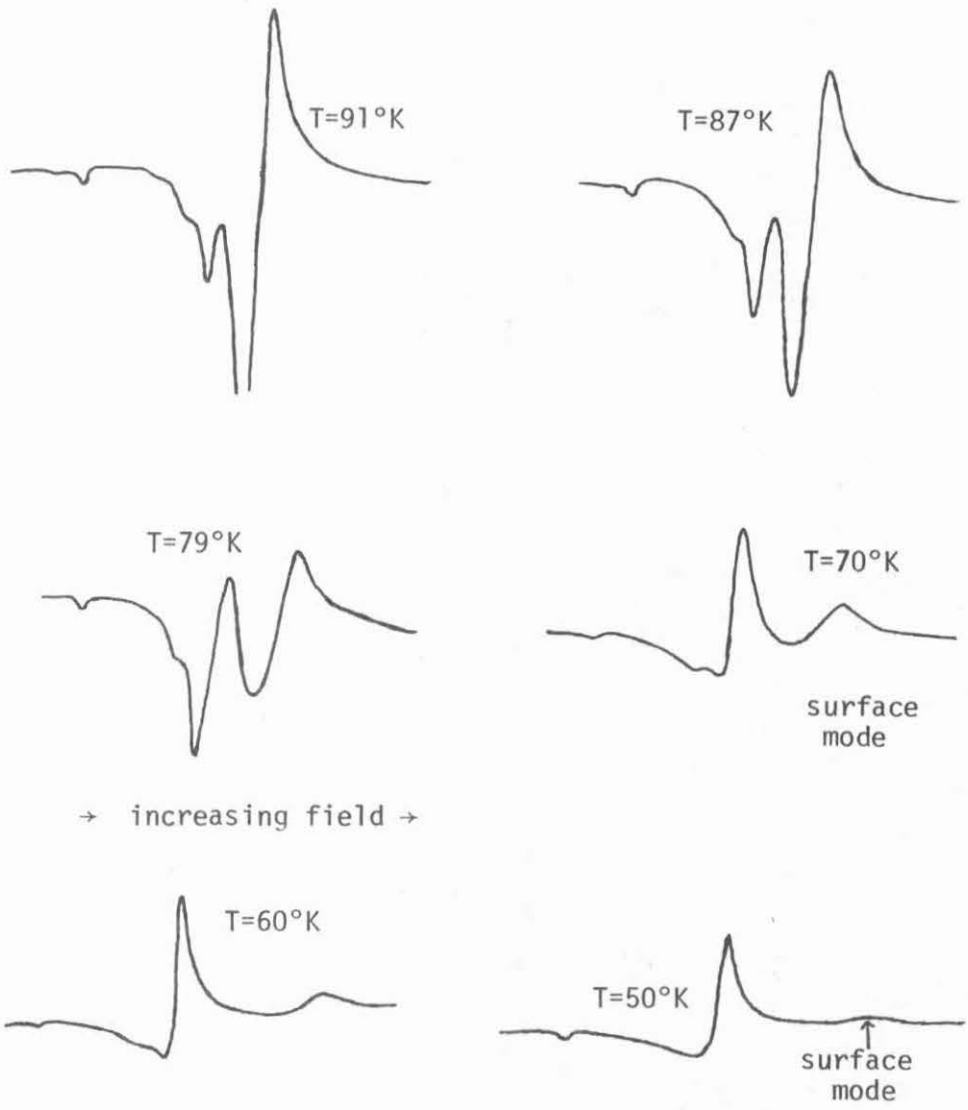

Fig. (6-10) Derivative absorption curves at six temperatures taken at perpendicular resonance for sample CIT3. The curves show the formation of the perpendicular resonance surface mode and that it has almost vanished at T=50°K.

for sample OSU 1. The experimentally observed mode does not continue to shift in field position as predicted by the model. Further from Fig. (6-10) it can be seen that with decreasing temperature the mode decreases in intensity; it was not detected at temperatures below 43°K. This rapid decrease in intensity would be expected if the mode continued to move away from the uniform mode as predicted by the model, but it would not be expected if the mode remained roughly stationary as indicated by the experimental data.

If the surface layer model is to represent the experimental data at low temperatures, some other cause must be found to account for the behavior observed. There is one mechanism at low temperatures that has not yet been considered. In the analysis the net magnetization on the surface side of the compensated region was assumed aligned anti-parallel to the magnetization in the bulk of the film, this alignment being due to exchange interaction between neighboring Fe sites. Since exchange is not the only torque acting on the magnetization, complete alignment may not be achieved and some sort of quasi-domain wall may be generated; the effects of such a quasi-wall on the resonance boundary conditions are unknown and not easily calculated.

The temperature dependence of the parallel resonance mode spacings for a film with two surface modes as measured by Yu is shown if Fig. (6-11). Since there is some question about the interpretation of this data, the following quotation is extracted from their paper. "Without exception, it is found that the high-field surface mode, the quasi-symmetric surface mode, is observed

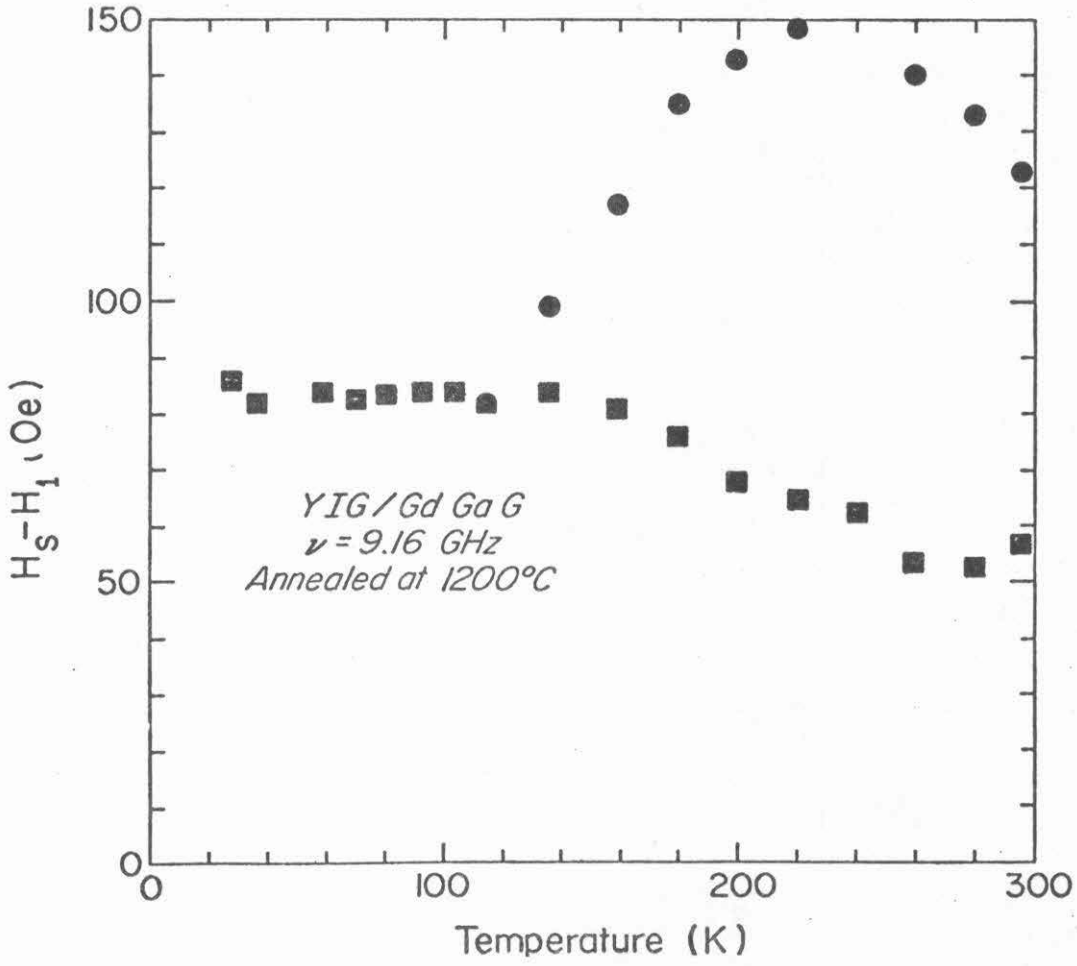

Fig. (6-11) Separation of the first body mode and the first and second surface modes, respectively, at parallel resonance as a function of temperature for a YIG film annealed at 1200°C. After Yu et. al. (1975)

to shift downward and becomes degenerate with the low-field surface mode.. The data points are the resonance-field separations between the two surface modes and the first body mode. At a temperature near 100°K, these two surface modes become degenerate in their resonance-field positions. Below this temperature, this surface mode is observed to appear at a nearly constant field separation above the first body mode."

Physical data for this film is not given, but it is believed similar to OSU 2 except for somewhat greater thickness. For the same reasons that OSU 1 was used in the calculations for temperature dependence, OSU 2 is used here; this dependence is shown in Fig. (6-12). In this figure the mode positions with respect to the uniform mode position have been computed and plotted assuming that the properties of the air-film interface are constant. Note that the behavior for the higher temperatures is in qualitative agreement with the above; that is, the quasi-symmetric mode increases in field position away from the body modes then "shifts downward". However, at the lower temperatures the two surface modes are not degenerate. It has been pointed out earlier that the surface layer model does not predict the low temperature behavior accurately. This is believed due to the supposed invalid approximation of anti-parallel spins in the diffusion region. If this is indeed true for the diffusion region produced by annealing at 1000°K then it probably has a larger effect on films annealed at 1200°K; that is, the diffusion region is thicker and closer to the thickness of a typical domain wall ($\sim$ 1500Å in YIG). In any event, the following may explain some of the

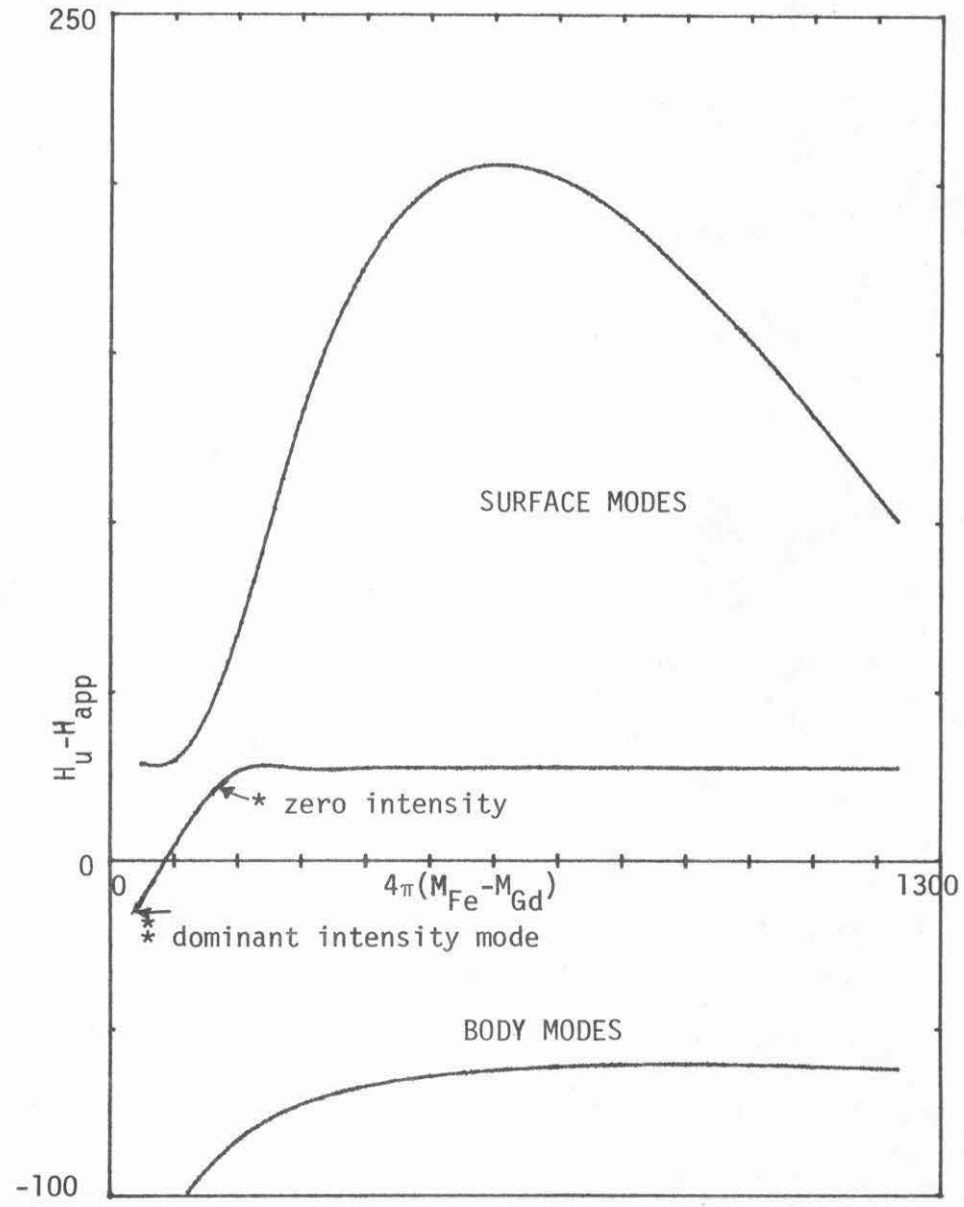

Fig. (6-12) The calculated temperature dependence of the magnetic field separation of the positions of three parallel resonance spin wave modes, H_{app}, from the position of the uniform mode, H_u, for sample OSU2.

discrepancy between the above calculations and the description of the experimental data; however, it is speculation! In Figs. (6-11) and (6-12) the second mode is a quasi-antisymmetric mode. It can be shown that at the position marked by a * this mode is nearly antisymmetric and has at most a very small excitation. Within the temperature range $*-_{*}^{*}$ in Fig. (6-12) this quasi-antisymmetric mode grows in intensity and becomes a large absorption mode. Therefore, a similar transition from surface mode to nearly vanishing antisymmetric surface mode to large body mode in a small temperature range may have resulted in a misinterpretation of the experimental data. If the air-film interface also has properties dependent on temperature as has been observed by Omaggio (1974) at perpendicular resonance the behavior might be even more complicated and difficult to interpret.

6.5 Comparison of Frequency Dependence Data

The frequency dependence of the experimental mode positions is dependent on the orientation angle of the applied field. At perpendicular resonance there is little dependence. For ion implanted films at perpendicular resonance Omaggio and Wigen (1974) reported no frequency dependence at room temperature. The uniaxial and tensorial models predict no frequency dependence at perpendicular resonance. The surface layer model contains a frequency dependence at perpendicular resonance if the gyromagnetic ratio of the bulk and surface regions are different; however, this effect is smaller than the experimental resolution.

At any other angle the experimental data show a frequency dependence. The parallel resonance configuration was chosen for comparison because the equilibrium position of $\overline{M}_o$ is not a function of the applied field strength. The largest observed effect was in the position of the parallel resonance surface mode. The measured mode separations at 6 and 25 GHz for sample CIT 2 are presented in Table (6-4). The calculated separations for the surface layer and uniaxial models are also given. Note that both models predict the experimental behavior; this is not surprising considering the agreement shown in Fig. (3-11) between K_s and the surface layer with $\gamma_b = \gamma_s$. The tensorial model has no frequency dependence, unless $K_{||}$ or $K_{\perp}$ has a frequency or field dependence.

6-6 Discussion and Conclusions

The data presented in this thesis are believed to show the following:

1. The observed phenomena cannot be explained by the uniaxial and tensorial models.
2. The observed phenomena are explained by surface regions with magnetic properties different from the bulk properties. These regions were approximated by uniform surface layers. In the case of low temperatures where the model predicts behavior which is not observed, it is believed that other assumptions made to facilitate computations are not valid.

The extent to which each of the three models predicts the experimental data is summarized below. Also discussed is the microscopic

TABLE (6-4)

Parallel Resonance	Experimental		Calculated Surface Layer		Calculated Uniaxial	
	5.966 GHz	25 GHz	5.966 GHz	25 GHz	5.966 GHz	25 GHz
surface mode-1st body mode	69.	101.3	68.3	100.1	69.2	101.6
1st body mode-2nd body mode	71.9	70.7	72.5	70.7	79.5	77.3
Perpendicular Resonance						
1st body mode-2nd body mode	54.3	53.3	57.2	57.3	51.7	51.7
1st body mode-3rd body mode	165.2	160.0	164.5	165.0	151.2	151.2

SAMPLE CIT 2

model for the tensorial surface anisotropy field at the film-substrate interface proposed by Wigen and Puszkarski (1976).

The perpendicular uniaxial anisotropy has been used by many workers to match experimental data in metal films. In these films this model and the surface layer model cannot be distinguished. In permalloy a 22Å half magnetization surface layer is equivalent to a K_s = .22 ergs/cm^2; this represents a significant anisotropy and an insignificant (11Å) change in the total film thickness. However, YIG samples cut from the same wafer but with different annealing histories must have significantly different thicknesses when this model is used to match the experimental data; for example, the thickness required for an annealed sample is as much as 400Å thinner than that required for an unannealed sample or sample annealed at a lower temperature (see Table (6-1)). This thickness difference cannot be understood in terms of a surface interaction alone. In addition to the above, this model cannot explain the following phenomena.

1) Temperature dependence of the critical angle (see Fig. (3-13)).
2) The observed linewidth and intensity variation with mode number and orientation of the applied field (see Tables (6-2) and (6-3)).

This model does, however, predict the observed room temperature frequency dependence if the values of K_s and film thickness are chosen to match the spectra at one frequency (see Table (6-4)).

The tensorial model was proposed by Yu et al (1975); in effect this model is a generalization of the Puszkarski (1970) model which assumes the surface spins are affected by a surface field that is independent of the magnetization. The tensorial model assumes a surface anisotropy field dependent on the mean orientation of the magnetization, but not on the instantaneous orientation. As in the case of the uniaxial anisotropy this model cannot explain why the required thickness for an annealed sample is as much as 400Å thinner than that required for an unannealed sample or sample annealed at a lower temperature (see Table (6-1)). In addition to the above, this model does not explain the observed linewidth and intensity variation with mode number and orientation of the applied field (see section (6-3)). This model can be made to match the observed frequency dependence and the variation of the critical angle with temperature; however, these are not physically meaningful unless some understanding of the origin of $K_{\perp}$ and $K_{||}$ is established. Wigen and Puszkarski (1976) proposed a microscopic model for $K_{\perp}$ and $K_{||}$ that combines two independent mechanisms. The first mechanism involves an isotropic static mean field interaction between the Gd^{3+} and Fe^{3+} cations in a diffusion region at the film substrate interface; this field is dependent on the temperature and applied field. The second field arises from a uniaxial energy in the Hamiltonian which is proportional to $\langle(\bar{S}\cdot\bar{n})^2\rangle$; it is proposed that this term is due to Fe^{2+} interacting with strong crystal field gradients at the interface. The latter anisotropy is considered independent of the temperature and

applied field. The isotropic term increases in magnitude with decreasing temperature. Therefore, the desired temperature dependence of $K_{\perp}$ and $K_{||}$ is qualitatively generated. To explain the effects of changing the frequency on the spectra, it was proposed that the isotropic term was field dependent. The hypothesis that Fe^{2+} is present at the surfaces was tested (Wigen et al (1976)) by observing a photo-induced change in the spectrum of a film at low temperatures (less than 100°K); in view of the effects observed in Si^{4+} doped YIG (Gyorgy et al (1970)) this is considered good evidence for the presence of Fe^{2+}. Assuming that the effects of the surface regions are lumped into $K_{\perp}$ and $K_{||}$, I feel that this model cannot be correct for the following reasons:

1) Only the static effects of the above mechanisms are included. The dynamic effects are not second order and unimportant. For example, if the assumed tensorial field depends on the instantaneous position of the magnetization the boundary conditions on $\overline{m}$ are changed and are in fact identical to that of the perpendicular uniaxial anisotropy with $K_s = K_{||} - K_{\perp}$ (see Appendix I).
2) If an interaction between the Fe^{3+} and Gd^{3+} exists it has to be in a finite region; the material in this region will be ferrimagnetic and should be treated dynamically as such.
3) The Fe^{2+} is probably distributed throughout the surface region; therefore, the plausible effect is an anisotropy like that observed in bulk materials. A temperature dependence is strongly suggested by the photo-induced effects (i.e., if

white light can change the effect then thermal agitation probably can).

The effects of inhomogeneous films have been considered by many workers at perpendicular resonance (Portis (1964), Sparks (1970), Bajorek and Wilts (1971)); however, due to the mathematical complications, work at the other angles has been limited. In this thesis the effects of inhomogeneous surface regions are considered by assuming uniform surface layers with properties that are averages of the actual properties. The results from this model are summarized below:

1) The film thickness required for an annealed sample is slightly greater than the thickness required for an unannealed sample or sample annealed at a lower temperature (samples cut from the same wafer). This is consistent with a diffusion process (see Table (6-1)).
2) The linewidth and intensity variation with mode number and orientation can be explained by making the plausible assumption that the surface layer has a larger damping constant than the bulk (see Tables (6-2) and (6-3)).
3) The room temperature frequency dependence of this model is the same as experimentally observed (see Table (6-4)).
4) The temperature dependence of the critical angle is qualitatively explained down to the critical temperature (see Fig. (6-10)). The temperature dependence of the surface mode spacings are qualitatively explained down to the critical temperature (see Figs. (6-11) and (6-12)). Below the

critical temperature the assumptions that the magnetization in the surface regions is anti-parallel to the magnetization in the bulk is believed invalid.

5) Although not addressed explicitly, the effects of Fe^{2+} can easily be incorporated into the surface layer model by an additional anisotropy like that observed in bulk materials.

Below the critical temperature a significant portion of the diffusion region is believed to have a magnetization that has passed through compensation. If exchange was the only torque exerted on the spins the above magnetization would be anti-parallel to the magnetization in the bulk. However, a variation in direction is believed to exist producing a quasi-domain wall; the effects of this variation are not known. It is therefore apparent that more work is necessary before all resonance phenomena in YIG films are fully understood. This thesis has introduced a model which may explain the origin of many of these phenomena; the phenomena not explained are believed to be due to mechanisms (like the variation in the direction of M mentioned above) which are not easily incorporated into the computations.

REFERENCES

Akhiezer, A. I., Bar'yakhtar, V. G., and Kaganov, M. I., Soviet Phys. Uspekhi 3, 567 (1961)

Ament,W. S., and Rado, G. T., Phys. Rev. 97, 1558 (1955)

Bailey, G. C., and Vittoria, C., Phys. Rev. B 8, 3247 (1973)

Bajorek, C. H., and Wilts, C. H., J. Appl. Phys. 42, 4324 (1971)

Brown, S. D., Henry, R. D., Wigen, P. E., and Besser, P. J., Solid State Comm. 11, 1179 (1972)

Calhoun, B. A., Smith, W. V. and Overmeyer, J., J. Appl. Phys. 29, 427 (1958)

Geller, S., J. Appl. Phys. 31, 30S (1970)

Gilleo, M. A., Geller, S., Phys Rev. 110, 73 (1958)

Gyorgy, E. M., Sturge, M. D., Van Uitert, L. G., Heilner, E. J., and Grodkiewicz, W. H., J. Appl. Phys. 44, 438 (1973)

Gyorgy, E. M., Dillon, Jr., J. F., Remeika, J. P., I.B.M. J. of Research 14, 321 (1970)

Henry, R. D., Besser, P. J., Heinz, D. M., and Mee, J. E., IEEE Transactions 9, 535 (1973)

Kittel, C., Phys. Rev. 110, 1295 (1958)

Kobayashi, T., Barker, R. C., Bleustein, J. L., and Yelon, A., Phys. Rev B 7, 2373 (1973)

Landau, L. and Lifshitz, E., Physik Zeits. Sowjetunion 8, 153 (1935)

Liu, Y. J., Ph. D. Thesis Yale U. (1974)

Macdonald, J. R., Ph. D. Thesis, Oxford U. (1950)

Morrish, A. H., The Physical Principles of Magnetism, John Wiley and Sons, New York (1965)

Omaggio, J. and Wigen, P. E., AIP Conf. Proc. 24, 125 (1974)

Pauthenet, R., Ann Phys. (Paris) 3, (1958)

Portis, A. M., Appl. Phys. Letters 2, 69 (1963)

Puzkarski, H., Acta Phys. Pol A 38, 217 (1970);38 , 899

Ramer, O. G., and Wilts, C. H., Phys. Stat. Sol. (b) 73, (1976)

Rosencwaig, A.,Tabor, W. J., and Pierce, R. D., Phys. Rev. Lett. 26, 779 (1971)

Sparks, M., Phys. Rev. B 1, 3831 (1970); 1, 3856 (1970); 1, 3869 (1970)

Stakelon, T. S., Yen, P., Puszkarski, H., Wigen, P. E., AIP Proceedings of the 21st Conference on Magnetism and Magnetic Materials (1976)

Stakelon, T. S., Annual Report, Ohio State Univ. NSF Report #4, RF project 3457 (1975)

Vittoria, C.,Ph. D. Thesis, Yale U. (1970)

Wangsness, R. K., Phys. Rev. 91, 1085 (1953); 93, 68 (1954); Am. J. Phys. 24, 60 (1956)

Wigen, P. E., Stakelon, T. S., Puszkarski, H., Yen, P., AIP Proceedings of the 21st Conference on Magnetism and Magnetic Materials (1976)

Yelon, A., Spronken, G., Bui-Thieu, T., Barker, R. C., Liu, Y. J., and Kobayaski, T., Phy. Rev. B 10, 1070 (1974)

Yu, J. T., Turk, R. A., Wigen, P. E., Phys. Rev. 11, 420 (1970)

Appendix I

I-1. Discussion of YIG Anisotropies and the Equilibrium Conditions on $\overline{M}_o$

The equations which describe the effects of anisotropies on the resonance process are given by Eq. (2-10) in terms of the anisotropy energy. The dominant anisotropies in YIG films are the cubic crystalline anisotropy and magnetostrictive anisotropy. The effects of the crystalline anisotropy in YIG are well described in terms of the standard first order expansion of the direction of $\overline{M}$ (i.e. $K_1 >> K_2$). The crystalline anisotropy energy is usually written in terms of the direction cosines of $\overline{M}$ from the cubic axes

$$E_A = K_1 [\alpha_1^2\alpha_2^2 + \alpha_2^2\alpha_3^2 + \alpha_3^2\alpha_1^2] + K_2 [\alpha_1^2\alpha_2^2\alpha_3^2] \quad \text{I-1}$$

When written in terms of the spherical polar coordinates of the text, the expression is different for different film orientations. For the K_1 term and the [100] oriented films

$$E_A = \frac{K_1}{2} [\sin^4\theta \sin^2 2\phi + \sin^2 2\theta] \quad \text{I-2}$$

For the [111] oriented films with ϕ measured from a $(\overline{11}2)$ axis

$$E_A = K_1 [\frac{\sin^4\theta}{4} - \frac{\sqrt{2}}{3} \sin^3\theta \cos\theta \cos 3\phi + \frac{\cos^4\theta}{3}] \quad \text{I-3}$$

If the tension is along the film normal, it is shown below that for the [100] and [111] oriented films the magnetostrictive anisotropy is uniaxial with easy or hard axis normal to the film plane. With the tensor components of the tension given by $\sigma_{ij}=\sigma\gamma_i\gamma_j$ (the direction cosines of the tension are γ_1, γ_2, γ_3), the magnetostrictive energy is (Morrish (1965))

$$E_M = \frac{-3}{2}\lambda_{100}\sigma\,(\alpha_1^2\gamma_1^2 + \alpha_2^2\gamma_2^2 + \alpha_3^2\gamma_3^2) - 3\lambda_{111}\sigma\,(\alpha_1\alpha_2\gamma_1\gamma_2 + \alpha_2\alpha_3\gamma_2\gamma_3 + \alpha_3\alpha_1\gamma_3\gamma_1) \qquad \text{I-4}$$

For the [100] oriented films and $\gamma_3=1$, $\gamma_1=\gamma_2=0$

$$E_M = \frac{-3}{2}\lambda_{100}\sigma\alpha_3^2 = \frac{-3}{2}\lambda_{100}\sigma\cos^2\theta \qquad \text{I-5}$$

For the [111] oriented films and $\gamma_1=\gamma_2=\gamma_3=1/\sqrt{3}$ the non-isotropic terms of the energy are

$$E_M = -\lambda_{111}\sigma\,(\alpha_1\alpha_2 + \alpha_2\alpha_3 + \alpha_3\alpha_1) \qquad \text{I-6}$$

It is easily shown that

$$\cos\theta = \frac{1}{\sqrt{3}}(\alpha_1 + \alpha_2 + \alpha_3)$$

therefore, for the [111] oriented film

$$E_M = \frac{-3}{2}\lambda_{111}\sigma\cos^2\theta \qquad \text{I-7}$$

The g_i's for Eq. (I-2) are

$$g_1(\theta,\phi) = \frac{-H_k}{8\pi M}\,[(3\sin^2\theta\cos^2\theta - \sin^4\theta)\sin^2 2\phi + 2\cos 4\theta\,] \qquad \text{I-8}$$

$$g_2(\theta,\phi) = \frac{-H_k}{8\pi M}\,[2\sin^2\theta\cos 4\phi + \sin^2\theta\cos^2\theta\sin^2 2\phi + \sin 4\theta\cos\theta/2\sin\theta\,]$$

$$g_3(\theta,\phi) = \frac{-3H_k}{16\pi M}\,[\sin^2\theta\cos\theta\sin 4\phi\,]$$

where $H_k = 2K_1/M$. The g_i's for Eq. (I-3) are

$$g_1(\theta,\phi) = -(H_k/8\pi M)[-8\sin^4\theta + 7\sin^2\theta - \tfrac{4}{3}\cos\theta\sqrt{2}\cos 3\phi\sin 2\theta\,(1 - \tfrac{8}{3}\sin^2\theta)] \qquad \text{I-9}$$

$$g_2(\theta,\phi) = -(H_k/8\pi M)[\frac{\sin^2 2\theta}{4} - \tfrac{4}{3}\cos^4\theta + \sqrt{2}\cos 3\phi\sin 2\theta\,(1 + \tfrac{2}{3}\sin^2\theta)]$$

$$g_3(\theta,\phi) = -(H_k/\sqrt{2}\,4\pi M)(\sin 3\phi)(2\sin\theta - 3\sin^3\theta)$$

The g_i's for a uniaxial anisotropy $E = -K_u \cos^2(\theta)$ (like E_M in Eq. (I-5) and (I-7)) are

$$g_1(\theta) = -(K_u/2\pi M^2)\cos 2\theta$$
$$g_2(\theta) = -(K_u/2\pi M^2)\cos^2\theta \qquad \text{I-10}$$
$$g_3(\theta) = 0$$

In general the equilibrium conditions can be determined from the requirement given by Eq. (2-11). The equilibrium conditions which are applicable to the experimental and calculated data presented in chapter 6 are presented here. For the [100] orientation with applied magnetic field, H_{app}, in a (100) plane at an angle β from the normal, the equilibrium condition is

$$0 = (4\pi M - 2K_u/M)\sin 2\theta - 2H_{app}\sin\beta - (H_k/2)\sin 4\theta \qquad \text{I-11}$$

where $K_u = -3\lambda_{100}\sigma/2$ from Eq. (I-5), and $H_k = 2K_1/M$. The equilibrium condition for the [111] oriented film with the applied field, H_{app}, at an angle β from the film normal in a plane defined by the normal and a line in the plane 30° from the $(\bar{1}\bar{1}2)$ axis are

$$0 = (H_k/\sqrt{2})\sin^2\theta\cos\theta\sin 3\phi + (\sqrt{3}H_{app}\sin\phi\sin\beta)/2$$
$$- (H_{app}/2)\cos\phi\sin\beta \qquad \text{I-12}$$
$$0 = H_{app}(-\cos\beta\sin\theta + (\sqrt{3}/2)\cos\theta\cos\phi\sin\beta + .5\cos\theta\sin\phi\sin\beta)$$
$$+ (4\pi M - 2K_u/M)\cos\theta\sin\theta - (H_k/2)[\sin^3\theta\cos\theta - (4/3)\cos^3\theta\sin\theta$$
$$-\sqrt{2}\cos 3\phi(\sin^2\theta - (4/3)\sin^4\theta)]$$

where $K_u = -3\lambda_{111}\sigma/2$, and $H_k = 2K_1/M$. Note that in Eq. (I-11) and (I-12) that the uniaxial anisotropy field substracts from $4\pi M$ and has an identical angular dependence. This is also true in the resonance equations.

I-2. Surface Boundary Conditions

The surface boundary condition is generally a statement that the surface anisotropy torque is balanced by a surface exchange torque. Since we are at the boundary of the ferromagnet, the surface exchange is related to the slope of the magnetization, $d\bar{m}/dn$, rather than to its second derivative. The anisotropy torque can be defined in terms of an equivalent surface field or a surface anisotropy energy. In the first case the surface torque requires the elementary calculation $\overline{M}x\overline{H}_s$ when the magnetization is perturbed from its equilibrium position. In the second case the torque can be obtained by taking appropriate angular derivatives of the energy function. If desired, calculation of these derivatives can be interpreted as calculation of an equivalent anisotropy surface field. An unresolved question is whether this surface field varies with the dynamic (small angle) motion of the surface magnetization or depends only on the equilibrium position of the magnetization or is completely independent of the orientation of $\overline{M}$. None of these assumptions complicate the analysis, they simply give different boundary conditions.

If the anisotropy energy is expressed in terms of the angular orientation of $\overline{M}$ (i.e.,θ and ϕ) then a satisfactory procedure is to define an equivalent anisotropy field which is at all times perpendicular to $\overline{M}$.

$$H_s = \overline{H}_{so} + \overline{h}_s$$

where $H_{so} = - \overline{\nabla}_m E_s/aM$, a is the lattice constant

$$\bar{\nabla}_m = \left(\bar{e}_\theta \frac{\partial}{\partial \theta} + \frac{1}{\sin\theta}\, \bar{e}_\phi \frac{\partial}{\partial \phi}\right)$$

$$\bar{h}_s = (1/M)\ (\bar{m} \cdot \bar{\nabla}_m)\ \bar{H}_{so}$$

$$(\bar{m} \cdot \bar{\nabla}_m) = \left(m_\theta \frac{\partial}{\partial \theta} + \frac{m_\phi}{\sin\theta} \frac{\partial}{\partial \phi}\right)$$

The field $\bar{H}_s$ is written as an expansion in terms of $\bar{H}_{so}$ the field when $\bar{M}$ is in its equilibrium position and $\bar{h}_s$ a small additional component which arises from a small displacement of $\bar{M}$ from its equilibrium position ($\bar{M} = \bar{M}_o + m_\theta \bar{e}_\theta + m_\phi \bar{e}_\phi$).

In the equilibrium position, the surface torque per unit area (on one atomic layer) is

$$\bar{T}_{so} = a\bar{M}_o \times \bar{H}_{so} \quad ,$$

and this is balanced by an equilibrium exchange torque between the surface spins and (for simple cubic lattice) the spins in the next atomic layer. With an arbitrary displacement $\bar{m}$, the surface torque becomes

$$\bar{T}_s = a(\bar{M}_o + \bar{m}) \times (\bar{H}_{so} + \bar{h}_s) + a(\bar{M}_o \times \bar{H}_{so} + \bar{M}_o \times \bar{h}_s + \bar{m} \times \bar{H}_{so})$$

where the second order term $\bar{m} \times \bar{h}_s$ has been omitted. For this same displacement, the exchange torque per unit area becomes

$$\bar{T}_{ex} = \left[-a\bar{M}_o \times \bar{H}_{so} + a(-m_\theta H_{s\phi} + m_\phi H_{s\theta})\ \bar{e}_r + \frac{2A}{M} \frac{\partial m_\phi}{\partial n} \bar{e}_\theta - \frac{2A}{M} \frac{\partial m_\theta}{\partial n} \bar{e}_\phi \right]$$

It will be noted that the first and second terms in $\bar{T}_{ex}$ are the negative of the first and third terms of $\bar{T}_s$, so the equilibrium condition $(\bar{T}_{ex} + \bar{T}_s) = 0$ becomes

$$t_s + t_{ex} = 0$$

$$\bar{t}_s = a\ (\ \bar{M}_o \times \bar{h}_s\ )$$

$$t_{ex} = \left(\frac{2A}{M}\frac{\partial m_\phi}{\partial n}\bar{e}_\theta - \frac{2A}{M}\frac{\partial m_\theta}{\partial n}\ \bar{e}_\phi\right)$$

When the anisotropy field is obtained in other ways which give a radial component, then one must include the θ and ϕ components of $\bar{m} \times \bar{H}_{so}$ which are not cancelled by the second term in the exchange torque.

$$\bar{t}_s = a\ [(-Mh_{s\phi} + m_\phi H_{sor})\bar{e}_\theta + (Mh_{s\theta} - m_\theta H_{sor})\bar{e}_\phi\ ]$$

It should be noted that the partial derivatives in $\bar{t}_{ex}$ do not include the static or equilibrium values of the derivatives which are required to balance the equilibrium torque $a\bar{M}_o \times \bar{H}_{so}$. The equilibrium values of the derivatives are much larger than the dynamic derivatives by a factor of the order of M_o/m since this is roughly the ratio of the surface torques balanced by these two components of the exchange torque.

Example 1 Uniaxial anisotropy $E_s = K_s \sin^2\theta$

$$\bar{H}_{so} = \frac{-K_s}{aM}\ \sin 2\theta\ \bar{e}_\theta$$

$$h_s = \frac{-2K_s}{aM^2}\ [\ \cos 2\theta\ m_\theta\ \bar{e}_\theta + \cos^2\theta\ m_\phi\ \bar{e}_\phi\ ]$$

$$t_s = \frac{2K_s}{M}[\ \cos^2\theta\ m_\phi\ \bar{e}_\theta - \cos 2\theta\ m_\theta\ \bar{e}_\phi\ ]$$

This gives the boundary condition given in equation (3-7).

Example 2 Tensorial field (Yu et al (1975)) (assumed constant with respect to dynamic $\bar{M}$ variations.

$$\bar{H}_{so} = [(H_{\perp}\cos^2\theta_o + H_{||}\sin^2\theta_o)\,\bar{e}_r + (H_{||} - H_{\perp})\sin\theta_o\cos\theta_o\,\bar{e}_\theta]$$

$$\bar{h}_s = 0$$

$$\text{Let } H_{\perp} = \frac{2K_{\perp}}{aM} \qquad H_{||} = \frac{2K_{||}}{aM}$$

$$t_s = \left[\frac{2K_{\perp}}{M}\cos^2\theta + \frac{2K_{||}}{M}\sin^2\theta\right](m_\phi\,\bar{e}_\theta - m_\theta\,\bar{e}_\phi)$$

This gives the boundary condition given in Eq. (3-11).

Example 3 Tensorial field but allowing it to vary with dynamic $\bar{M}$.

$$\bar{H}_{so} = [(H_{\perp}\cos^2\theta + H_{||}\sin^2\theta)\,\bar{e}_r + (H_{||} - H_{\perp})\sin\theta\cos\theta\,\bar{e}_\theta]$$

$$\bar{h}_s = \frac{1}{M}[(H_{\perp}\sin^2\theta + H_{||}\cos^2\theta)\,m_\theta\,\bar{e}_\theta + H_{||}\,m_\phi\,\bar{e}_\phi]$$

$$\bar{t}_s = \frac{2}{M}[(K_{\perp} - K_{||})\cos^2\theta\,m_\phi\,\bar{e}_\theta - (K_{\perp} - K_{||})\cos 2\theta\,m_\theta\,\bar{e}_\phi]$$

Note that this gives the boundary condition given in Eq. (3-7) with $K_s = (K_{\perp} - K_{||})$.

Appendix II

The elements of the determinants given in Eqs. (3-9a) and (3-10c) are given below.

$a_{11}=\Delta K \cos(2\theta) \cos(k_1 d/2)$

$a_{12}=-k_1 \sin(k_1 d/2) + K_o \cos(2\theta) \cos(k_1 d/2)$

$a_{13}= \Delta K \cos^2(\theta) \cos(k_1 d/2)$

$a_{14}= -k_1 \sin(k_1 d/2) + K_o \cos^2(\theta) \cos(k_1 d/2)$

$a_{21}= k_1 \cos(k_1 d/2) + K_o \cos(2\theta) \sin(k_1 d/2)$

$a_{22}= \Delta K \cos(2\theta) \sin(k_1 d/2)$

$a_{23}= k_1 \cos(k_1 d/2) + K_o \cos^2(\theta) \sin(k_1 d/2)$

$a_{24}= \Delta K \cos^2(\theta) \sin(k_1 d/2)$

$a_{31}= \Delta K \cos(2\theta) \cos(k_1 d/2)$

$a_{32}= -k_2 \sin(k_2 d/2) + K_o \cos(2\theta) \cos(k_2 d/2)$

$a_{33}= -RR^* \Delta K \cos(k_2 d/2)$

$a_{34}=-RR^* (-k_2 \sin(k_2 d/2) + K_o \cos^2(\theta) \cos(k_2 d/2)$

$a_{41}= k_2 \cos(k_2 d/2) + K_o \cos(2\theta) \sin(k_2 d/2)$

$a_{42}= \Delta K \cos(2\theta) \sin(k_2 d/2)$

$a_{43}= -RR^* (k_2 \cos(k_2 d/2) + K_o \cos^2(\theta) \sin(k_2 d/2))$

$a_{44}= -RR^* \Delta K \cos^2(\theta) \sin(k_2 d/2)$

where

$$k_2^2 = k_1^2 - \frac{A}{2\pi M^2} \{4|\Omega'|^2 + (g_1 - g_2 - \sin^2(\theta))^2\}^{1/2} \quad ;$$

K_{s1} , K_{s2} are the surface anisotropies at the two surfaces; and

$K_o = (K_{s1}+K_{s2})/2A$, and $\Delta K = (K_{s1}-K_{s2})/2A$

The elements of the determinant for the secular equation using asymmetric surface layers are:

$$0=a_{11}=a_{21}=a_{72}=a_{82}=a_{13}=a_{23}=a_{74}=a_{84}=a_{15}=a_{25}=a_{76}=a_{86}=a_{17}=a_{27}=a_{78}=a_{88}$$

$$a_{31}= \cos(k_{1b}D/2)$$

$$a_{41}= \sin(k_{1b}D/2)$$

$$a_{51}= \cos(k_{2b}D/2)$$

$$a_{61}= \sin(k_{2b}D/2)$$

$$a_{71}= -\cos(k_{1s1}L_1)$$

$$a_{81}= -\cos(k_{2s1}L_1)$$

$$a_{12}= -\cos(k_{1s2}L_2)$$

$$a_{22}= -\cos(k_{2s2}L_2)$$

$$a_{32}= a_{31}$$

$$a_{42}=-a_{41}$$

$$a_{52}= a_{51}$$

$$a_{62}= -a_{61}$$

$$a_{33}= a_{31}/R_b$$

$$a_{43}= a_{41}/R_b$$

$$a_{53}= -a_{51}\ R_b^*$$

$$a_{63}= -a_{61}\ R_b^*$$

$$a_{73}= a_{71}/R_{s1}$$

$$a_{83}=-a_{81}\ R_{s1}^*$$

$$a_{14}= a_{12}/R_{s2}$$

$$a_{24}= -a_{22}\ R_{s2}^*$$

$$a_{34}=a_{33}$$

$$a_{44}=-a_{43}$$

$a_{54} = a_{53}$

$a_{64} = -a_{63}$

$a_{35} = -k_{1b}\, a_{41}$

$a_{45} = k_{1b}\, a_{31}$

$a_{55} = -k_{2b} a_{61}$

$a_{65} = k_{2b} a_{51}$

$a_{75} = -k_{1s1}\, \sin(k_{1s1} L_1)$

$a_{85} = -k_{2s1}\, \sin(k_{2s1} L_1)$

$a_{16} = k_{1s2}\, \sin(k_{1s2} L_2)$

$a_{26} = k_{2s2}\, \sin(k_{2s2} L_2)$

$a_{36} = -a_{35}$

$a_{46} = a_{45}$

$a_{56} = -a_{55}$

$a_{66} = a_{65}$

$a_{37} = a_{35}/R_b$

$a_{47} = a_{45}/R_b$

$a_{57} = -a_{55}\, R_b^*$

$a_{67} = -a_{65}\, R_b^*$

$a_{77} = a_{75}/R_{s1}$

$a_{87} = -a_{85} R_{s1}^*$

$a_{18} = a_{16}/R_{s2}$

$a_{28} = -a_{26} R_{s2}^*$

$a_{38} = -a_{37}$

$a_{48} = a_{47}$

$a_{58} = -a_{57}$

$a_{68} = a_{67}$

The film characteristics are illustrated below.

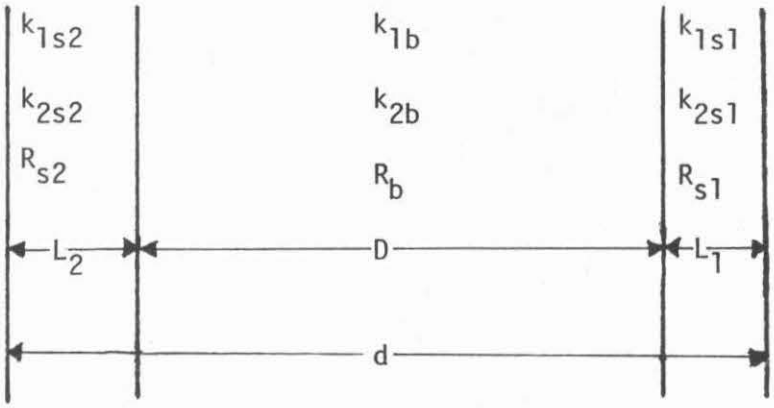

Appendix III

Amplitude of ferromagnetic spin-wave resonance in thin films

C. H. Wilts and O. G. Ramer

California Institute of Technology, Pasadena, California 91125
(Received 27 September 1974; in final form 17 October 1975)

The effect of conductivity on the spin-wave spectrum of thin Permalloy ferromagnetic films has been investigated. If conductivity effects are included and a simple surface anisotropy is assumed, it is known that the calculated mode locations and amplitudes for Permalloy films are in excellent agreement with some experimental data in the range 800–2700 Å in thickness. If conductivity effects are omitted, a much simpler calculation is possible, but the error in mode location and amplitude has been unknown. For both perpendicular and parallel resonance geometries, detailed calculations reported here have shown that mode locations are not significantly affected over the above thickness range, and that the main mode amplitude is in error by only 20% at 800 Å thickness. However, for 2000 Å thickness, the main mode amplitude is in error by a factor of 2.5.

PACS numbers: 76.50., 75.70.

INTRODUCTION

The existence of standing spin-wave modes in evaporated polycrystalline ferromagnetic thin films was established many years ago and the approximately quadratic dispersion has been used by several workers for measurement of the magnetic exchange constant.[1,2] At a fixed frequency, the modes were spaced in applied field approximately as the square of integers which describe (roughly) the number of half-waves in the standing-wave pattern. Using a semiclassical theory of spin-wave dispersion in an insulating medium, the observed deviations from a square law were explained qualitatively[3] by inhomogeneity in the film or by a surface anisotropy which provides partial pinning of the spins at the surface. Attempts to explain the observed amplitudes of the resonances have had only limited success.[4,5] However it is uncertain whether disagreements were due to poor samples, due to imposition of improper boundary conditions, due to the neglect of conductivity in the film, or due to inadequacy of the phenomenological model for magnetization dynamics.

Several papers in the last two decades have given a mathematical formulation for treatment of conducting media utilizing Maxwell's equations and the Landau-Lifshitz equation.[6–8] None of these have applied this formulation to a theoretical comparison with experimental data. A recent treatment by Bailey and Vittoria[9] is the first serious attempt to use this formulation to match experimental data. Mode locations were matched with very good accuracy, but due to an invalid approximation in treating the magnetic losses, the predicted amplitudes and linewidths for the higher (shorter-wavelength) spin-wave modes deviated widely from the experiment. After correction of this error,[10] the theoretical predictions were in good agreement with experiment for all modes observed in a set of four Permalloy films ranging in thickness from 800 to 2700 Å. Although the inclusion of conductivity effects greatly complicated the calculations, no effort was made by Bailey and Vittoria to confirm the importance of including this effect. The purpose of this paper is to compare the results of such accurate calculations with simple approximations which ignore the effect of conductivity.

Ferromagnetic resonance is observed with a static magnetic field applied in any direction with respect to the film. For simplicity of analysis, the experiments are often done with the magnetic field parallel or perpendicular to the film plane even though resonance at an oblique angle is a more powerful technique. Parallel and perpendicular resonance are the only cases considered in Ref. 9 and are therefore the only ones considered in this paper.

MATHEMATICAL FORMULATION

Since a quantum-mechanical treatment of this system is intractable, it is customary to use Maxwell's equations coupled with the Landau-Lifshitz phenomenological equation. In this equation $\mathbf{M}$ is treated as a vector of fixed magnitude which moves in reaction to the total effective field and a small phenomenological dissipative term provides an energy loss. These equations of motion have been amply discussed in the references cited earlier. However due to differences in notation, the Landau-Lifshitz equation is repeated here.

$$\frac{d\mathbf{M}}{dt} = -\gamma \mathbf{M} \times (\mathbf{H}_0 + \mathbf{h}_{rf} + \mathbf{h}_{ex} + \mathbf{h}_\lambda + \cdots). \tag{1}$$

The gyromagnetic ratio γ is taken to be a positive number so that a negative sign is explicitly used in Eq. (1); $\mathbf{H}_0$ is the static internal field including the static demagnetizing field; $\mathbf{h}_{rf}$ is the local rf magnetic field including both applied fields and rf demagnetizing fields. The term $\mathbf{h}_{ex}$ is an effective rf field due to exchange coupling between the adjacent nonparallel spins:

$$\mathbf{h}_{ex} = -(2Ak^2/M^2)\mathbf{m}, \tag{2}$$

where A is the exchange constant and k is the wave number of the spin wave $\mathbf{m} = \mathbf{m}_0 \exp[i(\omega t \pm ky)]$. The vector $\mathbf{m}$ is the rf component of $\mathbf{M}$, assumed small in magnitude compared to $\mathbf{M}$, and therefore (to first order) perpendicular to the equilibrium position of $\mathbf{M}$, i.e., $\mathbf{M} = \mathbf{M}_0 + \mathbf{m}$ where $\mathbf{M}_0$ is parallel to $\mathbf{H}_0$ and $\mathbf{m}$ is perpendicular to $\mathbf{H}_0$. The magnetic damping is treated phenomenologically by introducing $\mathbf{h}_\lambda$, an effective damping rf field field. It is written here in the Gilbert form[11]:

$$\mathbf{h}_\lambda = -\frac{\lambda}{(\gamma M)^2}\frac{d\mathbf{m}}{dt} = -\frac{\alpha}{\gamma M}\frac{d\mathbf{m}}{dt}. \tag{3}$$

The magnitude of the damping is described by the relaxation frequency λ, or by the dimensionless damping constant $\alpha = \lambda/\gamma M$. Additional fields to represent crystalline or uniaxial anisotropies are readily included. Since they do not contribute to the effects studied in this paper, they have been omitted.

The boundary condition on **M** is an unsettled matter although most workers invoke one of four situations: (1) spins unpinned, (2) spins completely pinned, (3) a uniaxial anisotropy energy with easy or hard axis along $\mathbf{H}_0$, or (4) a surface anisotropy energy with easy or hard axis perpendicular to the surface. The last of these appears to be more consistent with experimental results and is used both in Ref. 9 and here. The surface anisotropy energy is assumed to have the form $W_s = -K_s(\hat{n}\cdot\hat{v})^2$, where $\hat{n}$ is the outward pointing unit vector normal to the film surface and $\hat{v} = \mathbf{M}/M$ is a unit vector in the direction of **M**. However a layer of reduced magnetization or a surface layer of reduced demagnetizing field has an equivalent effect in "pinning" the magnetization at the surface if the anisotropy constant K_s and the surface layer thickness are given appropriate values.[3] In terms of the surface anisotropy, the boundary condition on **M** is

$$\frac{\partial m_\theta}{\partial n} + \frac{K_s}{A}\, m_\phi(\hat{n}\cdot\hat{v}_0)^2 = 0, \tag{4a}$$

$$\frac{\partial m_\theta}{\partial n} + \frac{K_s}{A}\, m_\theta[2(\hat{n}\cdot\hat{v}_0)^2 - 1] = 0, \tag{4b}$$

where $\hat{v}_0 = \mathbf{M}_0/M$, and θ and ϕ refer to polar coordinate directions with respect to the normal $\hat{n}$.

The solution to the above model is described below in greater detail than in Refs. 7 and 8 in order to facilitate comparison with the approximate solution developed later. The excitation is uniform linearly polarized electromagnetic radiation normal to the film surfaces. Appropriate boundary conditions are satisfied and power absorbed is calculated from the Poynting vector at the surface. Small-amplitude sinusoidal motion is assumed so that the equations are linearized. Calculations of the power absorbed and the steady-state standing-wave pattern are carried out by digital computer.

At a given frequency, amplitude of external rf field, static magnetic field, and film orientation, the calculation predicts the amplitude of **m** and **h** throughout the film and the power absorbed. The resonance condition is determined by locating a maximum in the power absorbed while sweeping either field or frequency. There are four components of the standing-wave pattern, each with a characteristic polarization and complex propagation constant k. For the case of perpendicular resonance, the response breaks up into circularly polarized pairs. One pair has positive precession (in the sense $-\mathbf{m}\times\mathbf{H}_0$), the other negative. Hence in the analysis, the external field is resolved into components of opposite circular polarization.

The following discussion relates to the positively polarized components which are the only ones that participate significantly in the resonance process. The two components are not in phase with each other and since even one component varies in both phase and magnitude through the film thickness, all components of **m** and **h** are described by complex numbers. In the discussion below, the subscripts (r) and (im) refer to real and imaginary parts of these complex numbers and subscripts 1 and 2 refer to the components corresponding to the two values of k, ordered so that $|k_1| < |k_2|$. The coordinate system is shown in Fig. 1, where the y axis is normal to the film. The basic normalization is to set the magnitude of the circularly polarized rf field at both surfaces equal to $\frac{1}{2}h_0$, with phase chosen so that at $t = 0$

$$h_x = h_{1_r}(\tfrac{1}{2}L) + h_{2_r}(\tfrac{1}{2}L) = \tfrac{1}{2}h_0,$$
$$h_x = -h_{1_{im}}(\tfrac{1}{2}L) - h_{2_{im}}(\tfrac{1}{2}L) = 0.$$

For fields and frequencies normally used in the laboratory for spin-wave spectra of metal ferromagnetic films, the components have the following characteristics at resonance: the component $h_{2_r}(y)$ is nearly independent of y and approximately equal to $\frac{1}{2}h_0$; the components $h_{2_{im}}$, h_{1_r}, and $h_{1_{im}}$ are all much smaller than h_0 for all values of y. The magnetization component $m_2(y)$ being proportional to $h_2(y)$ is also nearly independent of y, but is small. The component $m_1(y)$ is proportional to $h_1(y)$, but the proportionality constant is so large that $m_1(y) \gg m_2(y)$ even though $h_1(y)$ is small. The significant component $m_1(y)$ is largely imaginary and varies with y in a manner governed by the spin-wave k value, k_1. Since k_1 is nearly purely imaginary, the variation of m_1 is nearly sinusoidal. In otherwords, to a rough approximation h_{2_r} is equal to the external rf field and its degree of independence on y coupled with the smallness of h_{1_r} shows the degree to which the magnetic field is uniform in the metal. The resonance variation of **m** is described by $m_{1_{im}}$, which is roughly sinusoidal in y and 90° out of phase with the rf magnetic field, $\mathbf{h}_2$. All other components of **m** and **h** are small.

To summarize, the quantities of interest are as follows:

(1) applied field at resonance, $H_a = H_0 - 4\pi M$;

(2) spin-wave k value $\approx (k_1)_{im}$;

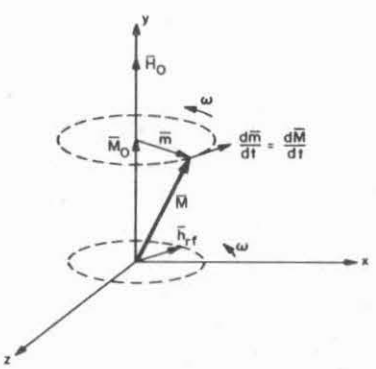

FIG. 1. Field relations at resonance in the perpendicular resonance configuration.

(3) resonance amplitude of $m \approx m_{1_{1m}}(0)$;

(4) relative surface amplitude of m (a measure of surface pinning) is approximated by the ratio

$$[m_{1_{1m}}(\tfrac{1}{2}L)]/[m_{1_{1m}}(0)];$$

(5) power absorbed per unit area equals the sum of Poynting vectors at the two surfaces.

Although the power absorbed is given directly, the power absorption due to resonance requires subtraction of the "background" power which is a significant part of the total for some modes. This is done most simply by plotting the power as a function of applied field, and drawing a smooth curve under the resonances.

Similar considerations hold for parallel resonance, except that the applied field is linearly polarized perpendicular to $\mathbf{M}_0$ and with amplitude h_0. There are three elliptically polarized components of $\mathbf{m}$ instead of two circular polarizations. In general one of these has positive polarization and describes the (roughly) uniform rf field driving the magnetization, the other of positive polarization is the resonant spin-wave mode, and the third of negative polarization is a surface component of negligible amplitude. The fourth component is linearly polarized but is not excited by the assumed external field.

AN APPROXIMATE SOLUTION

The simplest approximation for locating resonant modes neglects both conductivity and λ losses. Maxwell's equations neglecting conductivity and displacement current include the rf component of demagnetizing field due to the component of $\mathbf{m}$ perpendicular to the surface, $\mathbf{h}_m = -4\pi m_y \mathbf{e}_y$. Combining this with Eq. (1) gives simple relations for the mode locations. In the ferromagnetic insulator ($\sigma = 0$), if the λ losses are very small ($\alpha \ll 1$), the amplitude of resonance and power absorbed can be approximated by assuming the external driving rf field to penetrate the medium without attenuation or phase shift and the resulting magnetization variation to consist of purely sinusoidal or hyperbolic components again without phase shift.

If the driving torque integrated over the thickness is balanced against the dissipation torque also integrated over the thickness, the resonance amplitude is obtained. Note that these torques do not balance locally. However, the exchange interaction is so strong that insignificant changes in mode shape are able to provide the local torque balance without significant change in amplitude.

As discussed earlier for the case of perpendicular resonance, attention is focused on a positive circularly polarized magnetic field of amplitude $\frac{1}{2}h_0$ and frequency ω. For perpendicular resonance there is no rf demagnetizing field and the Landau-Lifshitz equation becomes simply

$$\frac{d\mathbf{m}}{dt} = -\gamma \mathbf{m} \times \hat{v}_0 \left(H_0 + \frac{2A}{M} k^2 \right) - \gamma M \hat{v}_0 + \mathbf{h}_{rf} + \alpha \hat{v}_0 \times \frac{d\mathbf{m}}{dt}. \qquad (5)$$

For positive values of K_s and for sufficiently small values of damping ($\alpha \ll 1$), all mode shapes are nearly simple sine waves with negligible phase shift through the film. At resonance, the relation between $\mathbf{M}$ and $\mathbf{h}_{rf}$ is shown in Fig. 1. The entire pattern rotates about $\mathbf{H}_0$ with angular velocity ω. The vector $d\mathbf{m}/dt$ is equal to the first term on the right-hand side of Eq. (5), so that the resonance condition is

$$\frac{\omega}{\gamma} = \left(H_0 + \frac{2A}{M} k^2 \right). \qquad (6)$$

The last two terms of the equation balance in the sense described earlier that the torque $M\hat{v}_0 \times \mathbf{h}_{rf}$ integrated over the thickness balances the dissipation torque $(\alpha/\gamma)\hat{v}_0 \times d\mathbf{m}/dt$ also integrated over the thickness.

Using a sinusoidal mode shape and the surface anisotropy boundary condition of Eq. (4) with $(\hat{n} \cdot \hat{v}_0) = 1$, it is not difficult to show that the secular equation for the resonant spin-wave k values is

$$[k - K_0 \cot(\tfrac{1}{2}kL)][k + K_0 \tan(\tfrac{1}{2}kL)] + (\Delta K)^2 = 0, \qquad (7a)$$

where L is the film thickness, K_{s_1} and K_{s_2} the surface anisotropies at the two surfaces, $K_0 = (K_{s_1} + K_{s_2})/2A$, and $\Delta K = (K_{s_1} - K_{s_2})/2A$. For our present purposes, it is adequate to consider the symmetric case $K_{s_1} = K_{s_2}$, in which case only half of the k values are taken (i.e., those corresponding to symmetric rather than antisymmetric mode shapes). The symmetric modes are obtained by setting the first factor of Eq. (7a) equal to zero.

$$[k - K_0 \cot(\tfrac{1}{2}kL)] = 0. \qquad (7b)$$

Recognizing the H_0 is the sum of the applied field H_a and the demagnetizing field $-4\pi M$, the resonance occurs at the field

$$H_a = 4\pi M + \frac{\omega}{\gamma} - \frac{2A}{M} k^2, \qquad (8)$$

where k is a solution of Eq. (7). Assuming the magnetization $\mathbf{m}$ has an amplitude $m_0 \cos(ky)$, where y is measured from the center of the film, the relative amplitude at the surface is $\cos(\frac{1}{2}kL)$. From the discussion following Eq. (6), it readily follows that the peak amplitude is given by

$$\frac{m}{M} = \frac{2\gamma h_0}{\alpha\omega} \frac{\sin(\frac{1}{2}kL)}{kL + \sin(kL)}, \qquad (9)$$

and the power dissipated per unit area of film is

$$P_0 = \frac{2h_0^2 \gamma M L}{\alpha} \frac{[\sin(\frac{1}{2}kL)]^2}{kL[kL + \sin(kL)]}. \qquad (10)$$

For the case of parallel resonance $\hat{v}_0$ is parallel to the z axis, $\hat{v}_0 = \mathbf{e}_z$. The field $\mathbf{h}_{rf}$ outside the sample is linearly polarized, $h_0 \mathbf{e}_x$, and the x component inside the film is assumed to have the same value. The boundary condition on $\mathbf{m}$ is given by Eq. (4) with $(\hat{n} \cdot \hat{v}_0) = 0$. The magnetization variation is no longer a circularly polarized spin wave, but is a linear combination of two elliptically polarized standing waves. It is easily shown from Eqs. (4) and (5) with $\hat{v}_0 = \mathbf{e}_z$ that these standing waves are either sinusoidal or hyperbolic, and are characterized by wave vectors $k_1 \mathbf{e}_y$ and $k_2 \mathbf{e}_y$. If the wave numbers are ordered so that $|k_1| < |k_2|$, then k_2 is usually imaginary for all modes, while k_1 is real for all modes except the first, in which case the sign of k_1^2 depends on the sign of K_s. The wave numbers k_1 and k_2 are obtained from the roots of a dispersion relation which

is somewhat more complicated than Eq. (7a):

$$\{+Rk_2[k_1 + K_0\cot(\tfrac{1}{2}k_1L)] + R^{-1}k_1[k_2 + K_0\cot(\tfrac{1}{2}k_2L)]\}$$
$$\{Rk_2[k_1 - K_0\tan(\tfrac{1}{2}k_1L)] + R^{-1}k_1[k_2 - K_0\tan(\tfrac{1}{2}k_2L)]\}$$
$$\times [Rk_2\tan(\tfrac{1}{2}k_2L) + R^{-1}k_1\tan(\tfrac{1}{2}k_1L)]$$
$$\times [Rk_2\cot(\tfrac{1}{2}k_2L) + R^{-1}k_1\cot(\tfrac{1}{2}k_1L)](\Delta K)^2 = 0, \qquad (11a)$$

$$k_2^2 = k_1^2 - (2\pi M^2/A)(1 + 4\Omega^2)^{1/2},$$

$$R = 2\Omega[1 + (1 + 4\Omega^2)^{1/2}]^{-1},$$

and

$$\Omega = \omega/4\pi M\gamma.$$

As in the case of perpendicular resonance, if the boundary conditions are symmetric, then $\Delta K = 0$, and the equation factors into separate relations for the symmetric or antisymmetric modes. The symmetric modes are those obtained by setting the first factor of Eq. (11a) to zero. With some simplification this becomes

$$\frac{K_0}{2k_1}\left(1 - \frac{1}{(1+4\Omega^2)^{1/2}}\right)\cot\left(\frac{k_1L}{2}\right)$$
$$+ \frac{K_0}{2k_2}\left(1 + \frac{1}{(1+4\Omega^2)^{1/2}}\right)\cot\left(\frac{k_2L}{2}\right) + 1 = 0. \qquad (11b)$$

Using Eq. (5) and the value of k_1 obtained from Eq. (11), the resonance field H_a is found to be

$$H_a = 2\pi M[(1 + 4\Omega^2)^{1/2} - 1] - (2A/M)k_1^2. \qquad (12)$$

The two components corresponding to k_1 and k_2 have quite different characteristics. For $K_s > 0$, the principal component corresponding to k_1 is hyperbolic in y for the main mode, and sinusoidal for all other modes. It has a positive precession and an ellipticity given by

$$(m_y/m_x)_1 = -iR. \qquad (13a)$$

The smaller component corresponding to k_2 is hyperbolic in y for all modes. It has negative precession and ellipticity.

$$(m_y/m_x)_2 = +i/R. \qquad (13b)$$

The amplitude of m_x at the center of the film can be written as the sum of the two components $m_x(0) = (m_{10} + m_{20})$, where

$$\frac{m_{20}}{m_{10}} = -\frac{k_1\sin(\frac{1}{2}k_1L)}{k_2\sin(\frac{1}{2}k_2L)}, \qquad (14)$$

and at the surface the amplitude is

$$m_x(\tfrac{1}{2}L) = m_{10}\cos(\tfrac{1}{2}k_1L) + m_{20}\cos(\tfrac{1}{2}k_2L). \qquad (15)$$

The maximum value of m_{x2} is $|m_{20}|\cosh(|\frac{1}{2}k_2|L)$. For thin films of typical ferromagnetic metals, it can be shown that this maximum value is about two or three orders of magnitude smaller than m_{10}. In consequence the amplitude of $\mathbf{m}$ and power absorbed can be approximated closely by ignoring m_2. With this approximation, the amplitude becomes

$$m_x(0) = \frac{4h_0\gamma M}{\alpha\omega}\left(\frac{1}{1+R^2}\right)\frac{\sin(\frac{1}{2}k_1L)}{k_1L + \sin(k_1L)}, \qquad (16)$$

and the average power absorbed per unit area of film is

$$P_0 = \frac{4h_0^2\gamma ML}{\alpha}\left(\frac{1}{1+R^2}\right)\frac{[\sin(\frac{1}{2}k_1L)]^2}{k_1L[k_1L + \sin(k_1L)]}. \qquad (17)$$

It should be noted that when k_1 is imaginary, Eqs. (16) and (17) should be used with k_1 replaced by the magnitude of k_1 and the sines replaced by hyperbolic sines.

It should be emphasized that the results given in Eqs. (6)—(17) are approximations based on assumptions of a uniform driving rf field, negligible phase shift of $\mathbf{m}$ and $\mathbf{h}$ through the film thickness, and sinusoidal or hyperbolic mode shapes. For insulators, small values of α, and for film thicknesses normally encountered, the errors are negligible.

TABLE I. Assumed properties of magnetic films.

Thickness (Å)	2023	790
$4\pi M$ (G)	11151.4	11216.7
A (erg/cm)	1.143×10^{-6}	1.143×10^{-6}
γ (Oe sec)$^{-1}$	1.8484×10^{7}	1.8484×10^{7}
α	0.00457	0.00455
σ (esu)	6.3×10^{16}	6.3×10^{16}
K_s (erg/cm^2)	0.275	0.200
f (GHz)	9.44	9.44

$\sigma = 6.3\times10^{16}$ corresponds to a resistivity of $1.426\times10^{-5}\,\Omega$ cm.

TABLE II. Predicted mode properties from insulator model.

Thickness		2023 Å				790 Å	
Mode No.		1	2	3	4	1	2
		Perpendicular resonance					
H_a (Oe)	Eq. (8)	14327.9	14011.7	13252.0	12005.3	14334.1	12588.6
k (cm^{-1}) $\times10^{-5}$	Eq. (7)	1.122	3.679	6.559	9.561	1.891	8.469
m_0/M	Eq. (9)	0.04073	0.00893	0.00337	0.00168	0.03736	0.00391
$m(\frac{1}{2}L)/m(0)$	$\cos(\frac{1}{2}kL)$	0.423	−0.837	0.939	−0.970	0.734	−0.979
Power (erg/cm^2) $\times10^{-7}$	Eq. (10)	1.732	0.0700	0.00933	0.00226	0.7107	0.00495
% power		100%	4.04	0.54	0.13	100%	0.70
		Parallel resonance					
H_a (Oe)	Eq. (12)	862.28	618.12			861.33	
k (cm^{-1}) $\times10^{-5}$	Eq. (11)	0.433	3.048			0.566	
$m(0)/M$	Eq. (16)	0.0616	0.00246			0.0634	
$m(\frac{1}{2}L)/m(0)$	$\cos(\frac{1}{2}k_1L)$	1.089	−0.990			1.019	
Power (erg/cm^2) $\times10^{-7}$	Eq. (17)	3.386	0.00248			1.338	
% power		100%	0.073%			100%	

In the cases of perpendicular and parallel resonance respectively, Eqs. (7)—(10) and (11)—(17) can be used to predict the location of the resonances, the spin-wave k value, the amplitude of the magnetization precession, the relative magnetization amplitude (effective pinning) at the surface, and the power absorbed. Only the first and last of these are experimentally observable. Equation (7) for dispersion, Eq. (8) for resonance field, and Eq. (10) for power dissipated in resonance are also obtained by the quantum-mechanical treatment of Puzkarski.[12] His Eqs. I 3.24 and II 1.8 reduce to Eqs. (7) and (10) in the limit that the lattice constant approaches zero. Similar equations for parallel resonance have not been found in the literature.

COMPARISON OF CALCULATION

For comparison of the approximations above with calculations which accurately include the effects of conductivity, two of the films tested experimentally and theoretically by Bailey and Vittoria[9] have been chosen. In particular a thick film (2023 Å) was selected where the effect of conductivity is expected to be significant, and a thin film (790 Å) where the effect of conductivity is expected to be small. The physical constants chosen in Ref. 9 have been used except that an average surface anisotropy has been assumed at both surfaces, the only effect being to eliminate excitation of the very small antisymmetric modes and to simplify the approximate calculations. The specific values of the physical constants are given in Table I.

In the case of perpendicular resonance, the spin-wave number k, mode location, magnetization rf amplitude, surface pinning, and power absorbed were calculated for the first four symmetric modes of the 2023-Å film and the first two symmetric modes of the 790-Å film. The results for the insulator approximation [Eqs. (7)—(17)] are given in Table II. For parallel resonance the same data are tabulated for the first two symmetric modes of the thick film and the first mode of the thin film. Only the larger in-plane component of **m** is tabulated.

For the more accurate conductivity model, in addition to the basic case, four other cases were considered corresponding to conductivity reduced by a factor of 10, 100, and 1000 and finally conductivity reduced by a factor of 1000 and α reduced by a factor of 10. Results for perpendicular resonance are given in Table III where they are also compared with data for the insulator ap-

TABLE III. Predicted mode properties in perpendicular resonance.

	Loss parameter		Thickness					
	σ	α	2023 Å				790 Å	
Mode No.			1	2	3	4	1	2
H_a (Oe)	6×10^{16}	0.0046	14327.7	14013.2	13252.3	12005.4	14334.1	12588.7
	6×10^{15}	0.0046	14327.9	14011.9	13252.0	12005.3	14334.1	12588.6
	6×10^{14}	0.0046	14327.9	14011.8	13252.0	12005.3	14334.1	12588.6
	6×10^{13}	0.0046	14327.9	14011.7	13252.0	12005.3	14334.1	12588.6
	6×10^{13}	0.00046	14327.9	14011.7	13252.0	12005.3	14334.1	12588.6
	Insulator model		14327.9	14011.7	13252.0	12005.3	14334.1	12588.6
k (cm^{-1}) $\times10^{-5}$			1.439	3.673	6.559	9.561	1.956	8.469
			1.190	3.679	6.559	9.561	1.901	8.469
			1.153	3.679	6.559	9.561	1.897	8.469
			1.149	3.679	6.559	9.561	1.897	8.469
			1.122	3.679	6.559	9.561	1.891	8.469
	Insulator model		1.122	3.679	6.559	9.561	1.891	8.469
% m_0/M			25.9	17.9	7.65	3.96	71.0	10.0
			67.5	21.4	8.21	4.11	94.6	10.4
			83.4	21.8	8.27	4.12	97.4	10.5
			85.5	21.9	8.28	4.12	97.7	10.5
			98.3	21.9	8.28	4.12	99.8	10.5
	Insulator model		100.0	21.9	8.29	4.12	100.0	10.5
Relative surface amplitude $m(\frac{1}{2})/m(0)$			0.071	−0.840	0.940	−0.970	0.702	−0.979
			0.277	−0.837	0.940	−0.970	0.726	−0.979
			0.322	−0.837	0.940	−0.970	0.728	−0.979
			0.327	−0.837	0.940	−0.970	0.728	−0.979
			0.422	−0.837	0.940	−0.970	0.734	−0.979
	Insulator model		0.423	−0.837	0.940	−0.970	0.734	−0.979
% power absorbed			39.1	3.26	0.50	0.13	81.7	0.66
			86.5	3.94	0.53	0.13	97.8	0.69
			98.4	4.01	0.54	0.13	99.8	0.70
			99.8	4.01	0.54	0.13	100.0	0.70
			98.4	4.03	0.54	0.13	99.8	0.70
	Insulator model		100.0	4.04	0.54	0.13	100.0	0.70

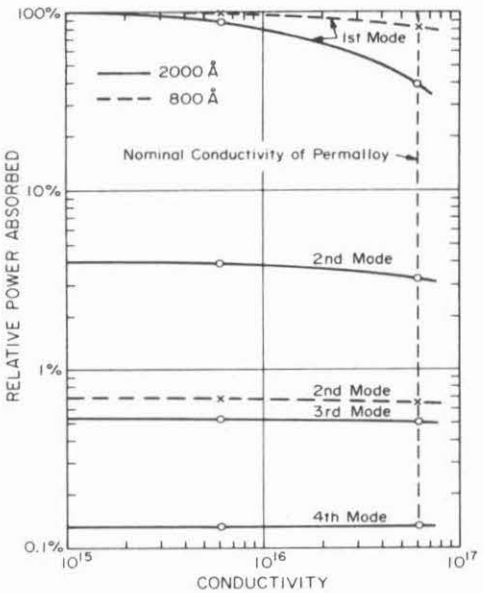

FIG. 2. Variation of mode intensities with conductivity for case of perpendicular resonance.

proximation. Five quantities are compared: applied field (mode location), wave number k, magnetization rf amplitude, surface pinning, and power absorbed. As remarked earlier, only the first and last of these are experimentally observable. It is immediately obvious that there is no significant difference in mode location. The main resonance for the thickest film is given within 0.2 Oe by the insulator theory. The second mode is the one which is most affected by conductivity effects, since it rides well up on the side of the main resonance for thick films. Even so, it is within 0.1 Oe for 790 Å, and the approximation deviates by only 1.5 Oe for 2000 Å. Reducing conductivity by a factor of 10 brings the two models in agreement within 0.2 Oe even for this mode of the thick film.

On the other hand the power absorbed by the 2000-Å film exhibits serious disagreement (factor of 2.5) for the first mode, moderate disagreement (20%) for the second mode, and good agreement only for the higher modes. In the case of the 790-Å film, even though the first mode is located by both models within 0.1 Oe, the amplitude of resonance is in disagreement by nearly 20%. However the amplitude of higher modes is in excellent agreement. Data for power absorbed by all modes is shown in Fig. 2.

Results for parallel resonance are shown in Table IV. There are fewer modes than for perpendicular resonance, but the results are in similar agreement except for two features: (1) the second (symmetric) mode of the thick film is in significant disagreement (16 Oe) for basic conductivity; (2) except for the lowest loss cases,

TABLE IV. Predicted mode properties in parallel resonance.

	Loss parameter		Thickness		
	σ	α	2023 Å		790 Å
Mode No.			1	2	1
H_a (Oe)	6×10^{16}	0.0046	862.04	602.3	861.34
	6×10^{15}	0.0046	862.28	615.6	861.33
	6×10^{13}	0.0046	862.28	617.9	861.33
	6×10^{13}	0.00046	862.28	618.12	861.33
	Insulator model		862.28	618.12	861.33
k (cm^{-1}) $\times10^{-5}$			a	3.152	a
			a	3.066	a
			0.625	3.058	0.696
			0.433	3.048	0.567
	Insulator model		0.433	3.048	0.566
% m_0/M			44.6	2.8	83.7
			89.0	3.8	98.0
			99.9	4.0	99.9
			98.7	4.1	99.7
	Insulator model		100%	4.0	100%
Relative surface amplitude $m(\frac{1}{2}L)/m(0)$			1.097	−0.997	1.019
			1.089	−0.997	1.019
			1.088	−0.996	1.019
			1.089	−0.990	1.019
	Insulator model		1.089	−0.990	1.019
% power absorbed			44.8	0.08[b]	83.6
			89.0	0.06[b]	97.9
			99.8	0.06[b]	99.8
			98.7	0.074	99.6
	Insulator model		100%	0.073%	100%

[a] The two k values are roughly equal in size so that it is not possible to assign the designation "spin-wave" component to either value.

[b] Mode amplitude extremely small, and shape of resonance highly asymmetric so that amplitude can only be estimated.

the main mode in parallel resonance is characterized by three k values, two of which are roughly of equal size. Neither can be clearly designated as belonging to the "spin-wave" component. Nevertheless, the observable quantities, mode location and power absorbed, are obtained for the main mode with essentially the same accuracy as in the case of perpendicular resonance. Although the field location of the second mode at 2023 Å is not obtained with high accuracy, its amplitude is less than 0.1%. It is unlikely that such a mode would be considered in attempting an accurate measurement of exchange constant.

Study of Tables I—IV and Fig. 2 shows that the conductivity must be decreased by a factor of 10 before the first mode amplitude is predicted with 10% accuracy at 2000 Å. For 800 Å, reduction of σ by a factor of 2 will give 10% accuracy. In any case the excellent agreement at low conductivity in all tabulated data of Tables III and IV demonstrates the validity in the correlation between the components of the two solutions discussed earlier, and the validity of the approximations used in the insulator model at least in the range of magnetic losses up to those observed in Permalloy films.

[1]Z. Frait, Phys. Status Solidi 2, 1417 (1962).
[2]C.H. Wilts and S. Lai, IEEE Trans. Magn. MAG-8, 280 (1972).
[3]C.H. Bajorek and C.H. Wilts, J. Appl. Phys. 42, 4324 (1971).
[4]P.E. Wigen, C.F. Kooi, and M.R. Shanabarger, J. Appl. Phys. 35, 3302 (1964).
[5]M. Sparks, Phys. Rev. Lett. 22, 1111 (1969).
[6]W.S. Ament and G.T. Rado, Phys. Rev. 97, 1558 (1955).
[7]J.R. MacDonald, Phys. Rev. 103, 280 (1956).
[8]C. Vittoria, G.C. Bailey, R.C. Barker, and A. Yelon, Phys. Rev. B 7, 2112 (1973).
[9]G.C. Bailey and C. Vittoria, Phys. Rev. B 8, 3247 (1973).
[10]C. Vittoria (private communication).
[11]The Landau-Lifshitz (LL) and Gilbert damping terms are exactly equivalent if in Eq. (1) one uses γ for the LL case and replaces it by $\gamma(1+\alpha^2)$ for the Gilbert case. For ferromagnetic metals this represents an insignificant change in gyromagnetic ratio of the order of 1 part in 10 000. The Gilbert form is somewhat easier to manipulate in the present context.
[12]H. Puzkarski, Acta Phys. Pol. A 38, 217 (1970); 38, 899 (1970).

Appendix IV

IV-1. Anisotropy Models

The perpendicular uniaxial anisotropy has been considered by many workers; it has been shown by Bailey et al (1973) that different or asymmetric surface anisotropies can be chosen in order to match experimental data in a set of permalloy films. When considering method one (presented in the text) Eqs. (4-6) and (4-7) are given by

$$2Z_o h^+_{xi} = \sum_{n=1}^{8} h_{xn} (Z_o + Z_n) e^{ik_n d/2} \qquad \text{IV-1a}$$

$$2Z_o h^+_{yi} = \sum_{n=1}^{8} h_{xn} \nu_n (Z_o + Z_n) e^{ik_n d/2} \qquad \text{IV-1b}$$

$$2Z_o h^-_{xi} = \sum_{n=1}^{8} h_{xn} (Z_o - Z_n) e^{-ik_n d/2} \qquad \text{IV-1c}$$

$$2Z_o h^-_{yi} = \sum_{n=1}^{8} h_{xn} \nu_n (Z_o - Z_n) e^{-ik_n d/2} \qquad \text{IV-1d}$$

$$Z_n = ick_n/4\pi\sigma' \qquad \text{IV-1e}$$

For the resonance calculations it was pointed out in section (4.1) that

$$h^+_{xi} = h^-_{xi} = h_o/2 \qquad \text{IV-1f}$$

$$h^+_{yi} = h^-_{yi} = 0 \qquad \text{IV-1g}$$

For transmission calculations (sometimes called antiresonance calculations), the following conditions are imposed (Liu (1974))

$$h^+_{xi} = h_o/2 \qquad \text{IV-2a}$$

$$h^-_{xi} = h^+_{yi} = h^-_{yi} = 0 \qquad \text{IV-2b}$$

The magnetic boundary conditions given by Eq. (3-7) can be written as

$$0 = \sum_{n=1}^{8} Q_n h_{xn} (ik_n + (K_{s1}/A) \cos^2\theta) e^{ik_n d/2} \qquad \text{IV-3a}$$

$$0 = \sum_{n=1}^{8} Q_n \nu'_n h_{xn} (ik_n + (K_{s1}/A) \cos 2\theta) e^{ik_n d/2} \qquad \text{IV-3b}$$

$$0 = \sum_{n=1}^{8} Q_n \, h_{xn} \left(-ik_n + (K_{s2}/A) \cos^2\theta \right) e^{-ik_n d/2} \qquad \text{IV-3c}$$

$$0 = \sum_{n=1}^{8} Q_n \, \nu_n' \, h_{xn} \left(-ik_n + (K_{s2}/A) \cos 2\theta \right) e^{-ik_n d/2} \qquad \text{IV-3d}$$

$$\nu_n' = m_\theta / m_\phi = i\pi_1/\Omega' = -\nu_n/\cos\theta \qquad \text{IV-3e}$$

A computer program has been written that solves the above equations for the eight unknowns (eight h_{xn}), and calculates the power absorbed by Eq. (4-4).

If the tensorial anisotropy (Eq. (3-11) were to be considered Eq. (IV-3) would be replaced by the following equations.

$$0 = \sum_{n=1}^{8} Q_n \, h_{xn} \left(ik_n + K_{T1}(\theta)/A \right) e^{ik_n d/2} \qquad \text{IV-4a}$$

$$0 = \sum_{n=1}^{8} Q_n \, \nu_n' \, h_{xn} \left(ik_n + K_{T1}(\theta)/A \right) e^{ik_n d/2} \qquad \text{IV-4b}$$

$$0 = \sum_{n=1}^{8} Q_n \, h_{xn} \left(-ik_n + K_{T2}(\theta)/A \right) e^{-ik_n d/2} \qquad \text{IV-4c}$$

$$0 = \sum_{n=1}^{8} Q_n \, \nu_n' \, h_{xn} \left(-ik_n + K_{T2}(\theta)/A \right) e^{-ik_n d/2} \qquad \text{IV-4d}$$

If method two is to be used Eqs. (IV-1) are replaced by Eqs. (4-13). The magnetic boundary condition equations remain unchanged.

IV-2. Perpendicular resonance with asymmetric anisotropies

In this orientation it has been shown that the polarization of the fields associated with a specific wave vector have either positive or negative circular polarization; and the linearly polarized input can be resolved into two oppositely polarized circular waves of half magnitude. Further, the two polarizations are completely uncoupled; one is made up of the positive precession wave vectors and the other the negative precession wave vectors. The wave vectors

are given by solutions to Eq. (2-18). The development is the same for both the positive and negative polarizations, therefore only the positive precession is treated. The K_s can be either the energy associated with either the perpendicular uniaxial or tensorial anisotropies.

The six boundary conditions come from the continuity of tangential components of $\bar{h}$ and $\bar{e}$ and pinning conditions on $\bar{m}$ at each surface. Since the polarizations are circular only the equations for h_x^+, h_x^-, $e_y^+ - e_y^-$ are used. The equations are:

$$\sum_{n=1}^{4} x_n e^{ik_n d/2} = h_x^+ = .5 \qquad \text{IV-5a}$$

$$-\sum_{n=1}^{4} x_n Z_n \sin(ik_n d/2) = e_y^+ - e_y^- \qquad \text{IV-5b}$$

$$\sum_{n=1}^{4} Q_n x_n (ik_n + K_1/A) e^{ik_n d/2} = 0 \qquad \text{IV-5c}$$

$$\sum_{n=1}^{4} x_n e^{-ik_n d/2} = h_x^- = .5 \qquad \text{IV-5d}$$

$$\sum_{n=1}^{4} Q_n (-ik_n + K_2/A) e^{-ik_n d/2} = 0 \qquad \text{IV-5e}$$

The power absorbed per unit area is then given by

$$P = \text{Re}\left[\frac{c}{8}\frac{h_o}{2}\left(e_y^+ - e_y^-\right)\right] .$$

IV-3. Surface Layer Model

The surface layer model is a simple extension of the cases already presented; it simply involves more unknowns and hence more equations. The mathematics are the same. In the most general case there are 24 unknowns. The magnetic boundary conditions imposed on $\bar{m}$ at the interfaces are given by Eq. (3-15). The spins at the outer surface

of the film are assumed free (i.e. $d\bar{m}/dn=0$). In each region of the film there are eight wave vectors and Eqs. (4-1)-(4-3) apply to each region. Since it is a trivial exercise to write down the equations necessary to solve for the power absorbed, only the case of perpendicular resonance with asymmetric surface layers is given below. One surface layer has properties with the subscript f, the other has properties with the subscript g. The magnetic boundary conditions at the z=D/2 interface are

$$\frac{1}{M_b}\sum_{n=1}^{4} Q_{bn}\, b_n\, e^{ik_{bn}D/2} = \frac{1}{M_g}\sum_{n=1}^{4} Q_{gn}\, g_n \qquad \text{IV-6a}$$

$$\frac{A_b}{M_b}\sum_{n=1}^{4} Q_{bn}\, b_n\, k_{bn}\, e^{ik_{bn}D/2} = \frac{A_g}{M_g}\sum_{n=1}^{4} Q_{gn}\, g_n\, k_{gn} \qquad \text{IV-6b}$$

The magnetic boundary conditions at the z=-D/2 interface are

$$\frac{1}{M_b}\sum_{n=1}^{4} Q_{bn}\, b_n\, e^{-k_{bn}D/2} = \frac{1}{M_f}\sum_{n=1}^{4} Q_{fn}\, f_n \qquad \text{IV-6c}$$

$$\frac{A_b}{M_b}\sum_{n=1}^{4} Q_{bn}\, b_n\, k_{bn}\, e^{-ik_{bn}D/2} = \frac{A_f}{M_f}\sum_{n=1}^{4} Q_{fn}\, f_n\, k_{fn} \qquad \text{IV-6d}$$

The equations specifying the continuity of tangential $\bar{h}$ at the + and -D/2 interfaces respectively are

$$\sum_{n=1}^{4} b_n\, e^{ik_{bn}D/2} = \sum_{n=1}^{4} g_n \qquad \text{IV-7a}$$

$$\sum_{n=1}^{4} b_n\, e^{-ik_{bn}D/2} = \sum_{n=1}^{4} f_n \qquad \text{IV-7b}$$

The equations specifying the continuity of tangential $\bar{e}$ at the + and -D/2 interfaces respectively are

$$\frac{1}{\sigma'_b}\sum_{n=1}^{4} b_n k_{bn} e^{ik_{bn}D/2} = \frac{1}{\sigma'_g}\sum_{n=1}^{4} g_n k_{gn} \qquad \text{IV-7c}$$

$$\frac{1}{\sigma'_b}\sum_{n=1}^{4} b_n k_{bn} e^{-ik_{bn}D/2} = \frac{1}{\sigma'_f}\sum_{n=1}^{4} f_n k_{fn} \qquad \text{IV-7d}$$

The equations specifying the free magnetic spins at the $z=D/2 + L_g$ and $z=-D/2 - L_f$ surfaces respectively are

$$0 = \sum_{n=1}^{4} Q_{gn} g_n k_{gn} e^{ik_{gn}L_g} \qquad \text{IV-8a}$$

$$0 = \sum_{n=1}^{4} Q_{fn} f_n k_{fn} e^{-ik_{fn}L_f} \qquad \text{IV-8b}$$

The equations specifying the continuity of tangential $\bar{h}$ at the $z= D/2 + L_g$ and $z= -D/2 - L_f$ surfaces respectively are (note that method two of the text is used here)

$$.5 = \sum_{n=1}^{4} g_n e^{ik_{gn}L_g} \qquad \text{IV-9a}$$

$$.5 = \sum_{n=1}^{4} f_n e^{-ik_{fn}L_f} \qquad \text{IV-9b}$$

Finally the condition specifying $e_y^+ - e_y^-$ is

$$e_y^+ - e_y^- = \frac{ic}{4\pi}\left[\left(\frac{1}{\sigma'_g}\sum_{n=1}^{4} g_n k_{gn} e^{ik_{gn}L_g}\right) - \frac{1}{\sigma'_f}\sum_{n=1}^{4} f_n k_{fn} e^{-ik_{fn}L_f}\right] \qquad \text{IV-10}$$

Appendix V

V-1. Approximations to Boundary Conditions

It was pointed out in section 4.3 that if the boundary conditions are such that the positive and negative spinwave branches uncouple then the approximate positive and negative precession wave vectors can be used to match the boundary conditions separately. Unfortunately, of the three models presented only the tensorial model falls into this class. Therefore, further approximations had to be made to simplify the calculations involving the other two. These approximations are presented in the following sections.

V-1.1 Uniaxial Perpendicular Anisotropy Approximation

For the uniaxial perpendicular anisotropy model the approximation was found by applying the similarity transformation U of Eq. (4-17) to the boundary condition given in Eq. (3-7). The result of this transformation is

$$\begin{vmatrix} \frac{d}{dn} + \frac{K_s^-}{A} & \frac{K_s R \sin^2\theta}{A(1 + |R|^2)} \\ \frac{-K_s R^* \sin^2\theta}{A(1 + |R|^2)} & \frac{d}{dn} + \frac{K_s^+}{A} \end{vmatrix} \begin{vmatrix} \mu_1 \\ \mu_2 \end{vmatrix} = 0 \qquad \text{V-1}$$

where $K_s^+ = K_s(|R|^2 \cos 2\theta + \cos^2\theta)/(1 + |R|^2)$

$K_s^- = K_s(\cos 2\theta + |R|^2 \cos^2\theta)/(1 + |R|^2)$

The approximation is to drop the off diagonal terms. The boundary condition for the positive precession spinwave branches is

$$\frac{d\mu_2}{dn} + \frac{K_s^+}{A} = 0 \qquad \text{V-2}$$

The approximate power absorbed can now be calculated as outlined in the text of chapter 4.

V-1.2 Surface Layer Model Approximations

For the surface layer model there are two approximations to Eq. (3-17) which will be considered. The first approximation yields an effective surface anisotropy with easy or hard axis along the equilibrium direction of the magnetization. In calculations involving this effective anisotropy the power absorbed in the surfaces is neglected; therefore, for thick layers a significant error exists in the calculated spinwave mode intensities. The second approximation gives an approximate boundary condition between the bulk and surface layers in which the positive and negative precession wave vectors are uncoupled. With this approximation the power absorbed due to the positive precession spinwave can be calculated. This calculation gives an accurate picture of the resonance process.

V-1.2.1 Surface Layer Effective Anisotropy

The first approximation to the surface layer problem is obtained by dividing the numerator and denominator of the right hand side of Eq. (3-17) by $A_b k_{2b} \tan(k_{2b}D/2)$, and dropping all terms remaining with $A_b k_{2b} \tan(k_{2b}D/2)$ in the denominator. The result is

$$A_b k_{1b} \tan(k_{1b}D/2) = \frac{-(k_{1s}T_{1s}(1 + R_s^* R_b)^2 + |R_s - R_b|^2 k_{2s}T_{2s})}{(|R_s|^2 + 1)(|R_b|^2 + 1)} \quad \text{V-3}$$

The secular equation for a symmetric film and boundary conditions given by an anisotropy with easy or hard axis along $\bar{M}_o$ and energy K_L is

$$A_b\, k_{1b} \tan k_{1b} D/2 = K_L \qquad \text{V-4}$$

Comparing Eq. (V-3) and (V-4) shows that the surface layer can be approximated by an effective anisotropy energy, K_L, given by the right hand side of Eq. (V-3). For this approximation of the surface layer the power absorbed can be calculated in the same manner as discussed for the other anisotropy models.

V-1.2.2 Surface Layer Approximate Boundary Condition

By making a further approximation to Eq. (V-3) an approximate boundary condition between the bulk and surface layer can be deduced. This approximation is to assume that $|R_s - R_b|^2 = 0$. With this approximation Eq. (V-3) becomes

$$A_b k_{1b} \tan(k_{1b} D/2) = \frac{-(k_{1s} T_{1s}(1 + R_s^* R_b)^2}{(|R_s|^2 + 1)(|R_b|^2 + 1)} \qquad \text{V-5}$$

An approximate boundary condition between the bulk and surface m_ϕ which gives this secular equation and the C in Eq. (3-18) with the same approximation is

$$\frac{1}{(1 + |R_s|^2)} \frac{m_{\phi b}}{M_b} = \frac{1}{(1 + R_b R_s^*)} \frac{m_{\phi s}}{M_s} \qquad \text{V-6a}$$

$$\frac{1}{M_b(1 + R_b R_s^*)} \frac{dm_{\phi b}}{dz} = \frac{1}{M_s(1 + |R_b|^2)} \frac{dm_{\phi s}}{dz} \qquad \text{V-6b}$$

The corresponding expression for m_θ is obtained by replacing m_ϕ by m_θ/R. By using Eq. (4-21) the approximate boundary for μ_2 is given by Eq. (4-24).

Appendix VI

Ferromagnetic Resonance Introduction

The theories of ferromagnetism propose that the magnetization is due primarily to the magnetic moment of the electron. Although the origin of this moment is quantum mechanical in origin, most of the phenomena involving ferromagnetism can be addressed classically. In this approach the ferromagnetic material is characterized by a magnetization, $\overline{M}$, which is associated with an opposite angular momentum $\overline{L} = \overline{M}/\gamma$ (γ is the gyromagnetic ratio). The motion of the magnetization is usually analyzed in terms of the Landau-Lifshitz equation. This equation is easily obtained by equating the rate of change of angular momentum and the torque ($\overline{M}x\overline{H}_{eff}$)

$$\frac{d\overline{M}}{dt} = -\gamma\overline{M}x\overline{H}_{eff} \quad .$$

In this equation $\overline{H}_{eff}$ is the total effective field acting on $\overline{M}$. The sources of these fields are presented in the text of the thesis.

Ferromagnetic resonance is a phenomenon in which the magnetization of a ferromagnetic sample exhibits a resonance when subjected to a harmonic magnetic field. The magnetic resonance is manifested by a maximum in the harmonic response of the magnetization or by a maximum in the power absorbed from the driving system. In a resonating elastic system, the resonances are found at (or near) the eigenfrequencies of the normal modes of the lossless elastic system. These modes are strongly dependent on the sample shape and boundary conditions; and the oscillations

can be treated by an analysis of the elementary excitations, phonons. Similarly in ferromagnetic bodies, the resonances are found at (or near) the eigenfrequencies of the normal modes of the lossless magnetic system. These modes are also strongly dependent on the sample shape and boundary conditions. The magnetic variations can be treated in terms of elementary excitations; these excitations are magnons in the quantum mechanical description and spinwaves in the classical description. The spinwaves are described by functions of the form $m_o e^{i(\bar{k}\cdot\bar{r}+\omega t)}$.

To eliminate the shape dependence in ferromagnetic resonance the samples are usually made in the form of thin films. These samples are then driven by an approximately uniform magnetic field applied in phase at both film surfaces. In this case the excitations are standing spinwaves with $\bar{k}$ normal to the film plane. Even with this simple geometry, the mode locations and intensities are dependent upon the magnetic boundary conditions at the surfaces. The normal modes of the system depend not only on the frequency, but on the static magnetic field which is used to ensure that the magnetic system is not broken up into magnetic domains and to establish the resonant frequency in a range convenient for experimental observation. The resonances can be excited as "lines" of the spinwave spectrum by sweeping the frequency at fixed magnetic field, or by sweeping the magnetic field at fixed frequency. For reasons of experimental convenience and accuracy the latter scheme is almost invariably used.

Spinwave spectra have been investigated for a number of reasons. In principle they provide one of the most accurate means of determining a number of the fundamental magnetic constants: saturation

magnetization, M , gyromagnetic ratio, γ , exchange constant, A , to name just a few. They also provide a powerful method of studying relaxation or loss processes in magnetic materials. However, to exploit the potential accuracy of this method in almost all of these applications it is necessary to have an accurate analytic statement of the boundary condition at the surface of a ferromagnet. It is surprising that this understanding remains elusive after 15 or 20 years of continuous research effort.